2017

Transverse Aeolian Ridges (TARs) on Earth and Mars: Analysis from a New Terrestrial Analog and a New Semi-Automatic Mapping Technique with a Large Sample Size

Foroutan, Marzieh

UNIVERSITY OF CALGARY

Transverse Aeolian Ridges (TARs) on Earth and Mars: Analysis from a New Terrestrial Analog and a New Semi-Automatic Mapping Technique with a Large Sample Size

by

Marzieh Foroutan

A THESIS

SUBMITTED TO THE FACULTY OF GRADUATE STUDIES

IN PARTIAL FULFILMENT OF THE REQUIREMENTS FOR THE

DEGREE OF MASTER OF SCIENCE

GRADUATE PROGRAM IN GEOGRAPHY

CALGARY, ALBERTA

JANUARY, 2017

ABSTRACT

Aeolian processes are the most dominant geological processes in the current environment of Mars. Studying other planets through terrestrial analogs is an important step in planetary science studies. One of the most enigmatic and mysterious aeolian features on this planet is known as Transverse Aeolian Ridges (TARs). In the present study, I described a terrestrial analog for TARs on Mars in the Lut desert of Iran. TAR-like features in this area have considerable similarities with Martian TARs in morphometry. This area represents a unique site to study the formation and evolution of these enigmatic features with the potential to develop a better understanding of TARs on Mars.

Furthermore, mapping small linear trending features such as TARs has been a restriction in planetary remote sensing. In this study, I present a new framework for mapping these features based on an Artificial Neural Network (ANN) algorithm known as Self Organizing Maps (SOM). Appropriate layer selection and network settings have been defined for mapping features with small footprints on satellite images. Accuracy assessment using different planetary images such as Worldview, Quickbird and HiRISE shows that this is a promising method in remote sensing analysis of these features. Moreover, this method can be applied in other disciplines for different purposes.

The new mapping technique was applied to satellite images in order to evaluate TARs on Earth and Mars. I produced a large sample set of these bedforms through Mars and Earth satellite images. Results from different metrics showed similarities between these features in the Lut desert and TARs on Mars. Interesting results have been acquired by using multi-temporal satellite images and morphometry analysis of TARs on both planets. The features have been classified into three different regions based on their migration rate, direction and location in this area. I define TARs that are unique to Mars from TARs that have the similar analogs on Earth.

ACKNOWLEDGEMENT

I would like to greatly acknowledge two internationally acclaimed scientists who helped me tremendously through this work: Prof. Shawn Marshall and Prof. James Zimbelman. Words cannot express how honoured I am to have worked with you both, I owe this thesis all to you and I wish I could repay all your kindnesses, considerations and helps. You guided me not only in science but also in my professional development teaching me how to become an independent scientist in my own right. Thanks for your trust, for letting me develop my own ideas and teaching me to be brave in science.

I would like to express my gratitude to my defense committee member Dr. Mozhdeh Shahbazi for her invaluable comments which improved my thesis. Also my internal committee member Dr. Yvonne Martin and the neutral chair Dr. John Matyas for their time. Special thanks to Ms. Paulina Medori, the graduate program administrator, for being such an amazing problem solver.

I would like to thank my wonderful friend Saghar. Many times I lost my hope and stopped and you pushed me to work more. I AM SURE THAT WITHOUT YOU I COULDN'T HAVE DONE THIS. Your friendship is the best gift from Canada. And thank you Jackie, for all your support and help. I am so happy that I have your beautiful voice on my first paper's slideshow. I would like to express my gratitude to Dr. Judy Chew for her care and encouragements, guidance and helps. Other wonderful people who helped me through my way: Jaya, Jeanna, Jane, Kevin, Robin, Lisa, Bart. Thank you all.

Last, but definitely not least, I would like to thank my wonderful family. My amazing mother Sedigheh, My brother Mohammad and my lovely sisters Leyla and Elaheh. I am nothing without you all. I couldn't have overcome all the difficulties in my life without your supports. Thank you!

I dedicate this work to my wonderful mother Sedigheh and the memory of my beloved father Mohammad Karim. I AM SUPER PROUD TO BE YOUR DAUGHTER.

TABLE OF CONTENTS

LIST OF FIGURES

LIST OF TABLES

LIST OF ABBREVIATIONS

ANN	Artificial Neural Networks
DDT	Dust Devil Track
DEM	Digital Elevation Model
DTM	Digital Terrain Model
HiRISE	High Resolution Imaging Science Experiment
LDD	Large Dark Dunes
MOC	Mars Orbiter Camera
MOC NA	Mars Orbiter Camera – Narrow Angle Images
MRO	Mars Reconnaissance Orbiter
PBRs	Periodic Bedrock Ridges
SRTM	Shuttle Radar Topography Mission
SOM	Self-Organizing Maps
TARs	Transverse Aeolian Ridges

CHAPTER 1

1-1 INTRODUCTION

Any planetary body within our solar system that has a dynamic atmosphere and a solid surface is subject to wind or aeolian processes. The best known examples are Earth, Mars, Titan and Venus – all of which have landforms indicative of aeolian sediment transport, either occurring presently or in the geological past (Greeley and Iverson, 1985; Bourke et al., 2010; Greeley, 2013). Mars, the most Earth-like planet, has been a major focus of research and interest for the last several decades and has revealed a rich array of aeolian features and landforms, including a wide variety of terrestrial analogs such as dust devil tracks (Rossi and Marinangeli, 2004), ventifacts (Greeley et al., 2002), yardangs (de Silva et al., 2010), mega-ripples (Zimbelman et al., 2009) and several types of sand dunes such as barchans (Bourke and Goudie, 2009), linear dunes (Radebaugh et al., 2010), star dunes (Silvestro et al., 2012), and domes (Szynkiewicz et al., 2010). Mars has a very "thin" atmosphere in comparison to Earth (i.e., about two orders of magnitude less dense than Earth's), but despite this, wind and associated aeolian processes dominate the current environment of Mars and result in several types of aeolian landforms of various scales active under current Martian conditions (Sullivan et al., 2005; Silvestro et al., 2011; Bridges et al., 2012b; Bridges et al., 2013; Sefton-Nash et al., 2014; Cardinale et al., 2016).

Our basic understanding and interpretations of aeolian geomorphology are based on aeolian processes and features that occur predominantly on Earth. However, from a planetary perspective, it can also be argued that surface processes are much more complicated on Earth because of the presence of water, vegetation and humans. These modifiers can convolute theoretical relations between the key system components: sediment grains and wind. As such, some aspects of aeolian processes that are difficult to assess on Earth may be easier to understand on other planets where these modifiers are absent. By investigating how landforms look and evolve on other planets, we can learn about processes that also occur on Earth and move closer to uncovering universal geomorphic transport laws (Thomas et al., 2005; Marchant and Head III, 2007; Church, 2010; Baker, 2014). The study of sand dunes, for example, was greatly advanced when a scaling law was developed for aeolian dunes on Mars, Earth and Venus, despite the differences in gravity and atmospheric density (Claudin and Andreotti, 2006). In this regard, a major thrust of aeolian geomorphological research is to establish the universal mechanics of processes that create and modify aeolian landforms.

Aeolian landforms are generally divided into granular bedforms (e.g., ripples and dunes) or features carved from bedrock (e.g., ventifacts and yardangs). A bedform is a repeating depositional feature,

whose genesis is through the action of a forcing fluid (e.g., air) resulting in the movement of the granular material, manifesting into characteristic surface morphology indicative of the flow parameters in operation (Hargitai and Kereszturi, 2015). There are lots of detailed bedform classifications by different authors and based on diverse characteristics. 'Dunes' and 'Ripples' are two

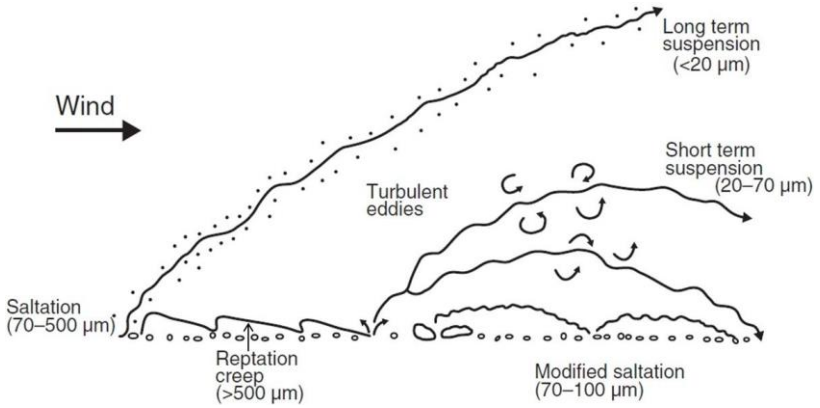

Figure 1.1. Schematic of the different modes of aeolian transport (Nickling and McKenna Neuman, 2009).

major classes based on bedform shape and dimension. Morphological differences arise from variability in particle size among these bedforms and the formation process. One of the key defining factors of bedform morphology is related to the mode of transport and accumulation of their composed particles or the initiation. Figure 1.1 indicates different types of transportation of particles by wind that influence their morphology.

Despite the wide array of analog aeolian landforms on Earth and Mars, there are also several enigmatic aeolian landforms identified on Mars that do not have well-defined analogs on Earth, like transverse aeolian ridges (TARs) (Ward, 1979; Thomas et al., 1999; Bourke et al., 2003; Balme et al., 2008; Zimbelman, 2010; Berman et al., 2011; Kerber and Head, 2012). TARs are believed to be a form of granular bedform unique to Mars (Fenton et al., 2015). They are generally brighter than the surrounding terrain and occur at a length-scale on the order of 10 meters (Figure 1.2). They occur singularly or number in the thousands and, while plentiful, they are not ubiquitous (Balme et al., 2008). The term "ridge" was chosen by Bourke et al. (2003) to describe these bedforms because it did not convey if the features were ripples, dunes, or something else entirely. Information and hypotheses about their composition, origin and formation, as well as the processes that control their distribution and activity, sediment source, age and superposition relationships are still limited. In the absence of direct measurements of formative processes and sedimentology, research on TARs has focused almost exclusively on their distribution and morphology. Observations from satellite imagery indicate

that TARs are widespread at low to mid-latitudes in the northern and southern hemispheres of Mars (Wilson and Zimbelman, 2004; Balme et al., 2008; Berman et al., 2011).

TARs have been described as "*About 10-m-scale, light- or medium-toned albedo relative to surrounding terrain, ripple-like aeolian bedform on Mars*" in the Encyclopedia of Planetary landforms (Hargitai and Kereszturi, 2015). Morphological measurements indicate their ridge planforms and patterns vary and include simple, sinuous, forked, networked, and barchan-like arrangements (Balme et al., 2008). However, despite their initial definition, their diversity in size, color, pattern and morphology of crestline, highlights a demand to define more detailed criteria for a new classification scheme (Foroutan, 2015). TARs tend to have sharp crests, symmetric transverse profiles and show no sign of recent movement (Zimbelman, 2010; Zimbelman and Scheidt, 2014).

From a critical review of the peer-review literature, the study of TARs and the development of hypotheses about TAR formation and evolution appear to have at least four limitations. First, introduced terrestrial analogs do not have enough similarities with TARs on Mars. Although there are some similarities between these features and some sort of aeolian deposits on Mars, they are not similar to typical TARs on Mars, which is considered to be unique to Mars (Fenton et al., 2014). Second, there is a limitation in initial mapping of these features or any other linear-trending features on all planets in order to further processing and spatial analysing. This is a critical issue because they have small footprints on satellite images and they are plentiful in their patches. So time-consumption and difficulties in manual mapping can prevent comprehensive investigation of small features such as TARs. Furthermore, previous terrestrial analogs of Martian aeolian bedforms were not studied using the same method, and different scales of multiple bedform superposition and interaction has never been analysed simultaneously on both planets. Comparing the forms of these aeolian activities with terrestrial analogs at a comparable time scale increases information about the atmospheric conditions and aeolian processes on Mars, because these bedforms play a critical role as a geological indicator of Martian surface evolution and history. Finally, sample sizes used for evaluating these features are small compared to their abundance on Mars and there is a lack of quantitative analysis of their morphology.

The overarching goal of this thesis research is to improve our understanding of TARs on both planets and advance mapping methodology. This will be accomplished by introducing the best terrestrial analog for TARs on Earth, developing a mapping technique for extracting crestlines of these bedforms on both planets, and making a comparison and metrics analysis using this new technique on a larger

sample size. We believe that this thesis will serve as a benchmark in TARs study and remote sensing mapping technique.

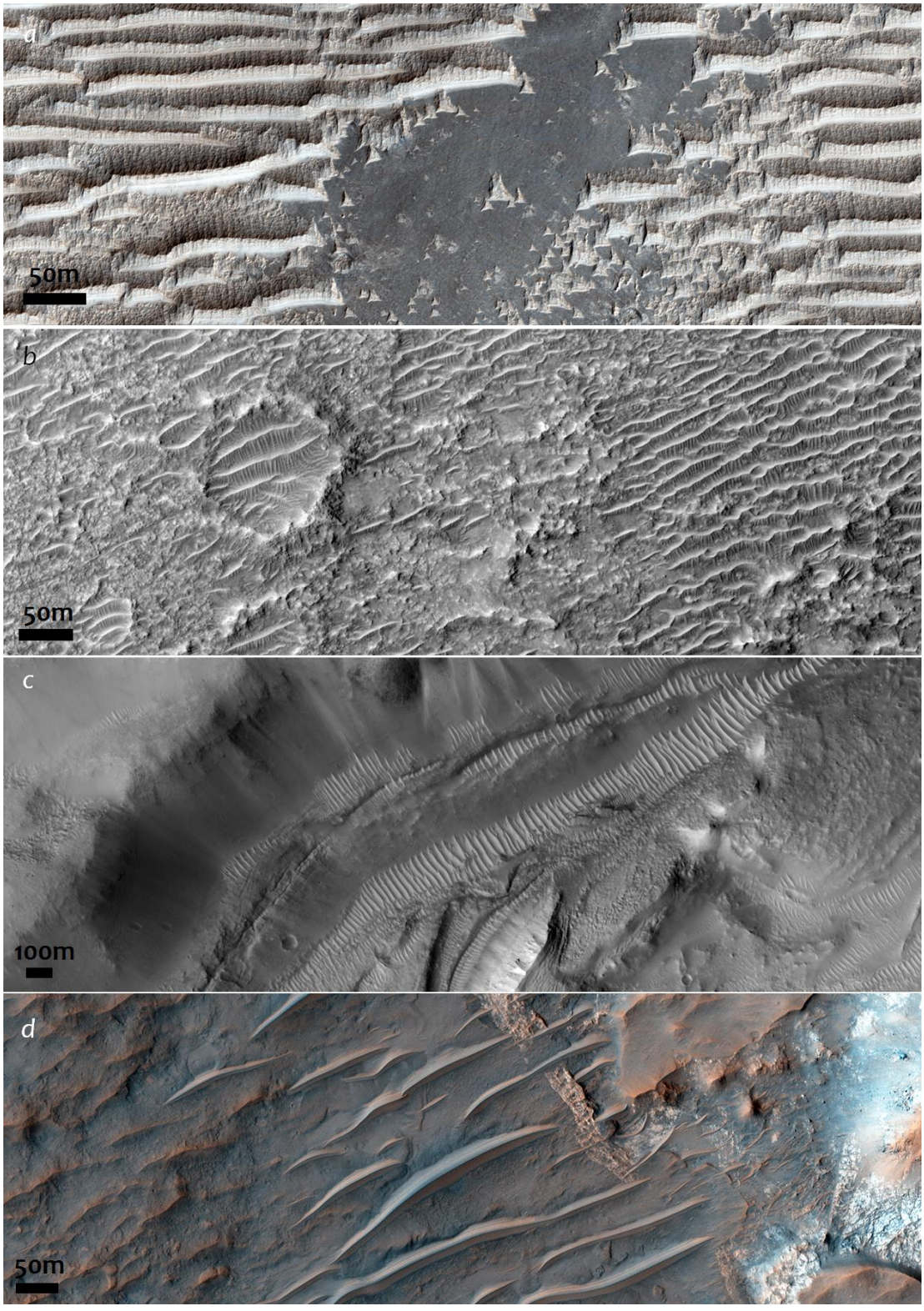

Figure 1.2. TARs on Mars: a) A specific morphology of TARs in Syria Planum (HiRISE - ESP_042124_1665), b) Centipede-shaped TARs in Terra Cimmeria (HiRISE - ESP_046085_1695), c) TARs in Mareotis Fossae (HiRISE - ESP_046131_2270), d) Banded TARs in Iapygia (HiRISE - ESP_020782_1610).

1-2 BACKGROUND

1-2-1 BRIEF OVERVIEW OF AEOLIAN PROCESSES ON EARTH AND MARS

Important advances have been made in our understanding of the processes of aeolian sediment transport on other planets, particularly in the last decade with the advent of high-resolution imaging sensors onboard satellites orbiting Mars, as well as several rovers successfully deployed on Mars (Craddock, 2011; Fenton et al., 2015). The study of aeolian processes and landscape dynamics on Mars, however, remains grounded in the classical work of Bagnold (1941). While Earth and Mars have many notable differences that affect the characteristics of aeolian transport and the resulting depositional features (Table 1.1), such as lower gravity and atmospheric density, the basic physics of windblown material is considered to be essentially the same. One of the most striking differences is related to the comparatively thin Martian atmosphere, which requires much higher wind velocities to accomplish the same effect as on Earth (Figure 1.3) (Greeley and Iverson, 1985; Greeley et al., 2000). Another important difference is the nature of sediment on Earth and Mars. It is suggested that two of the most important influences on terrestrial aeolian sediment are the dominance of quartz in granitic rocks and the past actions of large continental ice sheets (Greeley and Iverson, 1985; Chapman, 2007). However, neither of these factors is dominant on Mars; the crustal rocks on Mars appear to be mostly basaltic rather than granitic and there is no evidence of large-scale glaciation of the kind found on Earth (Smalley and Krinsley, 1979). Further, the absence of plate tectonics on Mars implies that the cycling of sediment is very different from Earth. On Earth, sediment is removed from the surface and incorporated into rocks through tectonics, whereas on Mars, it remains at the surface for billions of years to be moved around by the wind (Carr, 2006).

Table 1-1. Physical differences in key parameters and aeolian processes on Earth and Mars (Kok et al., 2012; Lorenz and Zimbelman, 2014).

Parameter	Earth	Mars
Gravity (m s^{-2})	9.81	3.71
Fluid density (ρ: kg m^{-3})	1.2	0.02
Particle density (ρ_p: kg m^{-3})	2,650	3,200
Dynamic viscosity (kg m^{-1} s^{-1})	1.78 x 10^{-5}	1.3 x 10^{-5}
Typical particle diameter (μm)	250	600
Density ratio (ρ_p/ρ)	2,200	160,000
Threshold friction speed (m/s)	0.2	1.5
Ratio of impact to fluid threshold speed	0.8	0.1
Typical saltation height (cm)	3	10
Typical saltation length (cm)	30	100
Minimum threshold friction speed (cm/sec)	15	160

Particle diameter most easily moved by winds (μm) 80 100

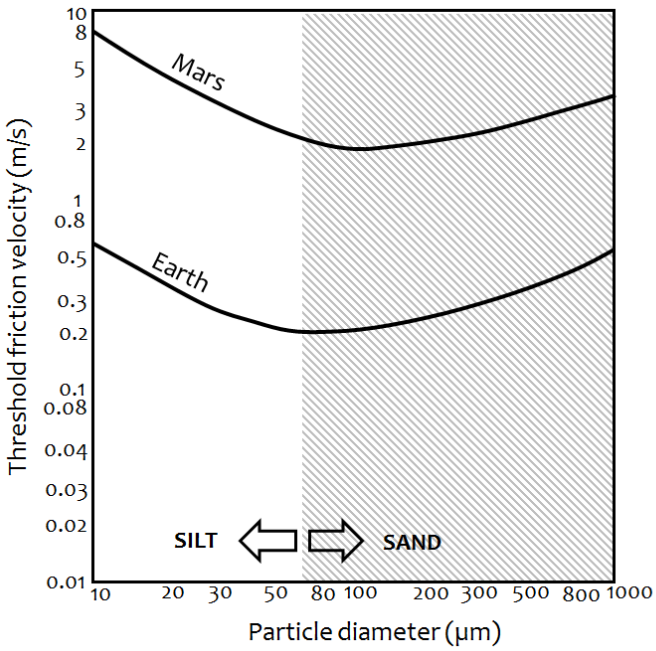

Figure 1.3. Wind speed needed to move particles of different sizes on the surface of Earth and Mars. The optimum particle size is about the hundred microns (75μm Earth, 115μm Mars).The shape of the curves for both planets are essentially the same. The difference between Mars and Earth is resulted from differences in atmospheric density and gravity (From Greeley and Iverson, 1985).

At a more detailed level, the lower gravity and atmospheric density on Mars creates conditions that favour the perpetuation of aeolian sediment transport once it is initiated. In order for a sedimentary particle to become mobilized, the wind shear stress must exceed the forces that keep the particle at rest. This is known as the fluid threshold shear stress (Bagnold, 1941). Once the grains are set into motion, there is another threshold known as the impact threshold, which is the minimum shear stress required to sustain particle mobility (Bagnold, 1941). For most conditions on Earth and Mars, the impact threshold is smaller than the fluid threshold because the transfer of momentum to the soil bed through particle impacts is more efficient than through fluid drag (Kok et al, 2012). On Earth, the impact threshold is ~80% of the fluid threshold (Bagnold, 1941), whereas on Mars the impact threshold is expected to be only ~10% of the fluid threshold (Kok et al., 2012). This occurs because the lower Martian gravity and air density allow sand grains to travel in higher and longer trajectories at a given launch speed, causing them to be accelerated by wind for a longer duration in a single hop than on Earth (Edgett and Malin, 2000; Yizhaq et al., 2014). It has been shown theoretically that these

differences result in Martian particles saltating 100 times higher and longer in trajectories (Figure 1.4) and 5–10 times greater in velocities than the same particles under Earth's gravity and atmospheric density (Almeida et al., 2008). Therefore, the aeolian feature sizes (length and height) on Mars are expected to be larger than those on Earth (Parteli et al., 2009).

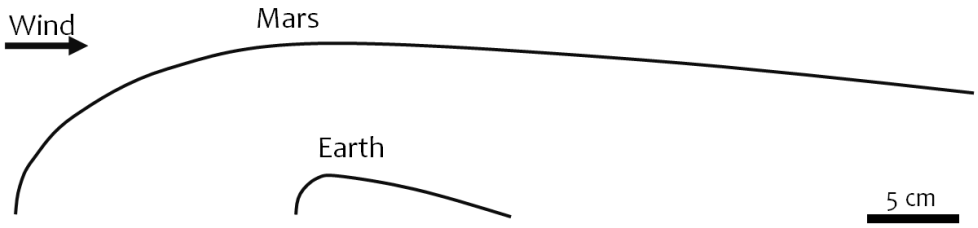

Figure 1.4. Schematic of typical saltation trajectories and scales on Earth and Mars.

1-2-2 MARTIAN ATMOSPHRE AND AEOLIAN ACTIVITY

Our understanding about Martian atmosphere and physics is largely built upon our comprehension of Earth's fluid dynamics. However, the environment of Earth is largely complicated because of the existence of water, vegetation and humans compared to Mars. Although there is no liquid water currently on Mars, evidence, such as the existence of geological fluvial features and phyllosilicates, suggest this planet has experienced a huge atmospheric evolution with a wetter period and thicker atmosphere about 3.9 GA ago (Noachian period). Furthermore, new high-resolution data from orbiters and landers give us remarkable detailed information of the present major geological agent on this planet, which is the wind.

Apart from Hadley circulation, Mars is the same as Earth and other rotating planets and is subject to some other factors that affect wind forces on this planet considerably. (i) Mars' greater Orbital eccentricity, (ii) huge Martian dust storms, (iii) its thin atmosphere; as well, (iv) condensation flows and (v) strong thermal tides are other factors that create pressure gradient and influence tidal winds. Surface pressures of this planet vary up to about 20% due to variations in CO_2 and H_2O components, resulting from seasonal changes in polar caps. It has atmospheric structured layers with different properties than other planets. Also, landers on Mars have recorded considerable diurnal variation in wind direction on this planet, which is evidence of a highly active aeolian environment of Mars.

Aeolian processes operate on all scales across Mars – from grains to landforms – and have played an important role in shaping the Martian surface throughout much of its geological history (Greeley et

al., 2000; Carr, 2006; Chapman, 2007). There are many theories about the history and past conditions of Mars, including landscapes indicating the presence of liquid water, but today it is a cold desert dominated by aeolian processes. Most of the high-resolution images taken of Mars' surface reveal TARs and sand dunes (typically referred to as Large Dark Dunes – LDDs), which are clear evidence of pervasive aeolian activity on this planet. Some studies suggest that aeolian processes on Mars might have been more vigorous or variable in the past (Edgett and Malin, 2000). While Mars' wind patterns are dominated by a Hadley-style circulation pattern, there are some notable differences in comparison to Earth because of its rotation rate, obliquity, and orbital eccentricity as well as the presence of polar caps and thermal continents (Barlow, 2008).

Present-day aeolian activity has been reported for many regions of Mars and includes evidence of ripple and dune migration, dust devils and resulting tracks, and planet-wide dust storms. Initial reports showed that some aeolian landforms are active today, as evidenced by downwind shifts of ripple crestlines and dune lee slopes (Silvestro et al., 2010; Chojnacki et al., 2011; Hansen et al., 2011; Bridges et al., 2012a; Bridges et al., 2012b; Fenton et al., 2014). However, Bridges et al. (2012b) showed that entire dunes were also moving in the Nili Patera dune field. The calculated sand fluxes were unexpectedly high and similar to dunes in the Victoria Valley, Antarctica, implying rates of landscape modification on Mars that are similar to cold polar deserts on Earth. As will be discussed, mobility of dunes and ripples on Mars has a significant implication for interpreting the formation and evolution of TARs.

1-3 TAR RESEARCH

TARs were first distinguished and noted in images from the Viking mission and the Mars Global Surveyor (MGS) Mars Orbiter Camera (MOC) mission (Zimbelman, 1987; Thomas et al., 1999; Malin and Edgett, 2001). Compared to LDDs, TARs are generally brighter and occur at a length-scale somewhere between ripples and dunes. Adapting aeolian bedform classifications developed from terrestrial studies is not straightforwardly applicable to TARs; hence the term "ridge" (Bourke et al., 2003) was chosen because it did not specify whether they are ripples or sand dunes or something else entirely.

Application of the term 'TARs' in different research papers includes a variety of different ripple-like aeolian deposits on Mars. There is no accepted description of TARs in the literature and, more recently, this nomenclature inconsistency has been debated. Most importantly for this proposed research, a number of studies have examined ripple-like features in Meridiani Planum, which is an area characterized by a large number of TARs (e.g., Sullivan et al., 2005; Fenton at al., 2015; Silvestro et al.,

2015). These studies separate ripple-like features from TARs based on orientation and further provide names for some of these non-TAR features, including 'plains ripples', 'plains-type ripples', 'patches of ripples', and 'ripple streaks'. Although separating these features based on their orientation is useful to distinguish TARs from other features, a careful survey of the differences in size and other morphologic characteristics between TARs and similar ripple-like features is needed. These differences could also help to recognize differences among TARs.

TARs are not homogenously distributed on Mars. They are commonly associated with outcrops of layered terrain in mid- to low-latitudes, often in local lowlands, and are comparably absent in the northern hemisphere and infrequent pole-ward of 35°N and 55°S. They also occur near the equator and in large southern-hemisphere impact craters (Wilson and Zimbelman, 2004; Balme et al., 2008; Berman et al., 2011). Berman et al. (2011) compared the pole-to-pole (45° longitude wide) distribution of TARs with General Circulation Model (GCM) climate data for various obliquity values. Although some agreement was found between present-day wind direction and TAR crestline orientations, the correlation between their distribution and shear stress was weak. In a more localized study of a region in the Meridiani Planum, Fenton et al. (2015) inferred that TARs formed by an easterly wind prior to about 200 ka, but their orientation was found to be inconsistent with present-day winds. What is also remarkable is that some LDDs in the region showed signs of migration (Chojnacki et al., 2011; Fenton et al., 2014), while adjacent TARs did not move. According to the principle of celerity, smaller (shorter) bedforms migrate faster than larger (taller) bedforms, assuming they are composed of the same sediment and subject to the same sediment flux. Collectively, these findings indicate that TARs may be relict features in some regions of Mars, and/or perhaps composed of different (coarser) sediment that reduces their mobility. However, it seems that TARs have been present on the surface in some regions of Mars for relatively long periods.

Although TARs have not yet been directly identified on any planet other than Mars (Fenton et al., 2015), two studies have documented terrestrial aeolian landforms that could serve as potential analogs. The two landforms are (a) the gravel-mantled mega-ripples in the Argentinian Puna (de Silva et al., 2013) and (b) reversing dunes (Zimbelman and Scheidt, 2014). The Puna mega-ripples have a length-scale similar to TARs and are believed to be contextually similar to granule ripples in the Meridiani Planum, Mars (de Silva et al., 2013). However, unlike the TARs measured by Zimbelman (2010) and Shockey & Zimbelman (2013), Puna mega-ripples often have asymmetric transverse profiles (Bridges et al., 2015). The largest mega-ripples also have topography amplified by the underlying bedrock topography,

which mimics that of the overlying bedforms. In the context of reversing dunes, Zimbelman & Scheidt (2014) found that the transverse profiles of large TARs and a 143 m tall reversing dune in Idaho are similar (symmetric), suggesting that TARs may have been developed under the influence of bimodal winds. However, the height of the reversing dune is 1-2 orders of magnitude greater than the height of TARs measured on Mars.

TARs may occur singly, but more commonly, they are found in groups or fields that range in size from a handful of features to hundreds. The arrangement of TARs within a field can vary substantially and presumably the pattern is an expression of processes, boundary conditions and the age of the field (Kocurek and Ewing, 2005; Ewing et al., 2006; Kocurek et al., 2010; Savage et al., 2014; Ewing et al., 2015). Previous work has examined TAR patterns in a qualitative manner using visual interpretation of satellite imagery (Bourke et al., 2003; Wilson and Zimbelman, 2004; Balme et al., 2008; Berman et al., 2011). Balme et al. (2008) provide the most rigorous treatment to date. The scheme is based on three levels. The first scheme considers their crestline morphology: simple, sinuous, forked, networked, and barchan-like. The second scheme considers topographic effects on TAR groupings: confined, controlled, influenced and independent. The third scheme considers the size of the grouping: patches, fields and seas. The main challenge with this approach is that a qualitative description creates ambiguities in the identification of particular patterns and weakens confidence in the outcome of any subsequent quantitative analysis. For example, these schemes do not describe other kinds of patterns, nor do they provide much in the way of insight into the processes.

The formation process of large ripple-like features, either Martian TARs or mega-ripples on Earth, is still under debate. However, observations from the first terrestrial analogs of TARs and wind tunnel studies by de Silva et al. (2013) and Bridges et al., (2015) suggested that they initiate as a result of trapped large particles in saltation or creep in low roughness of the surface. These large particles remain largely stable and grow by periodic vibration of clasts through wind gusts, which allows sand and silt to infiltrate the ripple interior (Figure 1.5). Also strong gusts of wind are found as a factor that cannot destroy the mega-ripples but can cause ripple migration (Yizhaq and Katra, 2015). On the other hand, Geissler (2014) suggested a new hypothesis that some TARs, in the Syria Planum, can be indurated dust deposits from dust carried by the winds in suspension millions of years ago. However, current conditions of Mars prevent us from real measurements that can test any of these hypotheses.

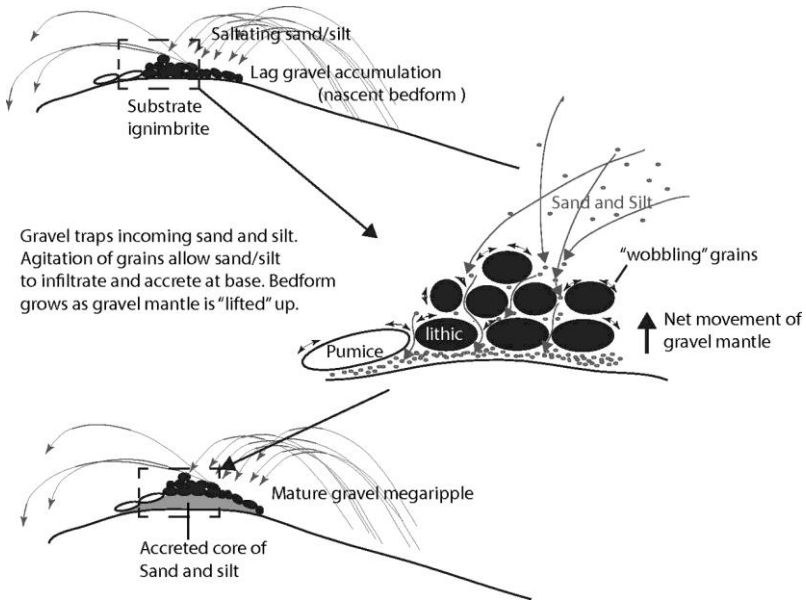

Figure 1.5. Schematic representation of one of the suggested formation mechanism of TARs by infiltration and accretion from de Silva et al. (2013).

In the absence of process measurements coinciding with the timescale of TAR formation and evolution, one approach commonly used in geology and geomorphology is to use morphology to infer process, or at least to develop initial ideas or hypotheses about process (es). This has been the leading research approach to the study of TARs thus far. The methodology has been based on geocoded satellite imagery and manual measurements of TAR length (L), width (W), height (H) and wavelength (λ). Whereas L is readily measured, measuring W and H is more difficult and requires 3D data, and λ is constrained by subjective positioning of transects over successive TARs. However, the most important deficiency is that our current information about TARs is based on an extremely small sample size, particularly when considering the pervasiveness of TARs on Mars. For example, the height of TARs has been measured using photoclinometry, which only works under ideal image and lighting conditions; therefore, what is known about the height of TARs on Mars is based on a sample size no greater than 60, all within the same area. Given the limited information available about TAR morphometry, the quantitative foundation for characterizing their form and inferring process (es) is limited. Further, in anticipation of future numerical models, the quantitative characterization of TAR morphometrics and patterns may be used to formally test hypotheses about their formation and evolution.

1-4 RESEARCH OBJECTIVES AND APPROACH

The review of research presented in the preceding discussion demonstrates that some progress has been made in describing TARs, but also shows that considerable work remains in terms of developing and testing hypotheses about their formation and evolution. The significant research gaps/problems in TARs studies can be described as (i) the lack of a suitable terrestrial analog, (ii) lack of any automated or semi-automatic methodology for mapping these small linear-trending bedforms, and (iii) a restricted quantitative understanding of TARs' morphometry regarding the lack of a sufficient sample size on Mars and absence of study to compare TARs to terrestrial analogs by remote sensing. In the current thesis we are trying to address these problems.

As stated, the goal of this thesis research is to improve our understanding about Martian TARs and evaluate the viability of a new terrestrial analog as well as a new mapping technique. These shortcomings will be addressed through the following objectives:

a. To introduce and investigate a viable terrestrial analog of TARs.

b. To test and advance the quantitative description of TARs by using a new methodology of mapping on Earth and Mars based on an Artificial Neural Network (ANN) algorithm.

c. To compare TARs and TAR-like features on both planets with a sufficient sample size from remote sensing for the first time.

Figure 1.6 indicates the flowchart of different steps of this thesis.

This is a manuscript-based thesis, written according to the Faculty of Graduate Studies, University of Calgary Thesis/Dissertation Guidelines. I was the primary person finding the research gaps and questions, designing the research, extracting the data, inventing the methodology, undertaking the analysis, creating the maps and graphical results, and writing the manuscripts. The first paper from this thesis entitled "Mega-ripples in Iran: A new analog for transverse aeolian ridges on Mars" has been published in the ICARUS journal. Dr. James R. Zimbelman, co-author of this paper and my co-supervisor, supervised the whole research, gave suggestions, comments and reviews that tremendously improved the manuscript. Two other manuscripts entitled "Semi-automatic mapping of linear-trending bedforms using 'self-organizing maps' algorithm" and "TARs on Earth and MARS" are currently under review in the Geomorphology and ICARUS journals, respectively. I am confident that this study will mark an important milestone for better understanding of TARs and aeolian processes on Mars.

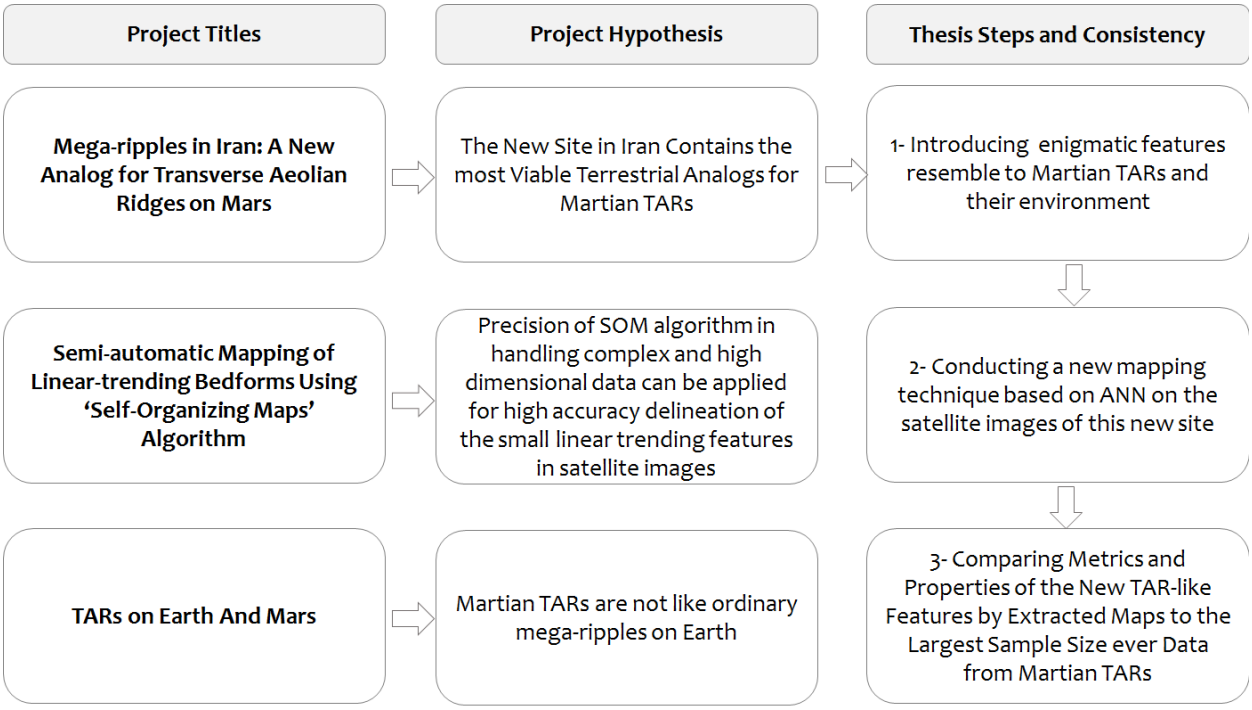

Figure 1.6. The flowchart indicates different projects of this thesis, their hypothesis and consistency.

1-5- REFERENCES

Almeida, M.P., Parteli, E.J.R., Andrade, J.S., Herrmann, H.J., 2008. Giant saltation on Mars. Proceedings of the National Academy of Sciences. 105(17), 6222-6226.

Bagnold, R.A., 1941. The Physics of Blown Sand and Desert Dunes. Chapman and Hall, London.

Balme, M., Berman, D.C., Bourke, M.C., Zimbelman, J.R., 2008. Transverse Aeolian Ridges (TARs) on Mars. Geomorphology. 101(4), 703-720.

Barlow, N., 2008. Mars: An introduction to its interior, surface and atmosphere. Cambridge University Press.

Berman, D.C., Balme, M.R., Rafkin, S.C.R., Zimbelman, J.R., 2011.Transverse Aeolian Ridges (TARs) on Mars II: distributions, orientations, and ages. Icarus. 213(1), 116-130.

Bourke, M.C., Williams, S.H., Zimbelman, J.R., 2003. The variability of TARs in troughs on Mars. LPSC XXXIV [CDROM].

Bourke, M.C., Goudie, A.S., 2009. Varieties of barchans form in the Namib Desert and on Mars. Aeolian Research. 1(1-2), 45-54.

Bourke, M.C., Lancaster, N., Fenton, L.K., Parteli, E.J., Zimbelman, J.R., Radebaugh, J., 2010. Extraterrestrial dunes: An introduction to the special issue on planetary dune systems. Geomorphology. 121(1), 1-14.

Bridges, N.T., Ayoub, F., Avouac, J., Leprince, S., Lucas, A., Mattson, S., 2012a. Earth-like sand fluxes on Mars. Nature. 485, 339-342.

Bridges, N.T., Bourke, M.C., Geissler, P.E., Banks, M.E., Colon, C., Diniega, S., Golombek, M.P., Hansen, C.J., Mattson, S., McEwen, A.S., Mellon, M.T., Stantzos, N., Thomson, B.J., 2012b. Planet-wide sand motion on Mars. Geology. 40, 31-34.

Bridges, N.T., Geissler, P.E., Silvestro, S., Banks, M.E., 2013. Bedform migration on Mars: Current results and future plans. Aeolian Research. 9, 133-151.

Bridges, N. T., Spagnuolo, M. G., de Silva, S. L., Zimbelman, J. R., Neely, E.M., 2015. Formation of gravel-mantled megaripples on Earth and Mars: Insights from the Argentinean Puna and wind tunnel experiments. Aeolian Research. 17, 49-60.

Cardinale, M., Silvestro, S., Vaz, D. A., Michaels, T., Bourke, M. C., Komatsu, G., & Marinangeli, L., 2016. Present-day aeolian activity in Herschel Crater, Mars. Icarus, 265, 139-148.

Carr, M.H., 2006. The surface of Mars. Cambridge University Press.

Chapman, M.G., 2007. The Geology of Mars: Evidence from Earth-based analogs. Cambridge University Press, Cambridge.

Chojnacki, M., Burr, D.M., Moersch, J.E., Michaels, T.I., 2011. Orbital observations of contemporary dune activity in Endeavour Crater, Meridiani Planum, Mars. Journal of Geophysical Research. 116(E7), E00F19.

Church, M., 2010. The trajectory of geomorphology Progress in Physical Geography. Progress in Physical Geography. 34, 265-286.

Claudin, P., Andreotti, B., 2006. A scaling law for aeolian dunes on Mars, Venus, Earth, and for subaqueous ripples. Earth and Planetary Science Letters. 252, 30-44.

Craddock, R.A., 2011. Aeolian processes on the terrestrial planets: Recent observations and future focus. Progress in Physical Geography. 36(1), 110-124.

de Silva, S.L., Bailey, J.E., Mandt, K.E., Viramonte, J.M., 2010. Yardangs in terrestrial ignimbrites: Synergistic remote and field observations on Earth with applications to Mars. Planetary and Space Science. 58(4), 459-471.

de Silva, S.L., Spagnuolo, M.G., Bridges, N.T., Zimbelman, J.R., 2013. Gravel-mantled megaripples of the Argentinean Puna: A model for their origin and growth with implications for Mars. Geological Society of America Bulletin. 125(11-12), 1912-1929.

Edgett, K.S., Malin, M.C., 2000. New views of Mars aeolian activity, materials, and surface properties: Three vignettes from the Mars Global Surveyor Mars Orbiter Camera. Journal of Geophysical Research. 105, 1623-1650.

Ewing, R.C., Kocurek, G., Lake, L.W., 2006. Pattern analysis of dune-field parameters. Earth Surface Processes and Landforms. 31(9), 1176-1191.

Ewing, R.C., Hayes, A.G., Lucas, A., 2015. Sand dune patterns on Titan controlled by long-term climate cycles. Nature Geoscience. 8(1), 15-19.

Fenton, L.K., Michaels, T.I., Chojnacki, M., Beyer, R.A., 2014. Inverse maximum gross bedform-normal transport 2: Application to a dune field in Ganges Chasma, Mars and comparison with HiRISE repeat imagery and MRAMS. Icarus. 230, 47-63.

Fenton, L.K., Michaels, T.I., Chojnacki, M., 2015. Late Amazonian aeolian features, gradation, wind regimes, and Sediment State in the Vicinity of the Mars Exploration Rover Opportunity, Meridiani Planum, Mars. Aeolian Research. 16, 75-99.

Foroutan, M., 2015. Ripple-like features on mars, characteristics and classification. 2015 GSA Fall Meeting. Geological Society of America.

Geissler, P. E., 2014. The birth and death of transverse aeolian ridges on Mars. Journal of Geophysical Research: Planets, 119(12), 2583-2599.

Greeley, R., Iverson, J.D., 1985. Wind as geological process on Earth, Mars, Venus and Titan. Cambridge University Press, Great Britain, Oxford.

Greeley, R., Kraft, M.D., Kuzmin, R.O., Bridges, N.T., 2000. Mars Pathfinder landing site: Evidence for a change in wind regime from lander and orbiter data. Journal of Geophysical Research: Planets (1991-2012). 105(E1), 1829-1840.

Greeley, R., 2013. Introduction to Planetary Geomorphology. Cambridge University Press.

Hansen, C.J., Bourke, M.C., Bridges, N.T., Byrne, C., Colon, C., Diniega, S., Dundas, C., Herkenhoff, K., McEwen, A.S., Mellon, M.T., Portyankina, G., Thomas, N., 2011. Seasonal erosion and restoration of Mars northern. Science. 331(6017), 575-578.

Hargitai, H., & Kereszturi, Á. (Eds.)., 2015. Encyclopedia of Planetary Landforms. Springer.

Kerber, L., Head, J.W., 2012. A progression of induration in Medusae Fossae Formation transverse aeolian ridges: evidence for ancient aeolian bedforms and extensive reworking. Earth Surface Processes and Landforms. 37, 422-433.

Kocurek, G., Ewing, R.C., 2005. Aeolian dune field self -organization – Implications for the formation of simple versus complex dune field patterns. Geomorphology. 72(1-4), 94-105.

Kocurek, G., Ewing, R.C., Mohrig, D., 2010. How do bedform patterns arise? New views on the role of bedform interactions within a set of boundary conditions. Earth Surface Processes and Landforms. 35(1), 51-63.

Kok, J.F., Parteli, E.J., Michaels, T.I. and Karam, D.B., 2012. The physics of wind-blown sand and dust. Reports on Progress in Physics, 75(10), p.106901.

Lorenz, R.D., Zimbelman, J.R., 2014. "Dune Worlds": How Windblown Sand Shapes Planetary Landscapes. Springer, Washangton, USA.

Malin, M.C., Edgett, K.S., 2001. Mars Global Surveyor Mars Orbiter Camera: Interplanetary cruise through primary mission. Journal of Geophysical Research. 106, 23429-23570.

Marchant, D.R., Head III, J.W., 2007. Antarctic dry valleys: Microclimate zonation, variable geomorphic processes, and implications for assessing climate change on Mars. Icarus. 192(1), 187-222.

Nickling, W. G., & Neuman, C. M., 2009. Aeolian sediment transport. In Geomorphology of desert environments (pp. 517-555). Springer Netherlands.

Parteli, E.J.R., Almeida, M.P., Durán, O., Andrade Jr., J.S., Herrmann, H.J., 2009. Sand transport on Mars. Computer Physics Communications. 180, 609-611.

Radebaugh, J., Lorenz, R.D., Farr, T., Paillou, P., Savage, C., Spencer, C., 2010. Linear dunes on Titan and earth: initial remote sensing comparisons. Geomorphology. 121(1-2), 122-132.

Rossi, A.P., Marinangeli, L., 2004. The first terrestrial analogue to Martian dust devil tracks found in Ténéré Desert, Niger. Geophysical research letters, 31(6). Geophysical Research Letters. 31(6), L06702.

Savage, C.J., Radebaugh, J., Christiansen, E.H., Lorenz, R.D., 2014. Implications of dune pattern analysis for Titan's surface history. Icarus. 230, 180-190.

Sefton-Nash, E., Teanby, N.A., Newman, C., Clancy, R.A., Richardson, M.I., 2014. Constraints on Mars' recent equatorial wind regimes from layered deposits and comparison with general circulation model results. Icarus. 230, 81-95.

Shockey, K.M., Zimbelman, J.R., 2013. Analysis of transverse aeolian ridge profiles derived from HiRISE images of Mars. Earth Surface Processes and Landforms. 38(2), 179-182.

Silvestro, S., Fenton, L.K., Vaz, D.A., Bridges, N.T., Ori, G.G., 2010. Ripple migration and dune activity on Mars: Evidence for dynamic wind processes. Geophysical Research Letters. 37(20), L20203.

Silvestro, S., Vaz, D.A., Fenton, L.K., Geissler, P.E., 2011. Active aeolian processes on Mars: A regional study in Arabia and Meridiani Terrae. Geophysical Research Letters. 38(20), L20201.

Silvestro, S., Fenton, L.K., Michaels, T.I., Valdez, A., Ori, G.G., 2012. Interpretation of the complex dune morphology on Mars: dune activity, modelling and a terrestrial analogue. Earth Surface Processes and Landforms. 37(13), 1424-1436.

Silvestro, S., Vaz, D. A., Di Achille, G., Popa, I. C., & Esposito, F., 2015. Evidence for different episodes of aeolian construction and a new type of wind streak in the 2016 ExoMars landing ellipse in Meridiani Planum, Mars. Journal of Geophysical Research: Planets, 120(4), 760-774.

Smalley, I.J., Krinsley, D.H., 1979. Eolian sedimentation on Earth and Mars: some comparisons. Icarus. 40(2), 276-288.

Sullivan, R., Banfield, D., Bell III, J.F., Calvin, W., Fike, D., Golombek, M., Greeley, R., Grotzinger, J., 2005. Aeolian processes at the Mars Exploration rover Meridiani Planum landing site. Nature. 436, 58-61.

Szynkiewicz, A., Ewing, R.C., Moore, C.H., Glamoclija, M., Bustos, D., Pratt, L.M., 2010. Origin of terrestrial gypsum dunes implications for Martian gypsum-rich dunes of Olympia Undae. Geomorphology. 121(1), 69-83.

Thomas, P.C., Malin, M.C., Carr, M.H., Danielson, G.E., Davies, M.E., Hartmann, W.K., Ingersoll, A.P., James, P.B., McEwen, A.S., Soderblom, L.A., Veverka, J., 1999. Bright dunes on Mars. Nature. 397, 592-594.

Thomas, M., Clarke, J.D., Pain, C.F., 2005. Weathering, erosion and landscape processes on Mars identified from recent rover imagery, and possible Earth analogues. Australian Journal of Earth Sciences. 52(3), 365-378.

Ward, A.W., 1979. Yardangs on Mars: Evidence of recent wind erosion. Journal of Geophysical Research: Solid Earth. 84(B14), 8147-8166.

Wilson, S.A., Zimbelman, J.R., 2004. Latitude-dependent nature and physical characteristics of transverse aeolian ridges on Mars. Journal of Geophysical Research. 109, (E10003).

Yizhaq, H., Kok, J.F., Katra, I., 2014. Basaltic sand ripples at Eagle Crater as indirect evidence for the hysteresis effect in Martian saltation. Icarus. 230, 143-150.

Yizhaq, H., Katra, I., 2015. Longevity of aeolian megaripples. Earth and Planetary Science Letters 422, 28-32. doi: 10.1016/j.epsl.2015.04.004.

Zimbelman, J.R., 1987. Spatial resolution and the geologic interpretation of Martian morphology: Implications for subsurface volatiles. Icarus. 71, 257-267.

Zimbelman, J.R., Irwin III, R.P., Williams, S.H., Bunch, F., Valdez, A., Stevens, S., 2009. The rate of granule ripple movement on Earth and Mars. Icarus. 203(1), 71-76.

Zimbelman, J.R., 2010. Transverse Aeolian Ridges on Mars: First results from HiRISE images. Geomorphology. 121, 22-29.

Zimbelman, J.R., Scheidt, S.P., 2014. Precision topography of a reversing sand dune at Bruneau Dunes, Idaho, as an analog for Transverse Aeolian Ridges on Mars. Icarus. 230, 29-37.

MEGA-RIPPLES IN IRAN: A NEW ANALOG FOR TRANSVERSE AEOLIAN RIDGES ON MARS

Journal: ICARUS

Authors: Marzieh Foroutan, James R. Zimbelman

Manuscript Status: Published (April 2016)

CHAPTER 2

MEGA-RIPPLES IN IRAN: A NEW ANALOG FOR TRANSVERSE AEOLIAN RIDGES ON MARS

ABSRTACT

A new terrestrial analog site for Transverse Aeolian Ridges (TARs) is described in this study. The Lut desert of Iran hosts large ripple-like aeolian bedforms, with the same horizontal length-scales and patterns of TARs on Mars. Different classes of TARs and different types of other aeolian features such as sand dunes, zibars, dust devil tracks and yardangs can be found in this area, which signify an active aeolian region. This area represents a unique site to study the formation and evolution of these enigmatic features, with potential relevance toward a better understanding of TARs on Mars.

2-1 INTRODUCTION

Transverse Aeolian Ridges (TARs) are small-scaled distinct morphological features with narrow transverse dimensions found mostly throughout the equatorial and mid-latitude regions of Mars. TARs can occur singularly or in groups that number in the thousands; they are abundant but not ubiquitous on Mars (Balme et al., 2008; Berman et al., 2011). The term "ridges" was first used by Bourke et al. (2003) because of their unknown origin. They could have formed either as small sand dunes or large ripples. Although they are found in variable ridge planforms and patterns (Bourke et al., 2003), it was revealed by Kerber and Head (2012) that types of TARs can sometimes grade into each other depending on the regional topography and wind regime. However, one of the most common and distinctive characteristics of TARs are their symmetric profiles (Zimbelman, 2010) and typical triangular cross-sectional shape (Kerber and Head, 2012).

The process responsible for forming TARs occurs over a wide range of elevations and geological formations on Mars (Bourke et al., 2003; Wilson and Zimbelman, 2004), but based on their proximity to layered terrain and steep slopes, Berman et al. (2011) argued that they formed from locally derived sediments. On the other hand, Geissler (2014) hypothesised TARs to be dust deposit features with examples in Syria Planum. TARs are currently inactive, which is demonstrated by superposition of slope streaks, large dark dune materials and occasional impact craters on TARs (Balme et al., 2008; Berman et al., 2015). Their distribution must be a result of both climate and wind regime, but information is still limited about their composition, origin, formation mechanisms, processes that control their distribution and activity, sediment source, age, and superposition relationships.

2-2 TERRESTRIAL ANALOG STUDIES

In planetary geology, a field site which possess a similarity in any aspect (physical, chemical, morphological) to other planetary bodies of the solar system is called a terrestrial analog. If the site is on Earth this can serve field facilities and can be used as references. Their particular attributes that resemble extraterrestrial features can be studied for understanding the origin and evolution of planetary features, which is a common approach in planetary geology and geomorphology (El-Baz et al., 1979; Gómez, 2011). Terrestrial analogs of TARs and their characteristics have been studied in order to investigate similar features in detail and develop hypotheses about their formation. TARs on Mars cannot be definitively classified as either ripples or dunes (Wilson and Zimbelman, 2004). Fryberger (1979) suggested that granule mega-ripples on Earth may develop in wind environments which display the least directional variability, but the general view remains that TARs appear to be unique to Mars (Fenton et al., 2015). Terrestrial analogs for TARs have been described by de Silva et al. (2013) in Argentinean Puna, where gravel-mantled mega-ripples are contextually and morphologically similar to small ripple-like TARs on Mars, which are quite unique mega-ripples on Earth (Figure 2.1-A). Another analog investigated by Zimbelman and Scheidt (2014) was a large reversing sand dune at Bruneau Dunes, Idaho, where precise profile measurements demonstrated that large TARs may be quite similar to either transitional or mature reversing sand dunes (Figure 2.1-B). The Bruneau Dunes are much larger than most TARs, and the Puna mega-ripples involve both pumice and lithics as gravel-sized surface coverings, so it is unclear at present how strong is the analogy of both locations to actual TARs on Mars. This work describes a new TAR analog site in the Lut desert of Iran (Figure 2.2) where aeolian bedforms have crest symmetry, crest sharpness, and horizontal length-scale that are very comparable to the most common TARs on Mars (Figure 2.3).

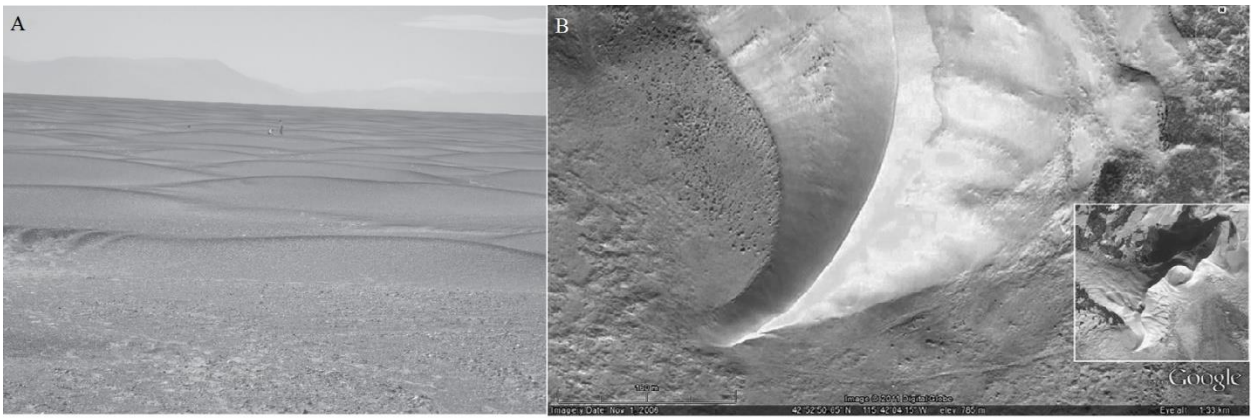

Figure 2.1. Terrestrial analogs of TARs: A) Gravel bedforms in the Campo Piedra Pomez. Located in the Puna Argentina, with heights of about one meter and wavelengths between 10 and 15 m (from de Silva et al., 2013). B) Bruneau Dunes, in central Idaho, U.S.; the Google Earth image shows the southern end of one large reversing dune, where precise topographic profiles were obtained, with an Inset showing all of the largest dunes, along with the lakes at the northern end of the dunes (from Zimbelman and Scheidt, 2014).

2-3 STUDY AREA

The new TAR terrestrial analog site is located in the hyper-arid Lut Desert (Dasht-e Lut) in southeast Iran, within an area of about 80,000 km^2 that is located between 29° 30' N to 30° 49' N latitude and 57° 47' E to 59° 53' E longitude (Figure 2.2). The Lut Desert contains many different kinds of aeolian landforms. However, the two most remarkable features in the Lut Desert are the deposition site at the eastern side of the basin, which is a low plateau covered with salt flats and containing some of the world's tallest sand dunes reaching heights of 300 m (Walker, 1986) and also the wind abrasion in the western part of the desert that has produced huge mega-yardangs up to 80 m tall and 120 km long in a NW-SE direction. The mega-yardangs developed in Pleistocene basin fill deposits (silty clays, gypsiferous sands) with an estimated thickness of 135–200 m (Gabriel, 1938).

In addition, this desert is located between two active strike-slip systems which contain several parallel fault strands on either side of the Lut desert; Gowk-Nayband and Sistan Suture Zone fault systems that are along the western and eastern margins of the Lut desert, respectively (Alen et al., 2004). The Lut desert depression contains several hundred meters of upper Pliocene to Pleistocene lacustrine silts over a basement of flat-lying Paleogene andesitic lavas and tuffs (Ehsani and Quiel, 2008). Several Quaternary basalt flows occur near the Nayband fault on the western edge of the Lut desert, and

further to the west, the anticlinal ridges of the Shahdad thrust belt are formed out of up to 3000 m of stratified marls containing gypsum, sandstone and conglomerates (Ehsani and Quiel, 2008).

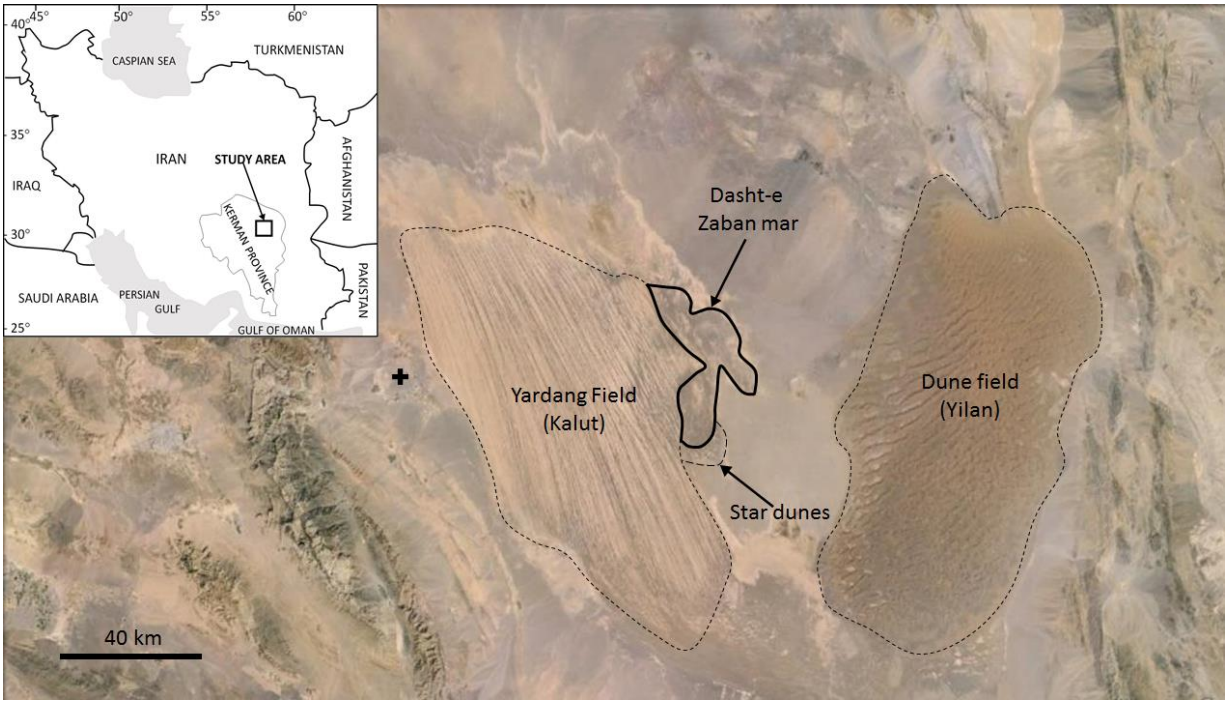

Figure 2.2. Google Earth image of the Lut Desert in Iran. An irregularly shaped region shows the location of the area with TAR-like features (Dasht-e Zaban mar). The site of mega-yardangs (elongate NNW-SSE), star-dunes and the Yilan erg are also shown. The cross mark is the location of the Ziyaratgah-e Deh Seif weather station in Shahdad village. Inset map shows regional context of the field area.

It has been demonstrated by Zambito and Benison (2013) that the Lut desert's playa, at the center part, is the best modern analog for the lower Nippewalla Group, which is an indication of hyperarid conditions more extreme than anywhere today. Moderate Resolution Imaging Spectro-radiometer (MODIS) Climate Model Grid (CMG) shows that the Lut Desert was the hottest area on Earth in the years 2004 to 2009 with a temperature up to 70°C (Mildrexler et al., 2011). Annual rainfall in this desert is less than 10 mm according to the weather station data. Based on wind records during the 1970–2013 period from the closest weather station (*Ziyaratgah-e Deh Seyf*) to the northwest of the study area (cross in Figure 2.2), the mean annual wind speed is 6 m/s. Strong winds in this area occur in April, with an average speed of 9.35 m/s. However, these reported weather records, such as high temperatures, need further precise investigation.

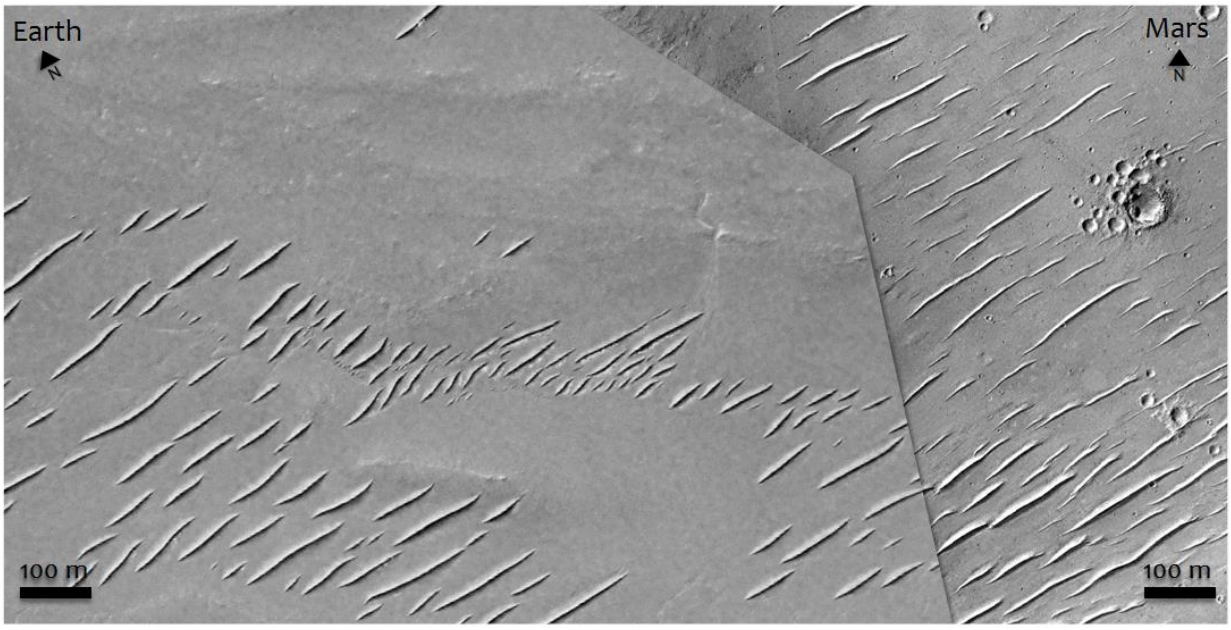

Figure 2.3. The morphological similarity of TARs on Mars (right) to the Lut Desert on Earth (left) is apparent when viewed at the same scale. Right, HiRISE (High Resolution Imaging Science Experiment) frame number ESP_037195_1625. left, WorldView-1 satellite image (50 cm/pixel) view of TAR-like features in the Lut desert of Iran.

2-4 DESCRIPTION OF TERRESTRIAL ANALOG OF TARS IN THE LUT DESERT

TAR-like features in the Lut Desert are located between two distinctive erosional and depositional sites, the mega-yardang region and a huge erg, respectively. The local name for this area is *Dashte-e Zaban mar*; it represents a pristine region that is quite difficult to access (Figure 2.2). TAR-like features are present here in many different shapes and wavelengths within an area covering about 250 km^2 (Figure 2.4). Terrestrial analogs of TARs that have been found in the Lut Desert are located in a lowland area ~200 m above sea level. They sit on Quaternary alluvial fan deposits surrounded by Dasht deposits (sand, silt, clay and conglomerate) and fine-grained lake deposits (Lut formation). Many forms and patterns that have been described in the literature for TARs on Mars (e.g., Balme et al., 2008; Bourke et al., 2003) can be found in the Lut Desert (Figure 2.4 & 2.5).

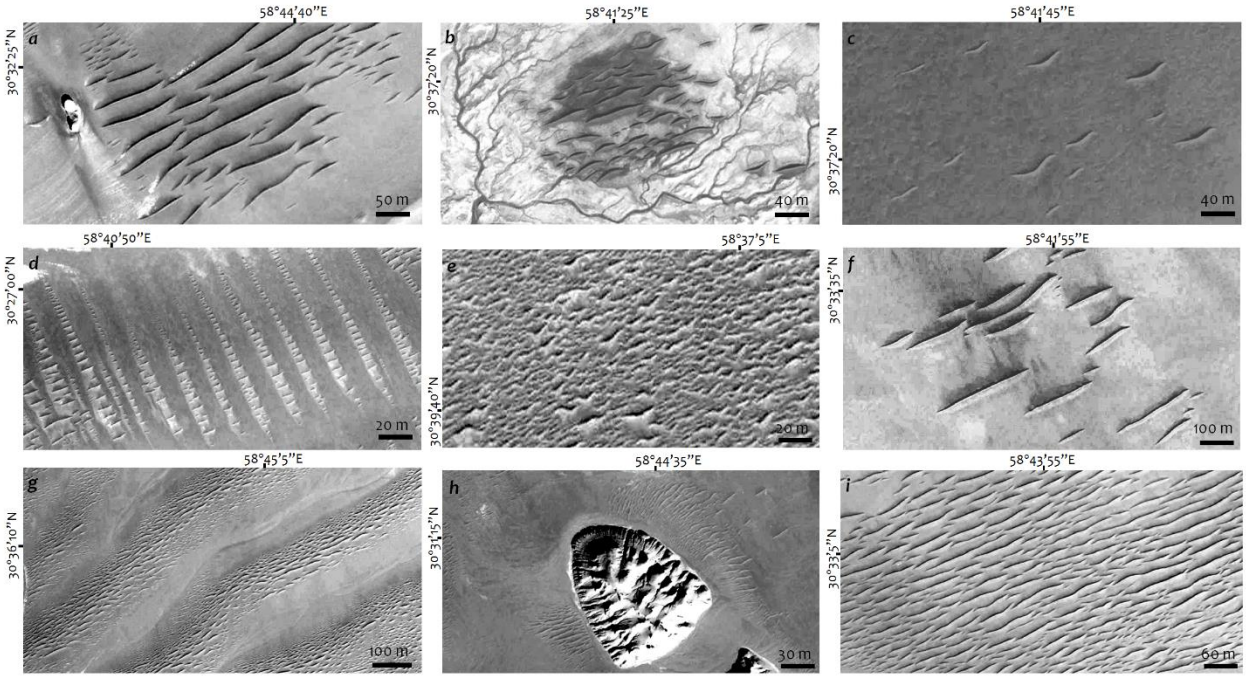

Figure 2.4. Examples of some of the different forms of TAR-like features in the Lut Desert. a) the largest TARs in the area are up to more than 3 meters in height; b) similar to influenced TARs, in the northern part of the study area; c) widely spaced TARs; d) 'raked' pattern of TAR-like features; e) analogs for barchan-like TARs; f) moderately spaced TAR-like features; g) sinuous TAR-like features, perhaps formed on transverse aeolian depositional features (e.g., zibars); h) similar to controlled TARs, and i) closely spaced TAR-like features.

Evaluation of the study area shows other interesting aeolian landforms near the TARs. There are star dunes southeast of the TARs area (Figure 2.2) and also barchan dunes nearby, which are superimposed onto the TAR-like features, the same stratigraphy that has been documented on Mars (Figure 2.6), and suggested a strong correlation between these two bedforms (Balme et al., 2015). Zibars are also present in the region, including in between TAR patches and perhaps beneath some TARs (Figure 2.4g). In some locations, the sediment grains are too coarse to form dunes with slip faces so they have accumulated into low relief zibars. In general, zibars are assumed to be oriented transverse to the prevailing wind and their wavelength in the study area is about 50 meters. Other aeolian landforms in this area have surface markings known in the literature as 'Dust Devil Tracks' (DDTs), which are surface tracks left by low pressure vortices formed from unstable, near-surface warm air generated by insolation; DDTs can be visible due to the entrainment or removal of dust (and possibly sand) along the path followed by dust devils. The occurrence of aeolian bedforms like sand dunes, zibars and DDTs

in the Lut desert indicate that a variety of different grain size particles are present throughout this area.

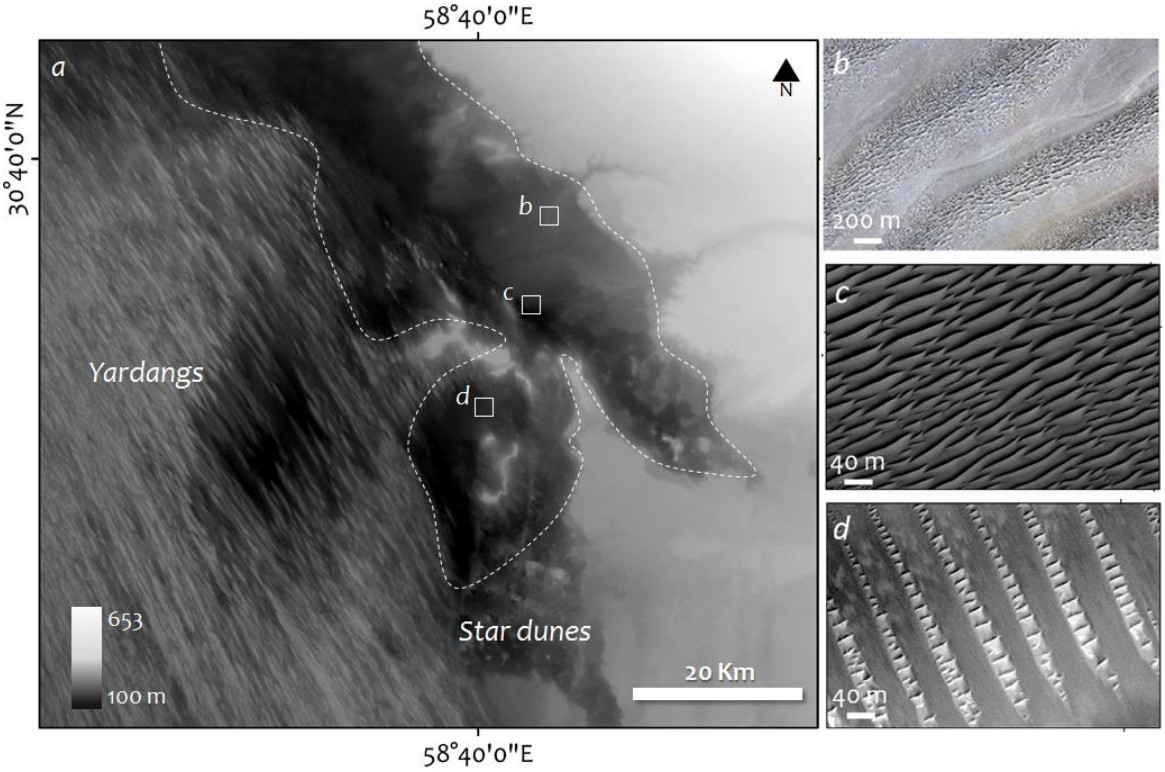

Figure 2.5. a) SRTM DEM (90 m resolution, UTM projection, WGS84 datum) of the study area showing the outline of the most concentrated region of TAR-like features; data obtained from http://srtm.csi.cgiar.org. Dashed line shows the area with highest concentration of TAR-like bedforms. Examples (locations outlined in SRTM image) of different TAR patterns seen in Google Earth images in parts b, and WorldView-1 satellite image in c and d.

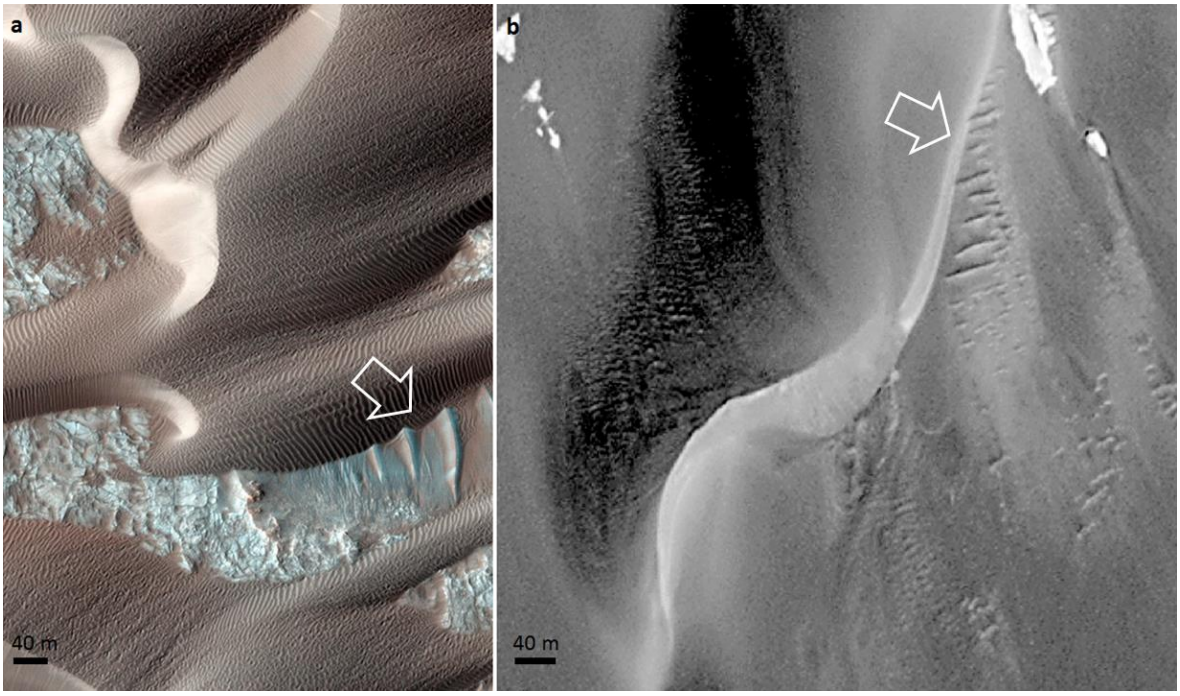

Figure 2.6. Barchan dunes superposed on TARs in Nili Patera, Mars (HiRISE ESP_018039_1890) and b) the same stratigraphic situation for barchan sand dunes and TAR-like features in the Lut desert (WorldView-1 satellite image).

The TAR-like bedforms are more concentrated in the central, eastern and northwestern portions of the study region (Dashte-e zaban mar). They exist as either isolated patches or larger collections of features and rarely as singular bedforms off by themselves as in the southern portion of the area. The widely spaced TAR-like features are found far removed from both the mega-yardangs and the sand erg. Features at the north part of the area are similar to barchan-like TARs (Figure 2.4-e). However, some patterns in the Lut desert are quite rare and enigmatic (Figure 2.5d). In the central and western portions of the region, close to small, highly eroded yardangs is a unique occurrence of an evenly 'raked'-appearing pattern of TAR-like features; these south-east-oriented features consist of small equally spaced bedforms (Figure 2.4-d). The 'raked' landforms are TAR-like features in parallel groups (i.e., of about 10 to 30 features) throughout the area; the TAR-like features have sharp boundaries and an overall 'spindle' shape. The 'raked' pattern could be evidence of either two successive aeolian formation episodes or of a special type of topographically influenced pattern.

Shuttle Radar Topography Mission Digitial Elevation Model (SRTM DEM) data of the study area (Figure 2.5) indicate that there is hardly any significant topographic relief within the study area. Consequently, there is no obvious regional-scale bedrock or topographic control on the distribution and morphology of the TAR-like features within the Lut Desert. Instead, it appears that their formation is controlled

only by aeolian mechanisms or processes. TAR-like features appear to be overlying alluvial deposits (such as alluvial fans) within the basin. SRTM DEM data show that the study area is located in a low-lying region with fluvial features (such as channels) bringing sediments into the region. This depression contains a veneer of aeolian sediment over most of the surface, but the majority of the sediment underneath the aeolian materials is probably alluvial fan deposits and other alluvium. In the northern part of the study area, which has a higher elevation than its surroundings, patches of TAR-like features are present that may have been created directly from the locally derived bedrock materials.

Based on the topographic control classification of Balme et al. (2008), the western portion of the study area consists of "influenced" patches of TAR-like deposits present both along and in between small yardangs. Some "confined" and "controlled" TAR deposits are found in the middle of the northern part of the study area, located in local depressions, but the majority of the TAR-like features fall within the "independent" class of topography-affected classification of Balme et al. (2008). In the southern part of the study region, deposited particles may become gradually smaller because the TAR-like bedforms slowly disappear as some different dune shapes become recognizable. According to the classification scheme of Balme et al. (2008) based on crestline morphology, most of the TARs in the study area have a simple morphology. Sinuous and barchan-like TARs tend to appear more often at the margins of the study area while forked types are very rare throughout the entire region and barchan-like ones are only observed at the north portion.

The bedforms' crest orientation is normal to the NE-SW trend of the yardangs. TAR-like landforms that do not share this dominant orientation are small, singular features or are strongly topographically dependent, which implies that the atypical bedforms were not formed by the regional wind regime. It is possible that the dominant wind direction is not unidirectional from NW to SE at this location, or perhaps the area is subject to a seasonal bimodal wind regime with strong wind directions separated by about 180°, as is the case for the reversing sand dunes at Bruneau Dunes in Idaho (Zimbelman and Scheidt, 2014). Comparison of winds in the Lut desert and Martian TAR regions require detailed calculations that take into account atmospheric pressure, gravity, and also temperature (White, 1979). In terms of bedform generation, the wind on Mars will need to blow many times faster than an 'equivalent' wind on Earth. However, the size of the feature may be more sensitive to the specific transport process involved (saltation, impact creep and suspension) than to either gravity or atmospheric pressure alone. It has been suggested by de Silva et al. (2013) that probably features on Mars took longer to form.

2-5 METHODOLOGY

Height is still one of the most important parameters of TARs. Rovers are unable to get close to the large aeolian depositional features and special conditions needed from orbital data for extracting height accurately. In this study, primary remote sensing analysis and photoclinometric measurements of the basic morphometric characteristics of the Lut Desert's TAR-like features, particularly their height, were extracted by using shadow length and in the ArcGIS environment. Our main data for these measurements are WorldView-1 satellite images with about 0.5 m/pixel resolution. We measured metrics of tens of TAR-like features and we tried to have our measurements from different locations in the area. Also, we used some field and ground photos acquired during 2011 to 2014 for visual evaluation and interpretation about their size and sediment size.

2-6 RESULTS AND DISCUSSION

Results show that they are not any taller than 4 m, and the majority are between 0.3 and 2 meters in height, comparable to the heights of the gravel-coated mega-ripples in the Puna (de Silva et al., 2013). The TAR features range in width and length from 1 to 30 and 7 to 300 meters, respectively. Wider and longer landforms are located mainly in the central part of the study area where there is less surface roughness, which means that they can be found directly on the bedrock. Barchan-like TARs are crescent-shaped, like their namesake dunes, but the crescentic TARs are far shorter than most barchan dunes. The majority of TARs, with more than 200 meters in crest length, occur on the central (flat) planar area.

Bagnold (1941) showed that on hard desert surfaces such as gravel fans (similar to the situation in the Lut Desert), sand grains bounce much higher and farther than on loose sand, so coarse-grained aeolian bedforms may be expected where both sand and coarse materials are abundant. Visual evaluation of available ground photos from the Lut Desert (Figure 2.7) reveal that the surface sediment is in fact coarse (i.e., much coarser than medium sand), although from these limited examples we cannot define specifically what the median grain size would be across the whole study area. Previous studies suggest that the surface particle size on Martian TARs is mostly in the coarse sand to gravel size range such as coarse grained ripples (e.g. Zimbelman, 2010). In some regions in the Lut Desert, cobble-sized alluvium or salt deposits between TAR-like features are recognizable from ground photos.

The location of the study area is in the middle of a large remote desert with harsh climate conditions, such as high temperatures and frequent sand storms, along with other non-geological dangers, which make in situ research almost infeasible. However, Figure 2.7 shows the approximate overall size,

symmetry, and lack of sinuosity for at least some TAR-like features in the Lut Desert, including a vertical view of the sediments on the surface of these features. Based on recent measurements of TARs on Mars (Balme et al., 2015), the size and shape of the features in the Lut desert are quite consistent with the previous suggestion that the differences of atmospheric density and gravity between Earth and Mars do not greatly alter the shape of aeolian features observed on both planets (Discussion section of Zimbelman et al, 2012), although the increased sand grain trajectories on Mars (relative to those on Earth) might lead to a larger overall size of an aeolian feature on Mars (Greeley and Iversen, 1985, pp. 94-98). Still, the similar overall size of the Lut features to at least some TARs on Mars suggests that the basic processes of either creep-induced coarse particle coatings or intense aeolian erosion of fine materials does not in itself seem to require that the Martian landforms be substantially bigger than their terrestrial counterparts.

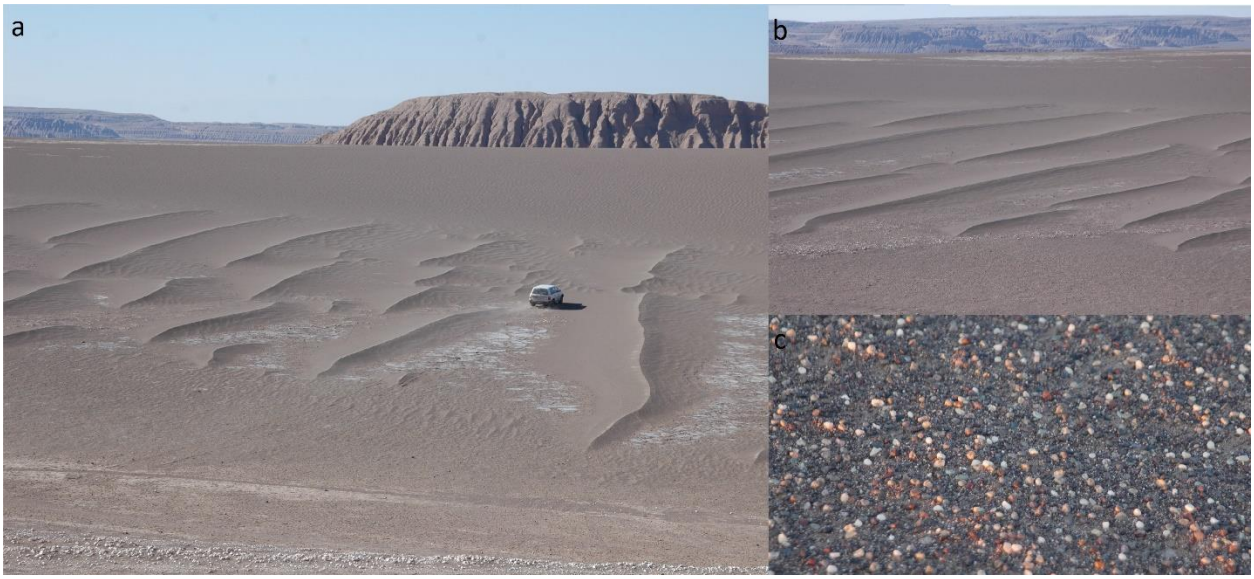

Figure 2.7. Pictures of TAR-like features from the study area in the Lut Desert: a) the approximate height of the features is evident in comparison to the vehicle nearby, suggesting a height of <1 m for the TAR features in this area (image: Mehrdad Ghazvinian, 2014); b) spectacular view of straight TAR-like features with no sinuosity (image: Mehrdad Ghazvinian, 2011); c) vertical photo from near the TAR-like features, with sediments of approximately 3-4 mm in diameter (image: Mehrdad Ghazvinian, 2014).

Based on field observations, grain sizes of these features are described to be about pea-sized (Figure 2.7c). Another observation regarding grain size is related to the existence of dark DDTs in the study area. Reiss et al. (2010) stated that dark DDTs might be formed on Earth and Mars only in regions where relatively fine-grained material is removed by the passage of dust devils, exposing coarser grain sizes not easily moved by the dust devils. The albedo difference caused by photometric changes due to the

geometric properties of the particle sizes might be visible only if the grain size differences are sufficiently large, indicating that DDTs were identified only in areas where coarse sand material is overlain by dust. This effect may be responsible for the rarity of DDT observations on Earth. Zibars, believed to form by the winnowing of smaller grains of sand from coarser materials, exist in the Lut Desert. Consequently, zibars are indicators of relatively coarse and poorly sorted sand, perhaps including both coarse sands and fine pebbles. All these observations highlight the variety of different grain sizes expected to be present within the study area.

In addition, the extraordinary temperature of this site leads to large temperature differences between day and night, which is the same as Martian global condition due to low atmospheric density and consequently, low heat retention. Furthermore, existence of unique hyperarid environmental indicators such as the modern analog for the lower Nippewalla Group, a rich array of aeolian landforms and its unusual untouched environment may emphasize the most evident similarity to Mars as compared to other analog sites.

2-7 CONCLUSION

A new site for terrestrial analogs of TARs is located in the middle of the Lut Desert in Iran between a field of mega-yardangs and a large sand erg. The TAR-like features at this location come in a variety of different populations and patterns within an area that covers about 250 km^2. Aeolian bedforms in this area have the same horizontal length-scale as TARs on Mars. The majority of TAR-like features occur on Quaternary sand sheet and alluvial fan deposits which are surrounded by salt-rich terrains. The features are located in a lowland that is less than 200 meters above sea level and they are also found in corridors between nearby yardangs. Based on superposition evidence, the TAR-like features in this area seem to be old relative to their neighboring aeolian and fluvial features, consistent with the current lack of any documented movement for TARs on Mars (Bridges et al., 2013). More studies need to be done to get information about the formation processes of these impressive features in the Lut Desert.

ACKNOWLEDGEMENT

The manuscript benefited greatly from the thoughtful review comments provided by Dan Berman and Paul Geissler.

2-8 REFERENCES

Allen, M., Jackson, J., & Walker, R., 2004. Late Cenozoic reorganization of the Arabia-Eurasia collision and the comparison of short-term and long-term deformation rates. Tectonics, 23(2).

Bagnold, R.A., 1941. The Physics of Blown Sand and Desert Dunes. Chapman and Hall, London.

Balme, M., Berman, D.C., Bourke, M.C., Zimbelman, J.R., 2008. Transverse Aeolian Ridges (TARs) on Mars. Geomorphology. 101(4), 703-720.

Berman, D. C., Balme, M. R., Rafkin, S. C., & Zimbelman, J. R., 2011. Transverse aeolian ridges (TARs) on Mars II: distributions, orientations, and ages. Icarus, 213(1), 116-130.

Berman, D. C, Michalski, J. R., Balme, M. R., 2015. Analyses of transverse aeolian ridges on mars. 46th Lunar and Planetary Science Conference Abstract #2210.

Bourke, M.C., Wilson, S.H., Zimbelman, J.R., 2003. The variability of TARs in troughs on Mars. LPSC XXXIV [CDROM] Abstract # 2090.

Bridges, N., Geissler, P., Silvestro, S., Banks, M., 2013. Bedform migration on Mars: Current results and future plans. Aeolian Research, 9, 133-155.

de Silva, S.L., Spagnuolo, M.G., Bridges, N.T., Zimbelman, J.R., 2013. Gravel-mantled megaripples of the Argentinean Puna: A model for their origin and growth with implications for Mars. Geological Society of America Bulletin. 125(11-12), 1912-1929.

Ehsani, A. H., & Quiel, F.,2008. Application of self organizing map and SRTM data to characterize yardangs in the Lut desert, Iran. Remote Sensing of Environment, 112(7), 3284-3294.

Fenton, L.K., Michaels, T.I., Chojnacki, M., 2015. Late Amazonian aeolian features, gradation, wind regimes, and Sediment State in the Vicinity of the Mars Exploration Rover Opportunity, Meridiani Planum, Mars. Aeolian Research. 16, 75-99.

Fryberger, S.G., 1979. Dune forms and wind regime. A Study of Global Sand Seas, USGS Professional Paper, US Geological Survey and United States National Aeronautics and Space Administration, Washington. 1052, 137– 169.

Gabriel, A., 1938. The southern Lut and Iranian Baluchistan. Geographical Journal. 92, 193–208.

Geissler, P. E., 2014. The birth and death of transverse aeolian ridges on Mars. Journal of Geophysical Research: Planets, 119(12), 2583-2599.

Kerber, L., Head, J.W., 2012. A progression of induration in Medusae Fossae Formation transverse aeolian ridges: evidence for ancient aeolian bedforms and extensive reworking. Earth Surface Processes and Landforms. 37, 422-433.

Mildrexler, D.J., Zhao, M., Running, S.W., 2011. Satellite finds highest land skin temperatures on Earth. Bulletin of the American Meteorological Society. 92, 855-860.

Reiss,D., Raack,J., Rossi,A.P., DiAchille,G., Hiesinger,H., 2010. First in-situ analysis of dust devil tracks on Earth and their comparison with tracks on Mars. Geophysical Research Letters.37, L14203.

Walker, A.S., 1986. Chapter 8: Plate E-19. M. Nicholas, S. Short, J. Robert, W. Blair (Eds.), Geomorphology from Space, NASA.

White, B.R. (1979) Soil transport by wind on Mars. Journal of Geophysical Research, 84, 4643-4651.

Wilson, S.A., Zimbelman, J.R., 2004. Latitude-dependent nature and physical characteristics of transverse aeolian ridges on Mars. Journal of Geophysical Research. 109, (E10003).

Zimbelman, J.R., 2010. Transverse Aeolian Ridges on Mars: First results from HiRISE images. Geomorphology. 121, 22-29.

Zimbelman, J. R., Williams, S. H., & Johnston, A. K., 2012. Cross-sectional profiles of sand ripples, megaripples, and dunes: a method for discriminating between formational mechanisms. Earth Surface Processes and Landforms. 37(10), 1120-1125.

Zambito, J. J., & Benison, K. C. 2013. Extremely high temperatures and paleoclimate trends recorded in Permian ephemeral lake halite. Geology, 41(5), 587-590.

Zimbelman, J.R., Scheidt, S.P., 2014. Precision topography of a reversing sand dune at Bruneau Dunes, Idaho, as an analog for Transverse Aeolian Ridges on Mars. Icarus. 230, 29-37.

CHAPTER 3

SEMI-AUTOMATIC MAPPING OF LINEAR-TRENDING BEDFORMS USING 'SELF-ORGANIZING MAPS' ALGORITHM

ABSTRACT

Increased application of high resolution spatial data, such as high-resolution satellite or Unmanned Aerial Vehicle (UAV) images from Earth, as well as High Resolution Imaging Science Experiment (HiRISE) images from Mars (McEwen et al., 2007), makes it necessary to develop semi-automatic and automated techniques capable of extracting their detailed information. Model validation based on multi-temporal images in different environmental management issues and geophysical problems such as climate change effects or aeolian bedform movement, such as ripples, illustrate the requirement for increasingly precise image-processing in the remote sensing discipline of different planets. This study presents a methodology based on an unsupervised Artificial Neural Network (ANN) algorithm, known as Self Organizing Maps (SOM), to achieve the semi-automatic extraction of linear or other small footprints, such as Martian Transverse Aeolian Ridges (TARs), from these high-resolution images in order to facilitate and speed up image analysis along with the accuracy of results.

3-1 INTRODUCTION

Mapping different types of minor linear-like features, such as aeolian ripples and glacial linear landforms, and extracting their morphometric and pattern information (whether on Earth and other planets) is challenging because of their small areal extent on satellite images and their large number or high density within small areas. Unfortunately, available feature extraction modules of remote sensing software, such as Envi, cannot efficiently recognize the size of these features. In order to spatially analyze small linear features such as ripple-like aeolian bedforms on Earth and other planets, other studies traced and digitized them manually (e.g., Ewing et al., 2010; Fenton et al., 2015; Pederson et al, 2015; Ewing et al, 2015). These manual techniques are time-consuming and subject to different types of human error, particularly in closely spaced and extensive bedform fields. In addition, previous frameworks for automatic and semi-automatic crestline extraction have been examined on mega-ripples and linear glacial features; however, these methodologies could not recognize those target

features, so they were not reproducible. An automatic digitizing technique has been introduced recently for aeolian features on Mars by Vaz and Silvestro (2014). However, their technique is not easily applicable to other satellite images since it needs an additional editing step, which could be more time-consuming for small linear features in complicated topographies.

The present study introduces a framework based on an unsupervised Artificial Neural Network (ANN) algorithm called Self-Organizing Maps (SOM) (Kohonen, 2001) to automate outlining bedforms for further spatial analysis of small linear features, which is still a problem. SOM is generally used for visualization of information that preserves the topological relationships captured in the input (Kohonen, 2001). It translates information relationships of high dimensional input data to a two-dimensional output grid in what is called the map. SOM initially was applied in engineering tasks, but it has been introduced to the geoscience community as a pattern recognition method used in geophysical inversion (Raiche, 1991). Gradually, several applications of this seminal method attracted scientists in other geoscience disciplines, such as the segmentation of remote sensing data like multispectral Landsat Thematic Mapper 5 (TM5) or ASTER data (Duda and Canty, 2002; Jianwen and Bagan, 2005), class modeling in agricultural chemistry (Marini et al., 2005), and information visualization and knowledge discovery in Geographic Information System (GIS) (Koua et al., 2006). Application of this method in geomorphometrical segmentation of bare earth and desert landforms (Ehsani et al., 2008; Foroutan et al., 2013) demonstrate that SOM is an efficient tool for analyzing aeolian landforms in hyper-arid environments, which provides useful information for terrain feature analysis in remote regions. However, these previous desert studies were based on geomorphometric elements derived from digital elevation models (DEMs), and this study's features were hundreds of meters in horizontal dimension. As an example in the gemorphometric segmentation work by Foroutan et al., (2013) with SOM, they used inputs that were calculated using elevation derivatives with first, second, and third orders to characterize the morphometric elements of the landforms.

In the study described here, high-resolution satellite images have been used as the primary input data, and other layers were extracted from these images depending on the properties of their bands and the characteristics of the features throughout the study area. Determination of the network design is the most important step in ANN algorithms. Other important issues for documenting small features by ANN in this project are the choices of the appropriate kernel size for each filter, the best dimensions for the output layer, and the number of iterations and the neighboring radius for the SOM network. We applied this framework to a large mega-ripple field in a hyper-arid desert and the results are both

promising and potentially successful. The introduced methodology with its associated high degree of accuracy can save a lot of time and should aid quantitative studies in different Earth and planetary science projects.

3-2 DATA AND METHODS

3-2-1 STUDY AREA

The study area for this research is a unique mega-ripple field in the Lut desert of Iran (Foroutan and Zimbelman, 2016). The region hosts millions of granule-covered mega-ripples with various spatial patterns and crest morphologies. These landforms are located in a lowland area about 200 m above sea level in an area of about 250 km^2 near the edge of a vast yardang field (Figures 3.1 and Figure 3.S1). For more information and detailed discussion about characteristics of this study area and the mega-ripple features, we refer the reader to the article introducing these enigmatic landforms (Foroutan and Zimbelman, 2016). Mega-ripples in this area are of great interest to planetary scientists because of their similar horizontal length-scale to mysterious aeolian bedforms on Mars known as Transverse Aeolian Ridges (TARs); the features in Iran are essentially identical to many TARs seen in high-resolution images of Mars (e.g., Zimbelman, 2010; Berman et al., 2011). Dimensions of these bedforms in the Lut desert range in width and length from 1 to 30 m and 7 to 300 m, respectively. Their height varies from less than 0.5 m to about 3 m.

3-2-2 SATELLITE DATA

Small granular mega-ripples cannot be easily identified in images with >2 m/pixel resolution, so these bedforms are best analyzed using satellite images with relatively high resolution. All bands of the natural color panchromatic QuickBird images, which have been Orthorectified, have been used as the main input data in this study, which is the best available for the area. QuickBird satellite collects both multi-spectral and panchromatic bands/images concurrently (Blue: 450–520 nm, Green: 520–600 nm, Red: 630–690 nm and near Infra-Red: 760–900 nm) (DigitalGlobe, 2008b). Capability for showing spatial variability at the fine scales represented by these images opened new horizons for field-scale remote sensing applications (Coops et al., 2006, Wu et al., 2008). The boundary of the acquired data for this project is illustrated in Figure 3.1. The selected area contains mega-ripples with many different patterns, sizes and spatial densities.

Figure 3.1. Study area in the Lut desert of Iran. The white outline shows the boundary of QuickBird satellite images used as the basic data for this study.

3-2-3 - SOM SELF ORGANIZING MAPS

Artificial neural networks are structured in layers of neurons, as processing units, which are inter-connected. Each output layer neuron is connected to all neurons in the input layer by synaptic weights or weight vectors. By adjusting the weights of an artificial neuron, desired output from the network can be obtained. This adjusting step, which is defined by a certain ANN algorithm, is called a learning process. SOM is an unsupervised artificial neural network algorithm invented and introduced by Kohonen in 1982 (Kohonen, 2001). The SOM characteristics such as learning ability, abstraction with topology preservation, and visualization can be applied to complex tasks in different disciplines (e.g., Marini et al., 2005). It has been applied in this study as a powerful classification algorithm with capability of delineating small linear features' details in satellite images.

The input layer in the SOM represents the input feature vector and thus has neurons for each measurement dimension. For remote sensing data, this would imply a separate neuron for each reflectance band or image. The output layer is a two-dimensional array of neurons where each output layer neuron is connected to all neurons in the input layer by weight vectors (Figure 3.2). Weights are

initialized randomly and the learning procedure modifies the initial weight of connections, or weight vectors, to best describe the spatial pattern of the features presented to them (Kohonen, 2001). The primary aim of the model is to let the weight vectors learn what is presented by the input vectors.

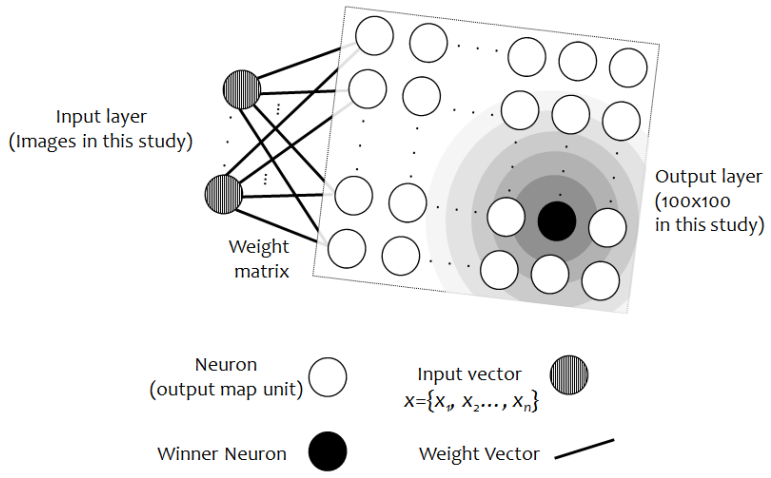

Figure 3.2. Simplified structure of the Self Organizing Maps. Lines show the connection between input and output neurons (weight vectors). Each input neuron is connected to all output neurons by weight vectors. Winner neuron update neighboring neurons based on their distance.

Network learning in SOM is an iterative process. Input data are represented by the vector $x=\{x_1, x_2\ldots, x_n\}$, where n is the number of input variables used for the network. During the classification, input vectors are presented to the network and, in each case, the output neuron with the minimum Euclidean distance between its weight vector and the input vector, is selected as the winner:

$$winner = \arg\ min_j \left(\sqrt{\sum_{i=1}^{n} \left(x_i(t) - w_{ij}(t) \right)^2} \right) \qquad (1)$$

where $x_i(t)$ is the input to neuron i at iteration t, and $w_{ij}(t)$ is the synaptic weight connecting output neuron j to the input neuron i at iteration t. The weight vector of the winner and output neurons within a neighborhood radius γ of the winner are then adjusted in the direction of the input vector:

$$w_{ij}(t+1) = w_{ij}(t) + \alpha(t)\left[x_i(t) - w_{ij}(t)\right] \qquad (2)$$

where $w_{ij}(t+1)$ is the adjusted weight and $\alpha(t)$ is the learning rate at iteration t. The weights of those neurons outside the neighborhood remain unadjusted. This competitive learning and lateral

interaction stage is known as coarse-tuning. The learning rate decreases gradually during the coarse-tuning stage from an initial learning rate ($\alpha_{\max}$) to a final learning rate ($\alpha_{\min}$), after a total number of iterations ($t_{\max}$):

$$\alpha(t) = \left(\frac{\alpha_{min}}{\alpha_{max}}\right)^{\frac{t}{t_{max}}} \qquad (3)$$

Consequently, the radius of the neighborhood decreases steadily during the coarse-tuning stage. A large initial neighborhood radius is usually chosen and it decreases until the weight of only the winning neuron is adjusted in the output layer. Coarse-tuning finally results in a fundamental organization (topology) of neuron weights that represent the underlying clusters in the input data. The final stage in SOM classification is labeling, which determines output neuron classes. At this stage, the basic structure of the input data has been topologically form to the SOM output layer, which finally define the classes' differences (Kohonen, 2001).

In comparison to other classification algorithms, SOM classification gave us more detailed separation between elements of mega-ripples, which means it has the ability to recognize our desired class of feature. The quantization error of the SOM algorithm is used as a performance criterion for classification results. The quantization error can be measured by defining the average distance of the input vectors to the cluster centroids by which they are represented.

3-3 RESULTS

3-3-1- SOM RESULTS

An important issue for documenting small features, such as mega-ripples, with ANN algorithms is finding inputs and adjusting the network to define these features in detail. The choices of suitable inputs and an appropriate kernel size for extracting each input layer, the best dimensions for the output layer, number of iterations and clusters, and the neighborhood radius for the SOM classification need to be adjusted carefully. Different sets of input layers and network adjustments have been tested to recognize the best resulting design for a framework that captures the crestlines of mega-ripples and their outlines with the highest accuracy. The best framework for capturing our target landforms has the input layers, including the main bands of the satellite image and two additional layers that were extracted from the initial image; one of these additional layers is the edge-

enhanced map, formed by using a Sobel edge detection filter and the second additional layer is the result of a High-pass spatial filter (Figure 3.4).

The Sobel operator is a directional filter, which calculates the gradient of the brightness intensity of each pixel in the image, giving areas of abrupt change (horizontal and vertical) relative to those of gradual change (Sobel, 1970). The High-pass filter removes the effect of low frequency components within an image, like 'geological noise' such as overlying dust devil tracks or salt deposits, while retaining the high frequency or dominant local variations and boundary between objects (Chavez et al., 1991). It uses a kernel with a high central value, surrounded by negative weights (Figure 3.3). Selection of filters and kernel sizes was done by comparing the results between several runs. The best results for satellite images, with about 0.5±0.1 m/pixel, were acquired by using 3x3 kernel size for the Sobel filter and 11x11 kernel size for the high-pass filter. The SOM was designed to sample all pixels in the input layers. Figure 3.3 indicates the final filters that have been used for our data.

$$A = \begin{bmatrix} -1 & -1 & -1 & -1 & -1 & -1 & -1 & -1 & -1 & -1 & -1 \\ -1 & -1 & -1 & -1 & -1 & -1 & -1 & -1 & -1 & -1 & -1 \\ -1 & -1 & -1 & -1 & -1 & -1 & -1 & -1 & -1 & -1 & -1 \\ -1 & -1 & -1 & -1 & -1 & -1 & -1 & -1 & -1 & -1 & -1 \\ -1 & -1 & -1 & -1 & -1 & -1 & -1 & -1 & -1 & -1 & -1 \\ -1 & -1 & -1 & -1 & -1 & 120 & -1 & -1 & -1 & -1 & -1 \\ -1 & -1 & -1 & -1 & -1 & -1 & -1 & -1 & -1 & -1 & -1 \\ -1 & -1 & -1 & -1 & -1 & -1 & -1 & -1 & -1 & -1 & -1 \\ -1 & -1 & -1 & -1 & -1 & -1 & -1 & -1 & -1 & -1 & -1 \\ -1 & -1 & -1 & -1 & -1 & -1 & -1 & -1 & -1 & -1 & -1 \\ -1 & -1 & -1 & -1 & -1 & -1 & -1 & -1 & -1 & -1 & -1 \end{bmatrix}$$

$$Bx = \begin{bmatrix} -1 & 0 & +1 \\ -2 & 0 & +2 \\ -1 & 0 & +1 \end{bmatrix} \rightarrow \text{X=Result of applying Bx}$$

$$By = \begin{bmatrix} +1 & +2 & +1 \\ 0 & 0 & 0 \\ -1 & -2 & -1 \end{bmatrix} \rightarrow \text{Y=Result of applying By}$$

$$B = \sqrt{X^2 + Y^2}$$

Figure 3.3 Matrices of high-pass and Sobel edge detection that were used for the QuickBird images of the study area.

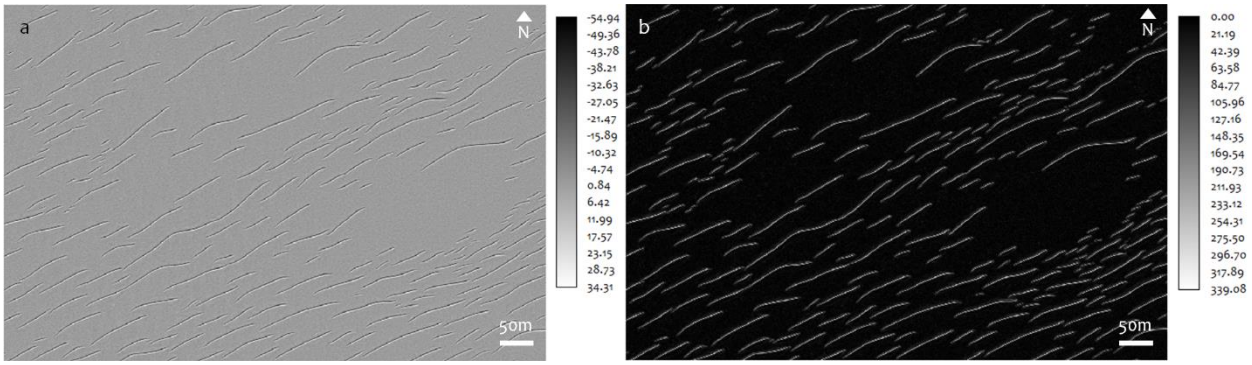

*Figure 3.4. Two layers resulted from a) high-pass filter with 11*11 kernel size and b) Sobel filter with 3*3 kernel size on the panchromatic image. These have been recognized to have the best results for linear features.*

The optimum size of the SOM output layer has been identified by considering 10 by 10 and 1000 by 1000 dimensions as the smallest and largest dimensions for a conductive classification result and defining the best output dimensions. This selection was done by evaluating the results of dimensions in between to identify the network with the least value of the quantization error. Finally, the optimum dimensions for the output layer, or SOM layer, was designed to have 100 by 100 neurons. The initial neighborhood radius of 142.42, the minimum learning rate, $\alpha(t)$, of 0.5 and the maximum learning rate of 1, have been used for this algorithm. All these values were determined as the most efficient and precise settings according to an evaluation of the smallest quantization error through several iterative runs of the network during an accuracy assessment. Post-classification steps are vectorization and conducting a smoothing algorithm to the desired class. Vectorization is accomplished by identifying and conjoining one side of the central cell's perimeter for our target class. The resulting line is stepped in order to get to the real shape we need to smooth out the line. For smoothing the resulting vector, the polynomial approximation with exponential kernel (Bodansky, et al, 2001) have been used by conducting a parametric continuous averaging technique. The smoothing tolerance of 10 was the best for our features.

QuickBird images of the study area consist of 4 tiles, each tile of which was processed separately. Getting TAR-like features' crestlines requires iteration of about 2.3e+6 for the described SOM setting, the final quantization error was ~ 0.001, which resulted in the desired classification. The final extracted shapefile contains all crest outlines in the area, which was ready for further spatial analysis. The flowchart in Figure 3.S2 summarizes the major steps used in this semi-automatic crestline extraction method. In addition, we tested our framework on a small portion of a WorldView-1 black and white image, which is the highest spatial resolution commercial imaging satellite with 0.5m resolution at

Nadir (DigitalGlobe, 2008a). The whole framework result was in perfect agreement with that obtained from the QuickBird image bands.

3-3-2- ACCURACY ASSESSMENT

Diversity of patterns and crest morphology of these features in the Lut desert enabled us to select different types of features for accuracy assessment of our methodology. About 600 features were randomly selected throughout the study area as our control points/features. Regarding our study area, this sample size is more than the required number of control points suggested in the literature (Lillesand et al., 2014). Mega-ripples in this area are not identical throughout the study area. Accordingly, sample features are also diverse in morphology such as linear, arcuate, barchan-like and they also form different patterns such as closely spaced, widely spaced or singular features. These random features have been digitized manually by photo-interpretation and independent from the results of the automatic method (Figure 3.5). Finally, the two results were quantitatively and qualitatively compared in order to validate the described methodology.

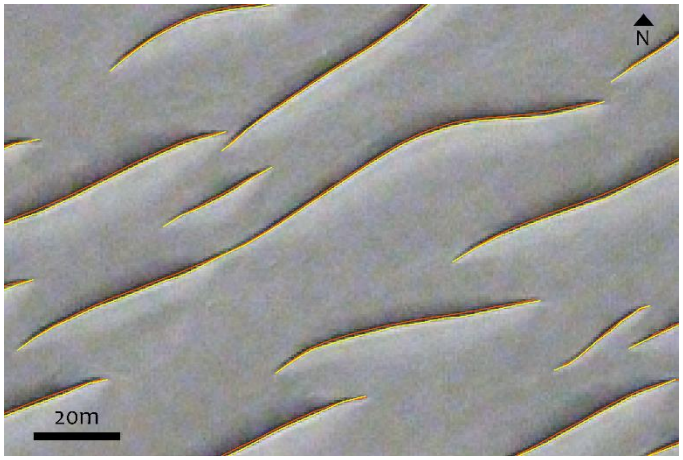

Figure 3.5. A portion of the study area, overlaying in two different crestline layer results by manual (yellow) and automatic (red) procedures.

Length, orientation and sinuosity are the first-hand metrics from the resulting crestline map of mega-ripples (Table 3.1). Plots in Figure 3.6 illustrate the comparison between cumulative probability distribution of length and sinuosity results of these two datasets. The rose plot in Figure 3.7 shows the orientation overlap of these data, which demonstrates a good agreement between manual and semi-automatic results. Based on the statistics analysis, a difference of 0.27° exists between the mean azimuth computed for datasets extracted from our method and manual procedure. In addition, an average difference in length of 1.1 m was obtained between the traditional and automatic mapping.

These values demonstrate the high level of accuracy for the methodology presented here. Table 3.S1 shows the statistical values of these two datasets for length, sinuosity and orientation. Such differences between results might happen in traditionally produced maps assessed by different users (e.g. Vaz et al., 2014). An overall comparison between each single feature from both methods shows most of the differences occur for the mega-ripples with the smallest footprints on the image. They are not considered to be mature mega-ripples and, as a result, can be ignored in many studies.

Table 3-1. Description of tested parameters for accuracy assessment.

Parameter for accuracy assessment	**Description of the parameter**
Length	Crestline length
Sinuosity	Crestline length / straight line distance between two endpoints of the feature
Orientation	The direction of the line from the horizontal line, considering the start and the end point (not all vertices)

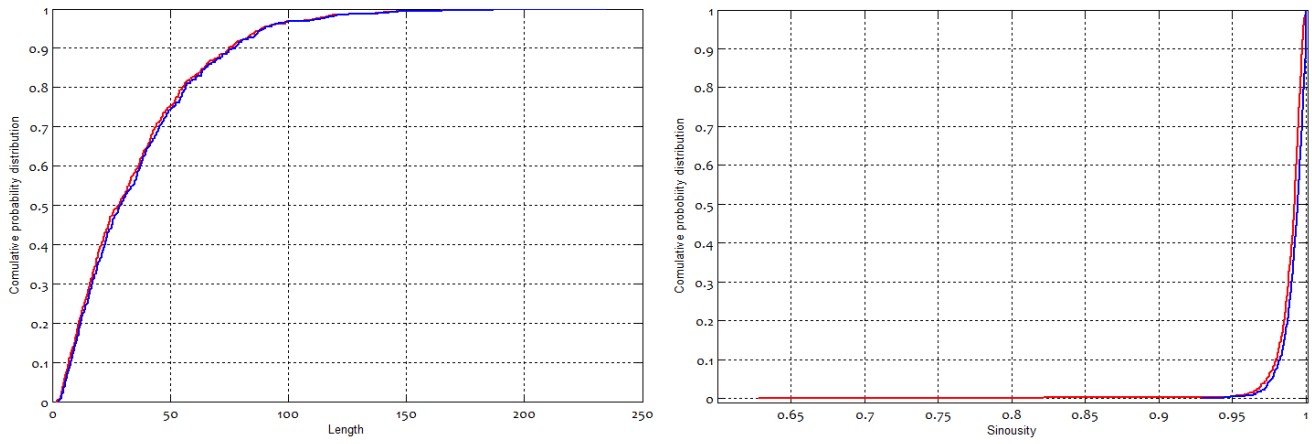

Figure 3.6. Cumulative probability distribution graphs of length (m) and sinuosity of the results of two different methods of extracting crestlines; red line shows the automatic results and blue line shows the manual results.

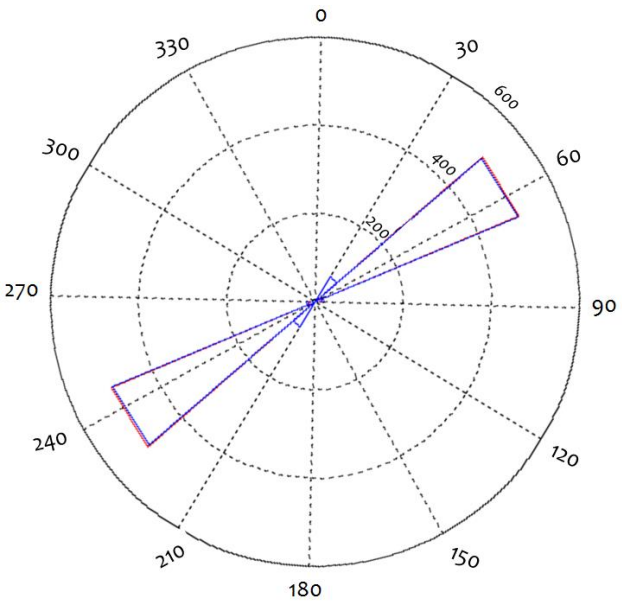

Figure 3.7. Features' orientation rose plot comparing two different methods; red is the automatic result and blue is the manual results. Results from both methods essentially overlap.

Based on the accuracy assessment results, the semi-automatic crestline extraction method proved to be very successful when applied to the Lut study area. More than 2 million mega-ripples with different morphologies were extracted by this method (Figure 3.8). Figure 3.9 shows resulting map within a portion of the study area. This methodology successfully extracted all bedform crestlines, including small barchan-like bedforms, along with some large wind ripples in the area with different topographic positions. Topographically influenced and confined bedforms and the ones in the immediate vicinity of other features were also captured with all details and less error. The methodology is simple, applicable and adjustable to diverse kinds of bedforms and linear features with the same horizontal length-scale as seen in high-resolution images.

The proposed methodology was also applied to HiRISE satellite images of the Martian surface (McEwen et al., 2007), which have a spatial resolution of about 25 cm per picture element. ANN results successfully mapped TAR crests observed in different topographic situations. All settings for the framework were the same as those applied to the Earth images. The results were as accurate as TAR-like features outcome in the Lut desert, likely facilitated by HiRISE's higher spatial resolution. In addition, features' overall length and the curved crests of some TARs comparatively had the lowest accuracy for the Earth images, but appear to have high accuracy in the HiRISE images, most likely because of the higher spatial resolution of these data. Figure 3.10 illustrates the results of the introduced framework applied to Martian TARs. It displays variable sizes at three different locations

on Mars, as well as within different topographic and geological settings. Such data should be amenable to quantitative comparisons between mapped crest trends for TAR-like features on both Earth and Mars, but such an analysis was not the intent of the present project (which is primarily focused on a demonstration of the utility of the ANN procedure).

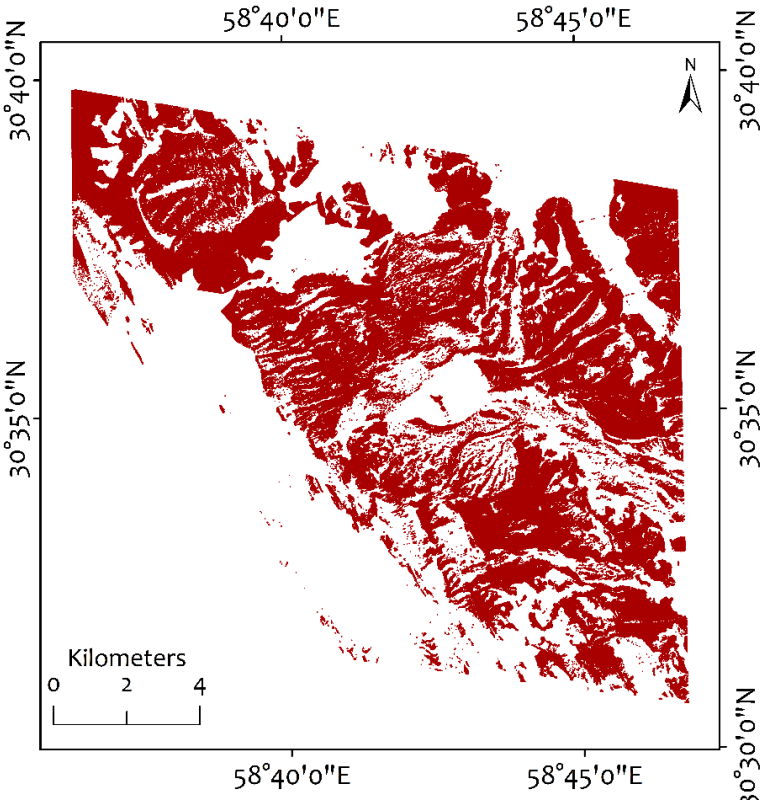

Figure 3.8. Crestline locations of more than 2 million mega-ripples that have been digitized by the framework presented in this study.

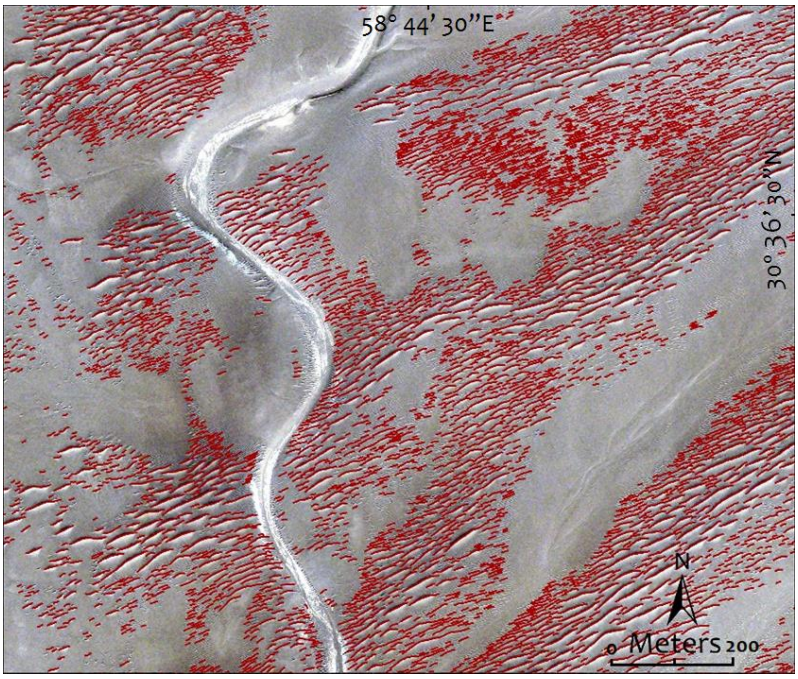

Figure 3.9. A portion of the mega-ripple field in the Lut desert of Iran, with an overlay of the extracted crestline layer (in red) on an image base. These results were derived from the SOM semi-automatic method.

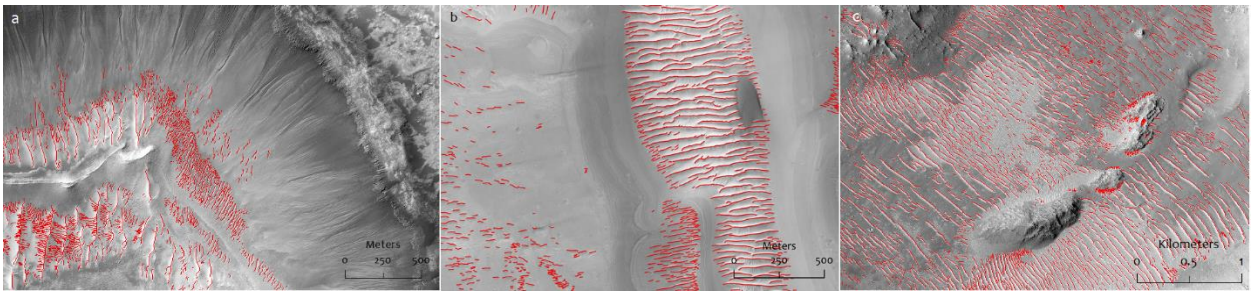

Figure 3.10. Crestline maps extracted by an introduced mapping framework for TARs on Mars observed in diverse topographic settings: a) TARs with variable sizes in Kaiser Crater (PSP_006820_1325); b) TARs in Noctis Labyrinthus, superimposed by LDD (ESP_044009_1730); c) TARs on the floor of an impact crater in Phlegra Dorsa (ESP_045503_2000).

3-4 CONCLUSION

A simple semi-automatic mapping framework is presented in this study. This methodology was conducted using high-resolution satellite images of a large mega-ripple field in Iran in order to digitize the aeolian bedforms. The suggested semi-automatic methodology has been evaluated for accuracy and the results are consistent with more traditional photo-interpretation. This method is capable of providing a precise delineation between small linear features, such as TARs and mega-ripples, and

other morphologic features present in the satellite images (e.g., the dry channel visible in Figure 3.9). This methodology has been successfully applied using high-resolution satellite images of both Earth and Mars. The network settings were examined in order to define ones that most accurately captured the mega-ripple crestlines and outlines from the images. This framework and module are applicable and adjustable to all types of images which contain linear features. The framework introduced in this work can facilitate and speed up image analysis along with improving the accuracy of the results. Furthermore, model validation based on multi-temporal images in different environmental management issues and geophysical problems, such as climate change effects and motion tracking in aeolian geomorphology, could greatly benefit from this precise image processing technique throughout the remote sensing discipline.

3-5 REFERENCES

Berman, D. C., Balme, M. R., Rafkin, S. C., & Zimbelman, J. R., 2011. Transverse aeolian ridges (TARs) on Mars II: distributions, orientations, and ages. Icarus, 213(1), 116-130.

Bodansky, E., Gribov, A., & Pilouk, M., 2001. Smoothing and compression of lines obtained by raster-to-vector conversion. In International Workshop on Graphics Recognition (pp. 256-265). Springer Berlin Heidelberg.

Chavez, P., Sides, S. C., & Anderson, J. A., 1991. Comparison of three different methods to merge multiresolution and multispectral data- Landsat TM and SPOT panchromatic. Photogrammetric Engineering and remote sensing, 57(3), 295-303.

Coops, N. C., Johnson, M., Wulder, M. A., & White, J. C., 2006. Assessment of QuickBird high spatial resolution imagery to detect red attack damage due to mountain pine beetle infestation. Remote Sensing of Environment, 103(1), 67-80.

DigitalGlobe, (2008a). WorldView-1 products quick reference guide, Longmont, CO, 2008. [Online]: http://digitalglobe.com

DigitalGlobe, (2008b). QuickBird imagery products: Product guide. Longmont, CO, 2008. [Online]: http://digitalglobe.com

Duda, T., Canty, M., 2002. Unsupervised classification of satellite imagery: choosing a good algorithm. International Journal of Remote Sensing 23, 2193–2212.

Ehsani, A. H., & Quiel, F., 2008. Application of self organizing map and SRTM data to characterize yardangs in the Lut desert, Iran. Remote Sensing of Environment, 112(7), 3284-3294.

Ewing, R. C., Peyret, A. P. B., Kocurek, G., & Bourke, M., 2010. Dune field pattern formation and recent transporting winds in the Olympia Undae Dune Field, north polar region of Mars. *Journal of Geophysical Research: Planets*, *115*(E8).

Ewing, R. C., Hayes, A. G., & Lucas, A., 2015. Sand dune patterns on Titan controlled by long-term climate cycles. *Nature Geoscience*, *8*(1), 15-19.

Fenton, L.K., Michaels, T.I., Chojnacki, M., 2015. Late Amazonian aeolian features, gradation, wind regimes, and Sediment State in the Vicinity of the Mars Exploration Rover Opportunity, Meridiani Planum, Mars. Aeolian Research. 16, 75-99.

Foroutan, M., Kompanizare, M., & Ehsani, A. H., 2013. Semiautomatic morphometric land surface segmentation of an arid mountainous area using DEM and self-organizing maps. Arabian Journal of Geosciences, 6(12), 4795-4810.

Foroutan, M., & Zimbelman, J. R., 2016. Mega-ripples in Iran: A new analog for transverse aeolian ridges on Mars. Icarus, 274, 99-105.

Jianwen, M., Bagan, H., 2005. Land-use classification using ASTER data and self-organized neutral networks. International Journal of Applied Earth Observation and Geoinformation 7, 183–188.Kohonen, T., 2001. Self Organizing Maps, 3rd Ed. Springer, New York.

Koua, E.L., MacEachren, A., Kraak, M.J., 2006. Evaluating the usability of visualization methods in an exploratory geovisualization environment. International Journal of Geographical Information Science 20, 425–448.

Lillesand, T., Kiefer, R. W., & Chipman, J., 2014. Remote sensing and image interpretation. John Wiley & Sons.

Marini, F., Zupan, J., Mageri, A.L., 2005. Class-modeling using Kohonen artificial neural networks. Analytica Chimica Acta 544, 306–314.

McEwen, A.S., et al., 2007. Mars Reconnaissance Orbiter's High Resolution Imaging Science Experiment (HiRISE), *Journal of Geophysical Research*, 112, E05S02, doi: 10.1029/2205JE002605.

Pedersen, A., Kocurek, G., Mohrig, D., & Smith, V., 2015. Dune deformation in a multi-directional wind regime: White Sands Dune Field, New Mexico. *Earth Surface Processes and Landforms*, *40*(7), 925-941.

Parikh, J. A., DaPonte, J. S., DiNicola, E. G., & Pedersen, R. A., 1992. Selective detection of linear features in geological remote sensing data. In *Aerospace Sensing* (pp. 963-972). International Society for Optics and Photonics.

Raiche, A., 1991. A pattern recognition approach to geophysical inversion using neural nets. *Geophysical Journal International*, *105*(3), 629-648.

Sobel I. E., 1970. Camera models and machine perception. Ph.D. Thesis, Electrical Engineering Department, Stanford University, Stanford, CA.

Vaz, D. A., & Silvestro, S., 2014. Mapping and characterization of small-scale aeolian structures on Mars: An example from the MSL landing site in Gale Crater. Icarus, 230, 151-161.

Wu, J., Bauer, M. E., Wang, D., & Manson, S. M., 2008. A comparison of illumination geometry-based methods for topographic correction of QuickBird images of an undulant area. ISPRS journal of photogrammetry and remote sensing, 63(2), 223-236.

Zimbelman, J. R., 2010. Transverse aeolian ridges on Mars: First results from HiRISE images. Geomorphology, 121(1), 22-29.

3-6 SUPPLEMENTARY MATERIAL

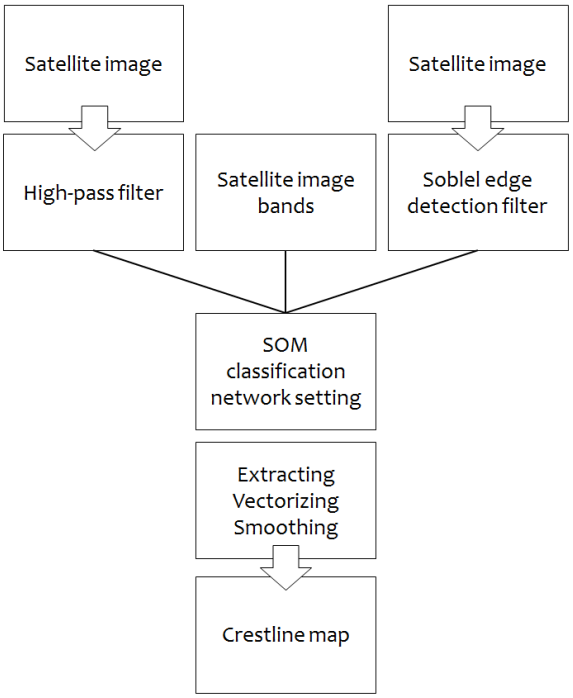

Figure 3.S1. Framework's flowchart for mapping small liner features.

Table 3.S1. Summary statistics for the two compared datasets from manual and automatic methods.

	Manual digitizing	**Automatic digitizing**
Length mean	64.72	64.99
Maximum Length	83.21	83.06
Minimum Length	48.87	48.09
Standard deviation of Length	5.99	5.96
Orientation mean	64.72	64.99
Maximum Azimuth	36.94	35.80
Minimum Azimuth	234.62	233.15
Standard deviation of Azimuth	2.77	2.23
Mean Sinuosity	0.99	0.98

Maximum Sinuosity	1.00	1.00
Minimum Sinuosity	0.92	0.62
Standard deviation of Sinuosity	0.008	0.018

CHAPTER 4

TRANSVERSE AEOLIAN RIDGES (TARS) ON EARTH AND MARS

ABSTRACT

Aeolian processes are the current dominant geological activity on Mars and decoding its surface features is important for identifying its history. Transverse Aeolian Ridges (TARs) on Mars are mysterious aeolian features, which are considered unique to Mars. TARs' origin, formation processes and sediment sources are still unknown. Using high-resolution satellite images and studying terrestrial analogs are the most important tools for resolving their mystery. TAR-like features in the Lut desert of Iran are outstanding analogs regarding the diversity and dimensions of aeolian and TAR-like features.

We used a new semi-automatic mapping methodology to map these bedforms in the Lut desert. Morphometry of more than 2 million TAR-like features in the Lut study area were extracted and evaluated in this study. We used HiRISE DTMs to acquire a sufficient sample size for Martian TARs and compare the morphometry of the Martian TARs to their terrestrial analogs on Earth. We studied these factors in order to get a better understanding of their formation controlling factors. Furthermore, this study presents a multi-temporal analysis of aeolian features at this site using satellite images. Finally, we classified TAR-like features in the Lut desert into four distinct groups in terms of their morphometry and response to wind activity.

4-1- INTRODUCTION

Large aeolian depositional linear bedforms have been studied using diverse names and explanations on different planets, such as ridges (Bagnold, 1941), granule ripples (Sharp, 1963), gravel ripples (Sakamoto-Arnold, 1988), mega-ripples (Ellwood et al., 1975), coarse-grained mega-ripples (Bridges et al., 2013), gravel mega-ripples (Yizhaq and Karta, 2015), gravel ridges (Dong et al., 2012), gravel-mantled mega-ripples (de Silva et al., 2013; Bridges et al., 2015) on Earth, as well as Transverse Aeolian Ridges (TARs) (Bourke, 2003) and plains ripples (Sullivan et al., 2005) on Mars. These features are different from simple ripples, also known as sand ripples, by their larger dimensions, different wavelengths, bimodal grain size (Yizhaq and Karta, 2015; Zimbelman et al., 2009; Lorenz and Zimbelman, 2014) and formation mechanism (Yizhaq and Karta, 2015). Our information about TARs on Mars is limited because

of the difficulties in getting samples, precise cross-sectional profiles, and wind profiles. MER rover Opportunity and MSL rover Curiosity images in a few places demonstrate bimodal grain size for small TARs on Mars (Balme et al., 2008, Berman et al., 2011). However, terrestrial analogs on Earth are the best choices for getting information about mysterious Martian features such as TARs. Different wind properties, grain sizes and formation mechanisms have been hypothesized for TAR origin, such as dust deposits (Geissler, 2014). Nevertheless, their formation mechanism on both planets is still under debate.

In planetary geomorphology, the lack of terrestrial analogs limits the ability to develop and test hypotheses about feature formation and evolution (Baker, 2014). There should be a clear difference in horizontal length-scale of the mega-ripples that are identified to be TAR-like features, which means all types of mega-ripples on Earth cannot be considered as terrestrial analogs of TARs. These bedform dissimilarities on Earth and Mars are suggested to be the result of their different atmosphere conditions (Berman et al., 2008). So, only large ripple-like features on Earth with close dimensions and wavelengths hint at the properties of Martian TARs. To date, three terrestrial analogs have been introduced for TARs. The first site is a mega-ripple field in the Puna, Argentina, which has been introduced by de Silva et al. (2013). Puna mega-ripples can be considered as a type of mega-ripples on Mars, known as plains ripples, such as the ripples in Meridiani Planum (Sullivan et al., 2005, Fenton et al., 2015). The second terrestrial analog has been introduced by Zimbelman and Scheidt (2014) as the Bruneau (reversing) sand dunes, Idaho, which are similar to large TARs on Mars, such as the ones in the Kaiser crater. Available satellite images imply that such huge TARs may be quite rare on Mars. The last analog has been introduced by Foroutan and Zimbeman (2016) in the Lut desert of Iran. Based on metrics for Martian TARs, the Lut bedforms are the most similar analog to common Martian TARs. Bedform metrics, location and wind properties of these three analog sites are different (Table 4.1).

Table 4 -1. Comparison among various aspects of all three terrestrial analogs for TARs in Argentina, United States and Iran.

Location	**Elevation of the area**	**Geology of sediments in the area**	**Wind speed (Monthly average)**	**Rare gusts**	**Well-developed Bedform amplitude**	**Wavelength**
Argentina, Puna	3000 m	late Pleistocene pyroclastic deposits,	9.7 – 13.9 m/s	66.7 m/s	2 m (bed- form itself only ~30 cm)	30 m <

		quartz-rich rhyolitic ignimbrites				
U.S, Bruneau dunes	750 m	Upper Pliocene to Middle Pleistocene	3 – 4.5 m/s (> 6 m/s)	10.3 m/s	122.2 m	-
Iran, Lut desert	250 m	upper Pliocene to Pleistocene lacustrine silts over a basement of flat-lying Paleogene andesitic lavas and tuffs	11 – 40 m/s	48 m/s	3.45	0.6 – 100m<

In this study, we extracted and analyzed the metrics of all TAR-like features and their aeolian activity in the Lut desert of Iran, with a brief comparison to other introduced analogs. Moreover, Martian TAR metrics acquired from previous studies have been applied to a larger sample size from HiRISE DTMs used in this study. The main effort of this paper is to make a comprehensive remote sensing analysis of the TAR-like features in the Lut desert of Iran and discuss the properties of these bedforms as the most similar analog to Martian TARs.

4-2- AN OVERVIEW OF TARS ON MARS AND ITS TERRESTRIAL ANALOGS

4-2-1- TARS ON MARS

Martian TARs are considered bright aeolian features compared with dunes and are located mostly in the equatorial regions on Mars. They are typically found in depressions such as troughs and crater floors (Balme et al., 2008). TARs come in different morphologies and patterns; for example, Valles Marineris contains TARs in its troughs with different crest morphologies and densities The typical form of TARs, known as "simple", mostly have sharp, pristine and symmetric crests (Berman et al., 2008, Zimbelman, 2010). In the southern hemisphere of Mars, most of the craters contain Large Dark Dunes (LDDs) and TARs together. The most massive TARs on Mars have been identified in the Kaiser Crater with the height of more than 8 meters and width and wavelength of hundreds of meters (Jessar et al., 2015) (the largest measured TAR in the literature so far is not necessarily the largest one on Mars). However, it should be mentioned that TARs' height is one of the most important and debated factors, which makes TARs different from regular dunes and ripples on Earth. Also height measurement is still

tricky and subject to several errors through orbital data alone. Our survey, using HiRISE images from different latitudes, indicates that having light- or medium-toned albedo cannot be a consistent indicator for TARs, since they appear with different albedo ranges relative to their surrounding area (Figure 4.1). In addition, color changes on TARs have been noticed in some areas such as in the Endeavour crater (Chojnacki et al., 2014), which demonstrates that TAR albedo, in many regions, cannot represent their sediment compositions. Previous studies measured TARs' height ranges from less than a meter to about 14 meters and width and length ranges of 7 to 45 and 10 to 700 meters, respectively (Table 4.2). It is worth mentioning that all of these data cannot define the exact range of TAR metrics as compared to their diversity and abundance on Mars. HiRISE images, which are the best images to study TARs, have covered only about 2% of all of the Martian surface.

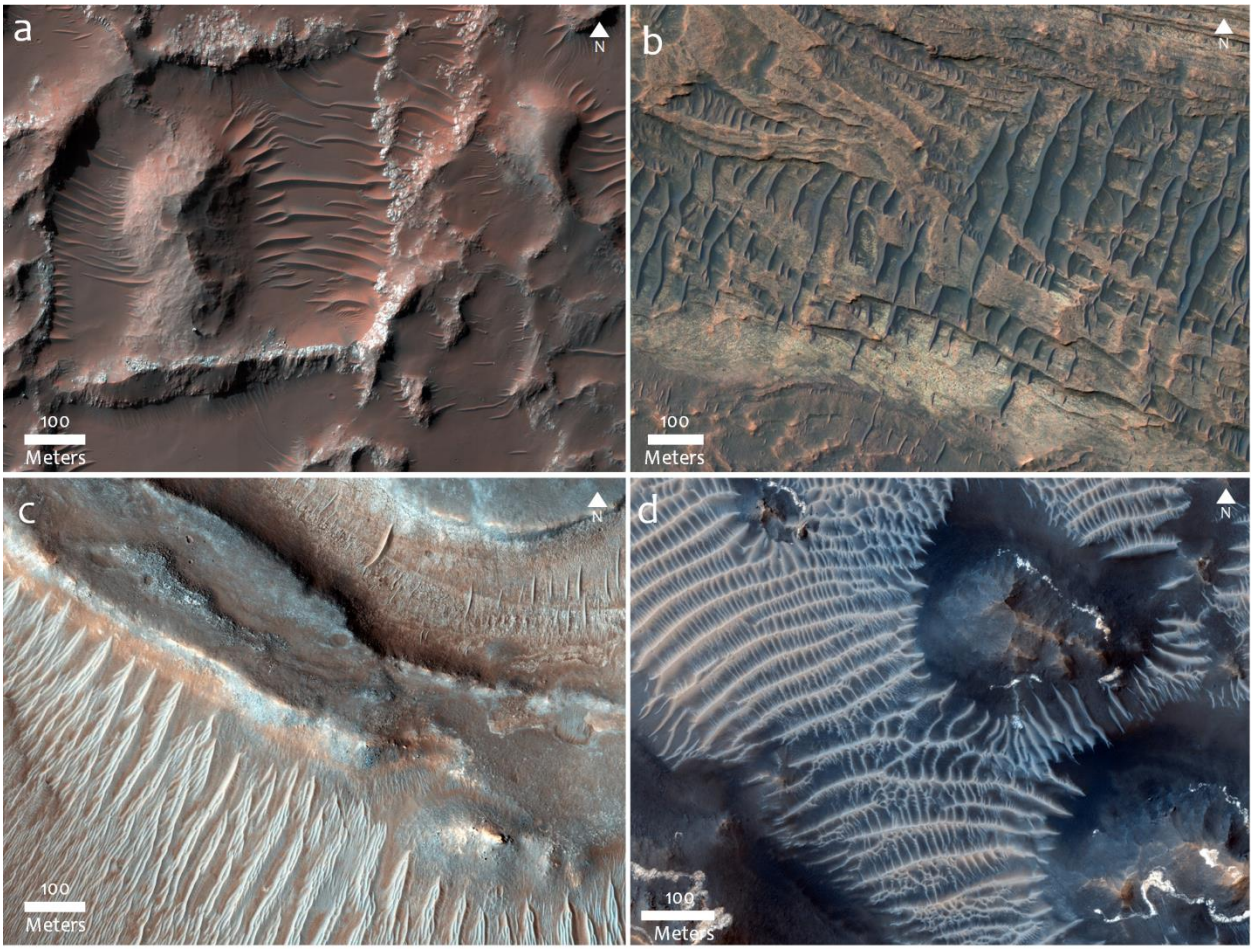

Figure 4.1. Examples of TARs with different ranges of albedo, indicating that their brightness cannot be an identifying characteristic for TARs: a) West Holden Crater; TARs in this area have the same albedo and probably the same material as their surrounding area (HiRISE PSP_010197_1540); b) Miyamoto Crater; here TARs are darker than their surroundings. Phyllosilicates have been detected at this site (HiRISE ESP_026378_1730); c) Syrtis Major; braided TARs with the same color and albedo as parts

of the bedrock (HiRISE ESP_038227_2020); and d) Noctis Labyrinthus; surrounding the bedrock knobs are networked TARs, pale ridges, with a complex interlinked morphology and clear light-toned albedo compared to the underlying surface (HiRISE ESP_033262_1725).

Small TARs in Meridinai Planum, described by Sullivan et al. (2005) as plains ripples, are considered to be armoured by coarse particles. Plains ripples are found everywhere in Meridiani Planum, while the TARs seem to be found primarily on the floor of craters; however, TARs and plains ripples appear to be influenced by the same set of winds (Fenton et al., 2015). Plains ripples were noted to have migrated (Golombek et al., 2010), yet TARs are considered to be static (Berman, et al., 2011). Despite TAR immobility, recently active aeolian features such as dust devil tracks (DDTs), fresh craters and LDDs have been noticed on TARs in Argyre Planitia, Nirgal Vallis and Nili Patera, respectively (Balme and Greeley, 2006; Zimbelman, 2003; Balme et al., 2008). These superimposition relationships could be evidence of TARs being older than other aeolian features. However, there are still several inconsistencies in the geomorphological explanation of these aeolian features (Foroutan, 2015).

4-2-2- TERRESTRIAL ANALOGS

PUNA: Puna mega-ripples in Argentina are considered to be the most extreme aeolian mega-ripples on Earth. Bedforms in this area have been formed on weakly indurated ignimbrites with strong control by the bedrock topography, so their wavelength is the result of this controlling factor rather than particle trajectories (de Silva et al., 2013). It has been demonstrated that these mega-ripples are morphologically and contextually similar to small ripple-like TARs or plains ripples. The bedrock control of these bedforms restricts their analogy to specific regions on Mars, which contain periodic bedrock ridges (PBRs) and TARs together. Their sediment size, with clasts up to 5 cm in diameter, makes them the coarsest-grained aeolian bedforms yet described on Earth (de Silva et al., 2013). However, limited close up images by rovers of Martian small TARs revealed the particle size of some TAR crests to be about 1–2 mm, with inter-ripple areas having 50–125 μm grains of basaltic sand and additional millimeter-scale concretion fragments along with intact concretions (Sullivan et al., 2005).

Areas with ripple-like features as TARs analogs in the Puna of Argentina can be classified to 5 distinct regions close to each other, with the base elevation of about 3000 m above the sea level in a high wind speed region. Monthly mean velocities are between 35 and 50 km h^{-1} with rare gusts as high as 240 km h^{-1} (Milana, 2009; de Silva et al., 2013). The main surface lithology in the basins is late Pleistocene pyroclastic deposits, quartz-rich rhyolitic ignimbrites, which are partly indurated and have been carved by the wind to produce yardangs and demoiselles (de Silva, 2010). Well-developed bedforms are

considered to have wavelengths of more than 30 m and present amplitudes of about 2 m. However, aeolian depositional bedforms comprise only ~30-60 cm of this topography (de Silva et al., 2013).

IDAHO: It has been demonstrated that TARs larger than 1 m in height compared favorably to profiles of reversing dunes (Zimbelman, 2010; Balme et al., 2011). The reversing sand dunes at Bruneau dunes, Idaho, are considered to be the best terrestrial analogs for large TARs (Zimbelman and Scheidt, 2014). These dunes have a maximum height of >122 m. The maximum height of TARs that has been reported to date is about 14 meters in Kaiser crater in the southern hemisphere (Jessar et al., 2015). The reversing dunes are located in an area with an elevation of about 750 meters above sea level in the center of an old cut-off meander of the Snake River, which was carved into lacustrine sediments of the Glenns Ferry and Bruneau Formations from the Upper Pliocene to Middle Pleistocene, respectively (Murphy, 1973).

The Bruneau Dunes sand consists of quartz, feldspar, and basaltic (iron-rich) particles in roughly equal proportions (Zimbelman and Scheidt, 2014). This analog is pretty similar in sediment albedo to the bright TARs, including large TARs in the Kaiser crater, and its sediment size is consistent with thermal inertia results of THEMIS data from TAR fields (Balme et al., 2008). Based on the closest weather station, the Bruneau area is subjected to a strong bimodal annual wind regime; minor winds can also blow from a variety of directions during spring and fall (Zimbelman and Scheidt, 2014). Data show the average monthly wind speed is 3 – 4.5 m/s, with rare gusts with maximum speed of 10.5 m/s. The annual bimodal winds typical of the Bruneau area may be similar to seasonal changes in wind patterns on Mars (Zimbelman and Scheidt, 2014).

LUT: TAR-like features in the Lut desert of Iran are in a depression with a maximum slope of about 0.3 degrees, located at the north-eastern fringe of a vast yardang field (Figures 5 and 6 from Foroutan and Zimbelman, 2016). A recent study of these yardangs shows that both fluvial and wind erosion produced these erosional features and they are currently young, active landforms (Maghsoudi et al., 2015). The sediments of these yardangs are composed of fine materials such as clay and silt with horizontal laminations, which has been demonstrated as a sign of suspended lacustrine fine-grained sediments. Some of these yardangs display cracks within clay-rich material, which is a sign of a dried pluvial lake (Maghsoudi et al., 2015). They also have some layers of gypsum and salt. Their layers display low sediment sorting, which indicates different sources for the initial sediments (Maghsoudi et al., 2015). Based on the situation of TAR-like features near these yardangs, and in some cases within their

corridors, it seems that these yardangs could be part of the source material for TAR-like features in this region.

TAR-like features in this area are covered by coarse particles with a diameter of 3-4 mm (Foroutan and Zimbelman, 2016). Most of these bedforms are similar to the majority of Martian TARs, which is called 'simple TARs' in the classification scheme introduced by Balme et al. (2008). Lut bedforms come in different spatial densities, the same as TARs on Mars. 'Barchan-like TARs' also exist on the bedrock in the northern part of the Lut area. One of the most distinguishing characteristics of TARs, which makes Lut's TAR-like features unique among the other terrestrial analogs, is their sharpness and symmetry of crests. In addition, superimposition of other aeolian features on these features, such as sand dunes and dust devil tracks, is quite exclusive compared to other terrestrial analogs. The location of these bedforms in the depression is in agreement with the situation of most Martian TARs.

4-3- METHODOLOGY

TAR-like bedforms in the Lut desert have been mapped by the Artificial Neural Networks (ANN) semi-automatic method described by Foroutan and Zimbelman (under review). There are more than 2 million bedforms in the Lut area. Crest length, wavelength, and sinuosity of these bedforms have been extracted from the initial crestline map. However, automatic extraction of the height and width of this bedform was not possible due to the local color and shadow changes in the satellite images, as well as salt accumulations among some parts of the site. So we selected about 2000 TAR-like features by cluster sampling and extracted height and width of these bedforms manually and by photoclinometry using 50 cm resolution WorldView satellite images, which is the best data available for this area.

The existing sample sizes in the literature for evaluating TAR metrics seems to be rather small (Table 4.2). Statistical theories suggest that to get a good estimate of a population parameter, the size of the sample is crucial, even more than the accuracy of the measurement (Spagnolo et al., 2012). To strengthen our deductions for both the Earth analogs and for Martian TARs, we selected TARs of different formats and patterns in diverse topographic settings from about 14 different DTMs all over Mars (Table 4.S1 and Figure 4.S1). We have digitized and extracted metrics of more than 2000 individual TARs (the same number as Earth), in order to do comparison and statistical analysis by using the extracted data from both planets.

Based on available orbital data and remote sensing studies of multi-temporal images, TARs are considered to be immobile on Mars, whereas LDDs move. We did the same remote sensing analysis

for TARs terrestrial analog in the Lut desert by using satellite images from 2004, 2008 and 2012. The semi-automatic mapping technique introduced by Foroutan and Zimbelman allow us to digitize, compare and produce a change detection map for further analysis of any change in aeolian features in the Lut desert. We believe that this study is unique regarding TARs/TAR-like features on both planets in two aspects of i) sample size, and ii) multi-temporal satellite image analysis.

4-4- RSULTS AND DISCUSSION

4-4-1 METRIC ANALYSIS

4-4-1-1 ALL TAR-LIKE FEATURES IN THE LUT DESERT

A density map of the study features in the area is illustrated in Figure 4.2 It can be deduced from a comparison of the derived density map with SRTM DEM that there is no relation between the spatial density of TAR-like features in this area and the topography. The highest density areas at this site are located in the northwest and northeast, which have the lowest (205 m) and the highest (456 m) elevation, respectively. Both locations seem to be relatively flat. TAR-like features in the dense northern areas, particularly in the northwest, are morphologically different and distinct from other bedforms in the area. They do not have clear wavelengths, large heights, and well-defined defect points. These saturated patches include small-dimension features (in height and width) with wavelengths less than 3 meters. These upwind features are supposed to be immature features or simple mega-ripples. They are close to blunt and barchan-like TARs and a continuum in form exists between immature and well-defined features. This spatial transition downwind is quite similar to Meridiani Planum bedforms (Balme et al., 2008), which are suggested be strong evidence of granular ripple origin of this location on Earth and Mars. However, there is a clear difference between these dense parts at north and close to the active yardangs and other dense fields far downwind. Figure 4.3 illustrates features in the northern high density areas (immature bedforms), compared to high density areas in the middle part of the study area (mature bedforms).

The southeastern borders of these dense northern patches contain individual TARs with well-defined defect points and larger wavelengths. We consider this transition as a kind of sediment sorting spectrum, which means the dense northern patches might contain the coarsest grain sizes. In addition, northern bedform wavelength and height are correspondingly smaller than the rest of the features in the south. The removal of the sediments in some parts of the pale underlined lacustrine sediments in the north part of the area shows the same mirroring relationship as in the Argentinian Puna and the Schiaparelli Crater on Mars (Figure 4.4). This is further evidence that may suggest the presence of

coarser grains in the northern part of the study area. The underlying geology, with a bright color, flat surface, and deep drainage, shows that it consists of soft sediments. The mechanism of mirroring features has been previously discussed for the Puna of Argentina (de Silva et al., 2013; Bridges et al., 2015). Towards the southeast, the bedforms gradually become more distinct in horizontal length, taller, with clear boundaries and defect points, and larger wavelengths and less highly dense patches. Simple well-developed features in the center of the study area are lying on an almost flat surface. The whole area seems to have a variety of different ripples and a similar diversity of ripple metrics can be seen in many locations on Mars, even in a relatively small area such as in the Kaiser crater.

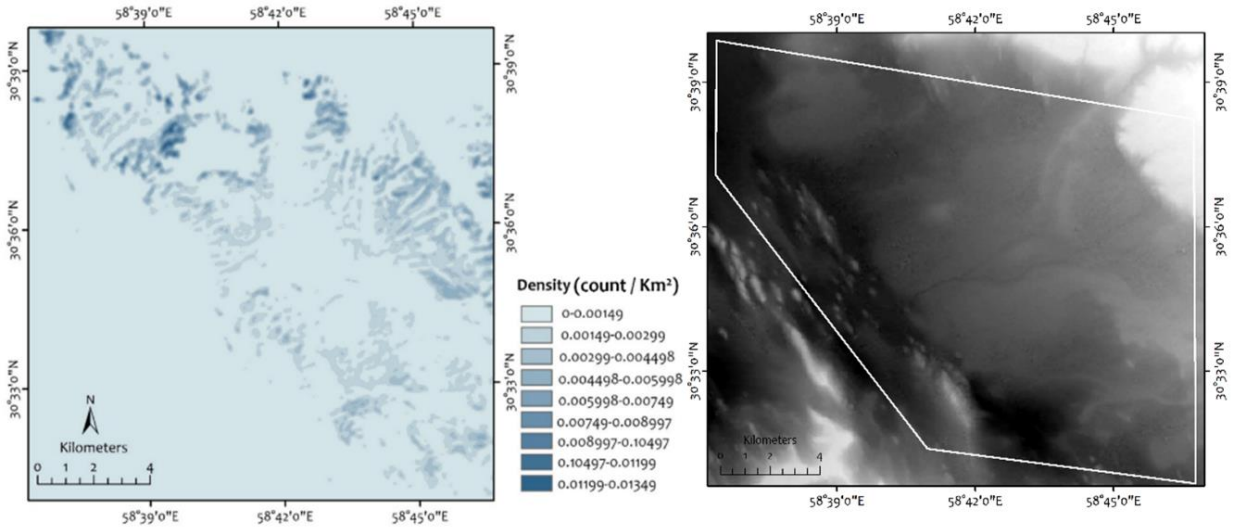

Figure 4.2. Density map of the study area and comparison to the 30m resolution SRTM DEM, which shows bedform density in this area is not controlled by topography. The white polygon shows border of the processed image (data).

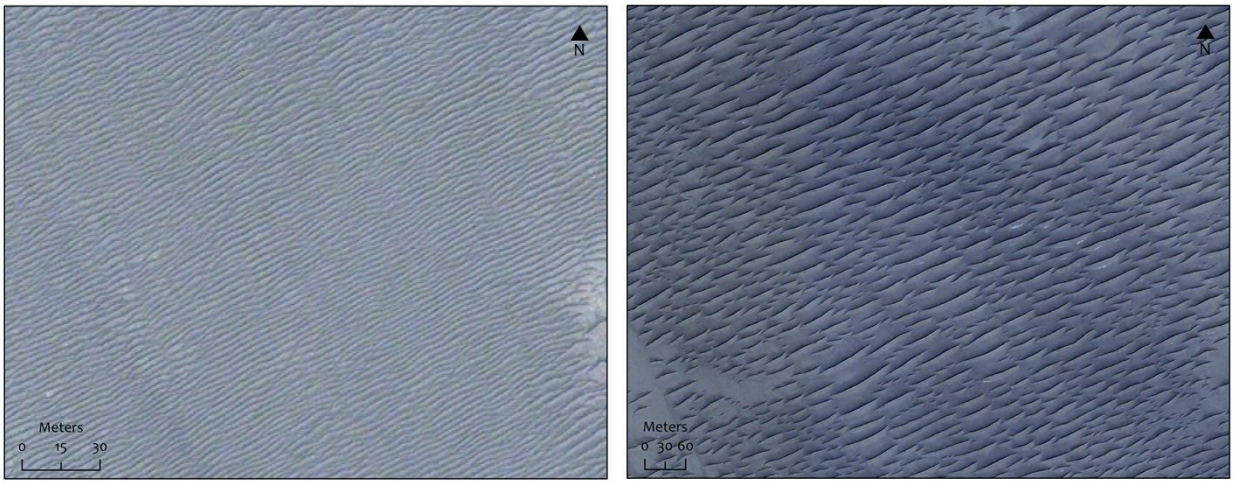

Figure 4.3. Saturated TAR-like features; left: northern part of the study area close to the yardang field; right: middle part of the study area at a relatively lower-elevation site. The scale of the left image is about 4 times larger than the right image, which shows features' different size.

Figure 4.4. Mirroring relationship with the bedrock, as well as the spectrum in the dimensions of the bedforms. Both demonstrate coarse grains occur in the northern region and the bedforms in this area are granular ripples.

We classified metrics using the extracted crestline map to identify the distribution of these metrics and recognize any relation they might have throughout the study area. Figure 4.5 illustrates the classified map and the probability distribution of the TAR-like features based on their crest length. Although different lengths for these bedforms can be found all over the study area, the map indicates longer features in the central parts of the individual patches and fields. However, a western trend for longer features is noticeable in the whole map. The longest features seem to be near small outcrops

and regions that are subject to concentrated winds or, in other words, topographic influence rather than being exposed to several wind directions. TAR-like features at the eastern side of the study area, without the protection and concentrating effect of winds on the yardangs, have short crest lengths. Furthermore, extra-long features, between 90 meters to 500 meters in crest length, are mainly located at the center of the site and in the middle of saturated patches and fields. The probability distribution of the crestline length shows that their length distribution is not normal, with an average value of about 7.21 meters and the standard deviation of 10.94 m. The crest lengths of about 80 percent of TAR-like features are less than 20 meters. Comparison to the crest length values of Martian TARs shows good agreement (Table 4.2).

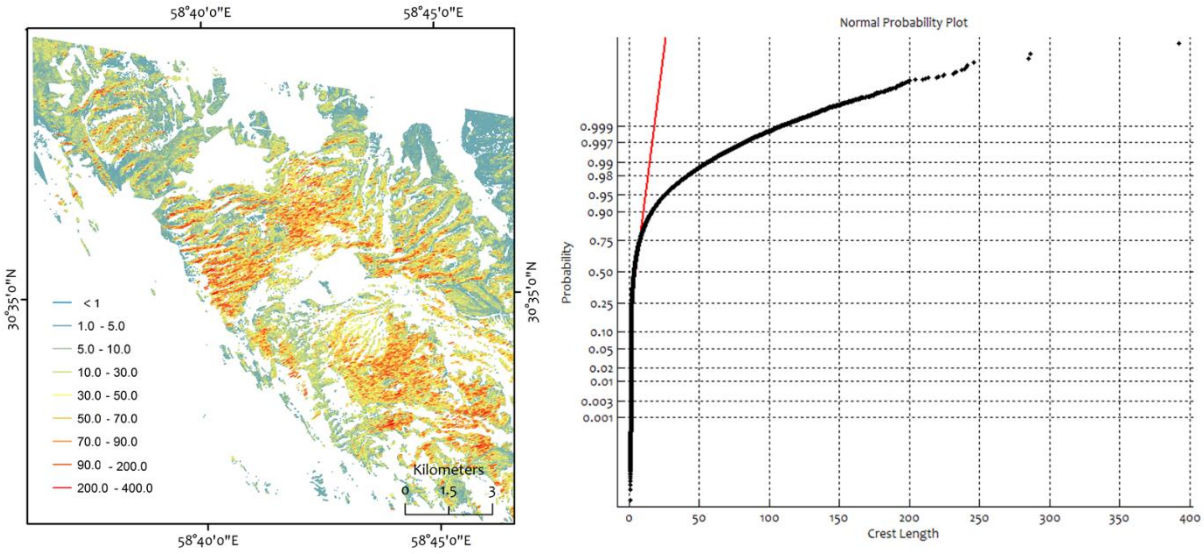

Figure 4.5. Classified crest length map of the TAR-like features and the probability distribution plot of this metric (black) comparing to the normal distribution (red).

A variety of different wavelength values can be found in the study area (Figure 4.6). As mentioned before, the lowest wavelength values for these features is in the dense northern part of the study area, ranging from less than two meters to tens of meters in the central saturated part. Average wavelength for barchan-like features in the north of the study area is about 2.5 m. Other parts of the site contain diverse wavelength values, from small saturated patches with about 5 meters up to hundreds of meters for features that can be identified as singly or widely spaced bedforms. Individual TARs exist in this site with a different spatial pattern, as observed on Mars (Balme et al., 2008). Comparing length and wavelength maps shows that there is a correlation between the longer features

and larger wavelengths in this area. There is a gradual increase in the length and the wavelength of these features along the main prevailing wind direction in each patch. This means that the features in the southern part of the patches have longer crestlines and wavelengths in comparison with northern features. The probability distribution of this metric shows that about 90 percent of these features have wavelengths of less than 10 meter (Figure 4.6).

The bedform orientation for the whole area has been illustrated in Figure 4.7 It can be concluded from the map that there is a change in the trend in orientation from northwest to southeast. In addition and apart from some influences of topography in some patches, the normal probability plot shows that there are different groups of orientation in this area. These orientation groups may indicate different stages of sedimentation. The influence of prevailing wind direction in different periods of time may suggest age and orientation differences in these bedforms. The diversity of wind patterns in this area will be discussed in the next section. The bedform trend of <45 degrees in the northwest part of the study area is close to the current yardang orientation. The slight difference in the orientation of the features could be a result of yardang evolution. The normal distribution graph of discussed metrics is illustrated in Figure 4.S2.

It is worth mentioning that one of the most important differences between the Lut bedforms and Martian TARs is the lack of bifurcation or branching, the same as features in Puna. The mechanism responsible for bifurcation has not been identified; however, Tanner (1967) hypothesized that it might reflect the sediment surface slope or elevation differences, which is rare in our study area.

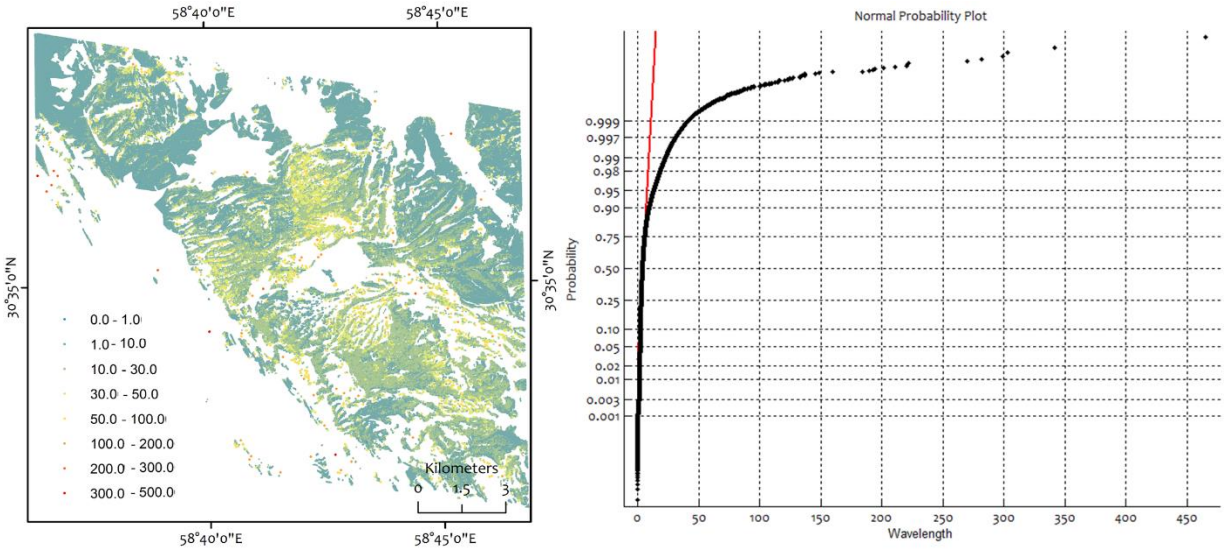

Figure 4.6. Classified bedform's wavelength in the Lut desert and the probability distribution plot of this metric (black) comparing to the normal distribution (red).

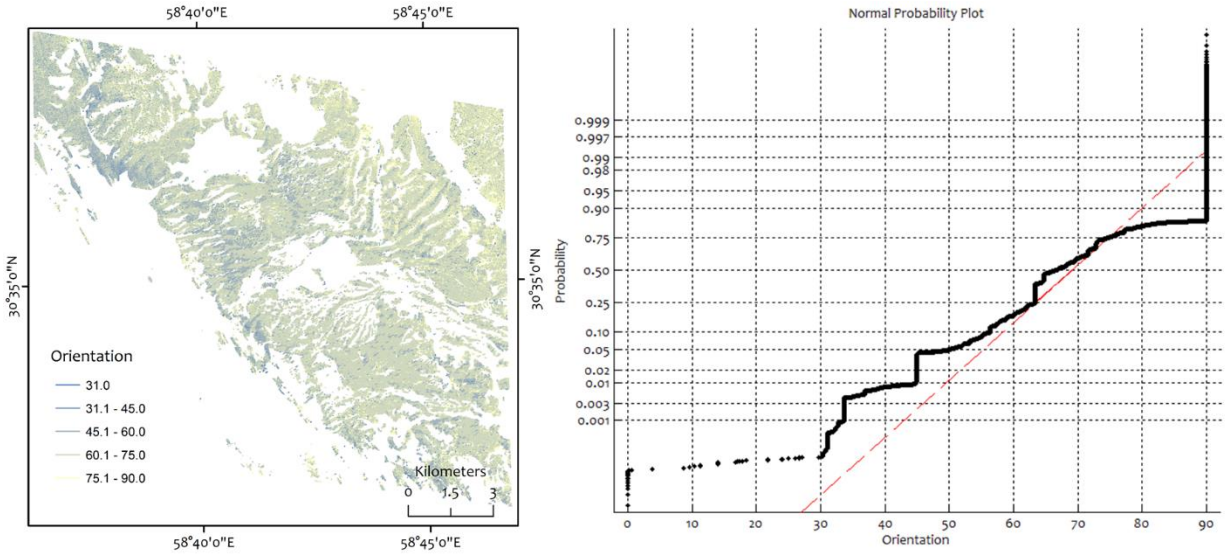

Figure 4.7. Bedform orientation in the study area and the probability distribution of the orientation (black) comparing to the normal distribution (red).

4-4-1-2- METRICS ON MARS WITH LARGE SAMPLE SIZE AND COMPARISON TO EARTH

Manually extracted height and width values of about 2000 features, by photoclinometry, on Earth show the highest features about 3.2 meters with a mean of about 0.5 meters. The exact minimum value of height cannot be extracted with the resolution of our satellite images (0.5 m); however, surface photos from the site show mega-ripples of about 10 cm as the shortest type. The maximum width of these features is about 25 meters with a mean of about 5 meters. Comparison between the metrics of these features showed that the tallest TAR-like features have wavelengths of about 50 meters and the smallest features are located in the saturated northern region. Nevertheless, for well-developed high-density TARs in the central part of the area, the wavelength is around 10 meters.

Table 4.2 shows a summary of metrics for Martian TARs obtained by different methodologies from previous studies, compared to our results from HiRISE DTMs, which shows almost the same range of the metrics in wavelength and length, and different ranges for height and particularly width. Height scaled by width previously has been evaluated as an important parameter for determining the origin of aeolian bedforms (Zimbelman et al., 2012). Figure 4.S3 illustrates this graph for bedforms in the Lut desert and two other terrestrial analogs (de Silva et al., 2013; Zimbelman et al., 2012), as well as data from Martian TARs studied by Shockey and Zimbelman (2013) and the metrics extracted in this study from 14 Mars DTMs. Results show a partial overlap (less than 50%) of Martian TARs both from the DTM results, and previously published data, with the Lut bedforms. Figure 4.S4 also illustrates the difference in some features in the Kaiser crater compared to other regions.

Table 4-2. Morphometric parameters of Martian TARs from different studies. Single values represent the average of the metric.

Source	***Sample size***	**H (m)**	**L (m)**	**W (m)**	λ (m)
Zimbelman (2000)	48	<1.5	80	11	35
Williams et al. (2002)		5.7	-	-	38
Bourke et al. (2003)	-	-	<100–700	-	-
Wilson & Zimbelman (2004)	<340	1-3	215	-	40
Bourke et al. (2006)	-	1-7.8	-	-	-
Balme et al. (2008)	-	-	<10-500	-	10-80
Zimbelman (2010)	12	1-8		7-45	7--100
Shockey and Zimbelman (2013)	60	2.3	-	22.6	-
Current Study	**2000<**	**0.2-12.5**	**13-610**	**1.5-195**	**5-210**

A closer look at the differences between Mars and Earth features on this graph in Figure 4.8 can show different conclusions. First, compared to the previous studies, the range of TARs width is significantly changed from less than 2 to about 200 meters and height to width ratio also seems to have a limitation of 0.5 on Mars (Figure 4.S3). Second, there is a clear difference between the range of width of TAR-like features on Earth and TARs on Mars. The significant relationship of aeolian bedform width to sediment availability may suggest different environmental conditions for these features on Earth and Mars. An abundance of aeolian processes, the dry conditions of Mars and availability of sediment material in any size range influences the morphometry of features and, as a result, expecting the same metrics for these features on both planets seems unrealistic. Distribution differences of 4 different metrics of TARs and TAR-like features and their comparison is illustrated in Figure 4.9, which emphasizes the difference in mean and distribution of parameters (i.e., stronger for width) of these features on both planets.

The correlation between metrics of the Lut TAR-like features is shown in Table 4.3. It can be deduced from the table that the correlation between TAR-like features' metrics are too strong for all parameters, while on Mars width and height are the only two parameters with considerable correlation. Also, comparative T-test results for Earth and Mars TARs can be found in Table 4.S2.

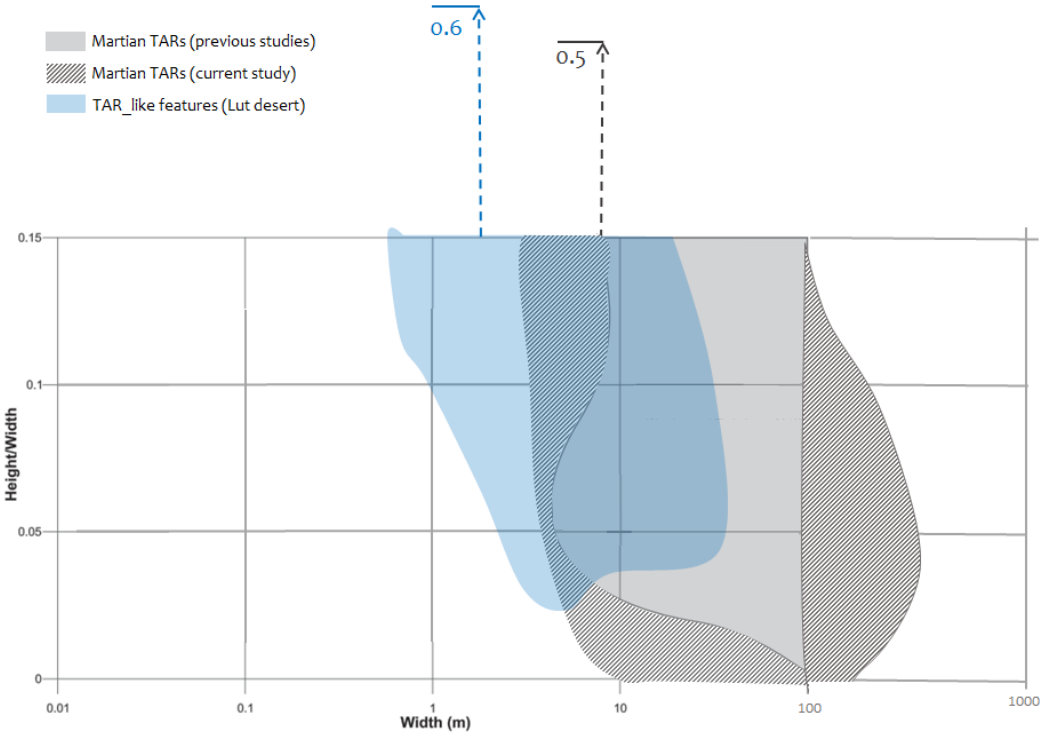

Figure 4. 8. Feature height scaled by width, shown as a function of feature width using a logarithmic scale, which shows partial overlap with new data extracted from HiRISE DTMs and also previous extracted data from Mars. Modified from de Silva et al., 2013.

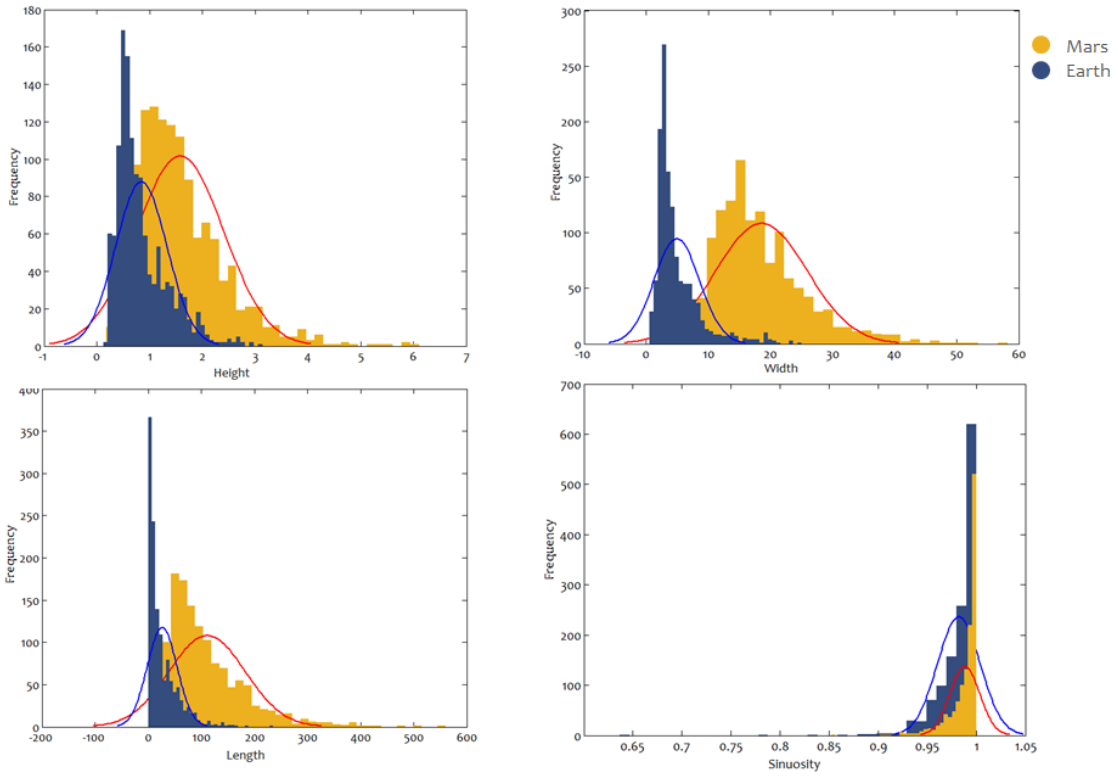

Figure 4.9. Distribution of morphometric parameters for TARs on Earth and Mars.

Table 4-3. Correlation between morphometric parameters on Earth and Mars.

	Crest length		Width		Height
Crest length	1				
Width	0.722	0.434	1		
Height	0.780	0.280	0.870	0.666	1
	Earth	Mars	Earth	Mars	

4-4-2- WIND ACTIVITY AND FEATURE EVOLUTION

4-4-2-1 WIND ACTIVITY IN THE LUT DESERT

The climatic condition of the Lut desert is harsh and it has been characterized as a hyper-arid desert (Ehsani and Queil, 2008). The closest weather station is about 80 km from the west side of the study area and the yardang field. Data from this station shows the annual rainfall is less than 10 mm, with the average mean daily temperature ranging from 11° to more than 40°C and the average annual wind

speed is more than 6 m/s. The strongest winds start in April with an average speed of more than 10 m/s. The prevailing wind in the area is known as the "wind of 120 days", which runs from NNW to SSE. It starts gradually in April and blows during the summer months and decreases during September. Figure 4.10 shows the wind record for 20 years in this region, which suggests the main geological process for yardang initiation and evolution.

The wind of 120 days, which is the strongest type of wind in this area, originates from the pressure gradient between the cold high-pressure system over the Hindu Kush Mountains and the summertime thermal low pressure typical system over the desert areas of eastern Iran and western Afghanistan. The wind is then strengthened by the channeling effect of the topography surrounding the region (Alizadeh-Choobari et al., 2014). Another originating area for this wind is proposed to be the Caspian Sea high pressure system at the north of Iran and also other less intensive high pressure systems in the north of Iran have been detected for these kinds of winds in different studies (e.g. Hamidian Pour et al., 2016). This wind gradually becomes hot throughout its path to south-east Iran, which affects the pressure gradient and intensifies the strength. We believe that the amalgamation of both regional and local sources initiate and intensify these types of winds in the Lut desert, which makes it so critical for surface modification and extensive dust storms.

The wind rose of this area has been extracted using the AWS Truepower's MesoMap® system (Figure 4.10 and Figure 4.55). In addition, data from the closest (Ziyaratgah-e Deh-Seif) and further (Zabol) weather stations show that there is a trend of more than one directional or bi-directional winds in the areas that are closest to the yardangs and relatively multi-directional winds farther from yardangs. The TAR-like features crestline map of the whole area confirms that stronger unidirectional or bi-directional winds can make ripples grow in length and wavelength. Star dunes at the south end of the study area and barchans at the southeastern end of the site show diverse types of winds in regions that are less protected and influenced by yardangs. Finally, available meteorological data as well as bedform symmetry can imply a periodic bimodal wind is responsible for formation and evolution of TAR-like features in the Lut desert, which can confirm previous suggestions of bimodal winds that are responsible for TARs formation.

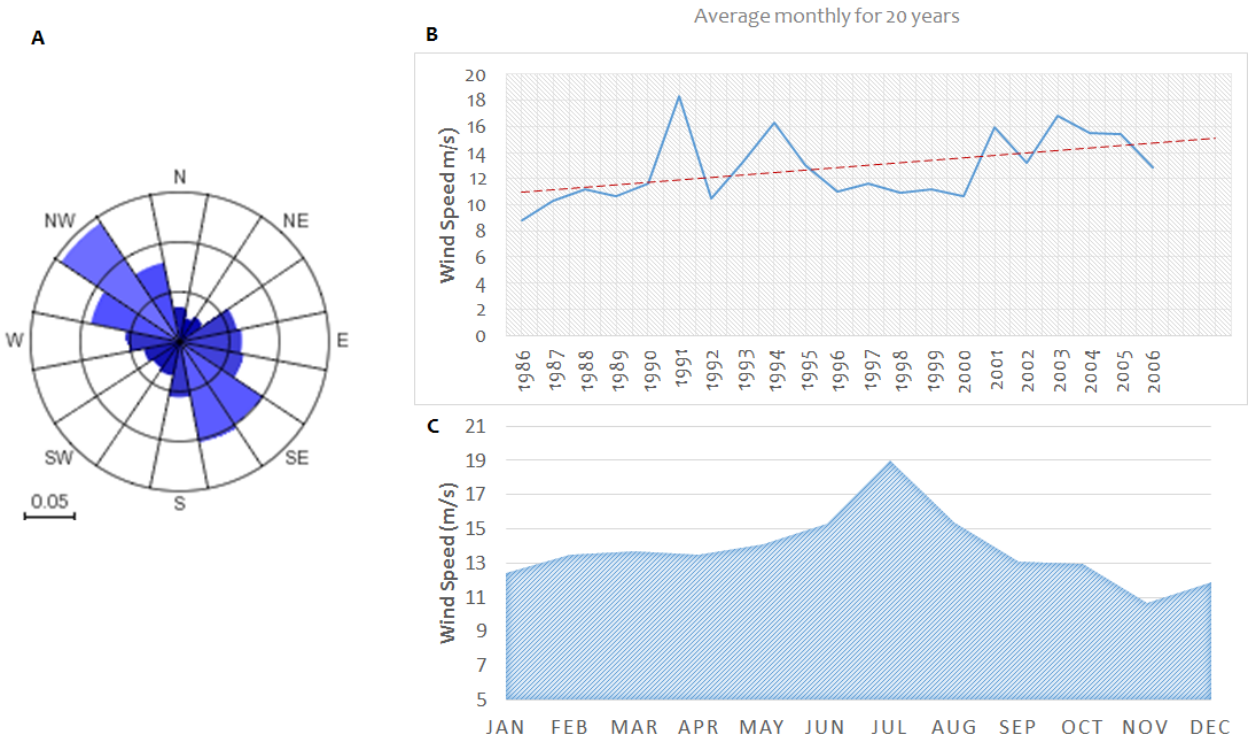

Figure 4.10. A) Wind rose of the study area in the Lut desert, extracted from AWS Truepower's MesoMap® system. B) Wind speed change during 20 years, which indicate an increasing trend during these years. C) Average monthly wind speed for 20 years data of this area (data from 'Ziyaratgah-e Deh-Seif" weather station).

4-4-2-2 EVOLUTION OF AEOLIAN FEATURES

Gradually from northwest to southeast the TAR-like features disappear and some different dune shapes become recognizable. The overall assessment of changes of aeolian features in the study area, through multi-temporal images and resulting change detection maps, show that most TAR-like features did not change or move during the eight-year period (2004-2012) covered by the images. However, some exceptions may shed light on the mystery of TARs on Mars. TAR-like features in the southern part of the study area, which are juxtaposed with active sand dunes, or ones that are pretty close to the yardang field, are the exceptions that have migrated during the study's timeframe. It may be expected that the migration direction of all aeolian features to be the same throughout the study area; however, this is not the case in this region. Although barchans could be a signature of unidirectional wind in the southern part of the study area, and a few TAR-like feature close and in between them have moved to the southeast, the same as barchan dunes (Figure 4.11). In contrast, we found that some parts of the study area have TAR-like features that clearly have moved in the opposite

direction to that of the sand dunes, with up to 2 meters migration during the eight years. These features are mostly in the northern part of the study area and near the yardangs fringe. There is another group of TAR-like features just before barchan dunes that have moved. The migrating TAR-like features make up less than 5% of the total number of features. Our preliminary study of the color and albedo of TAR-like features also indicate a difference between the albedo of stable and migrating features.

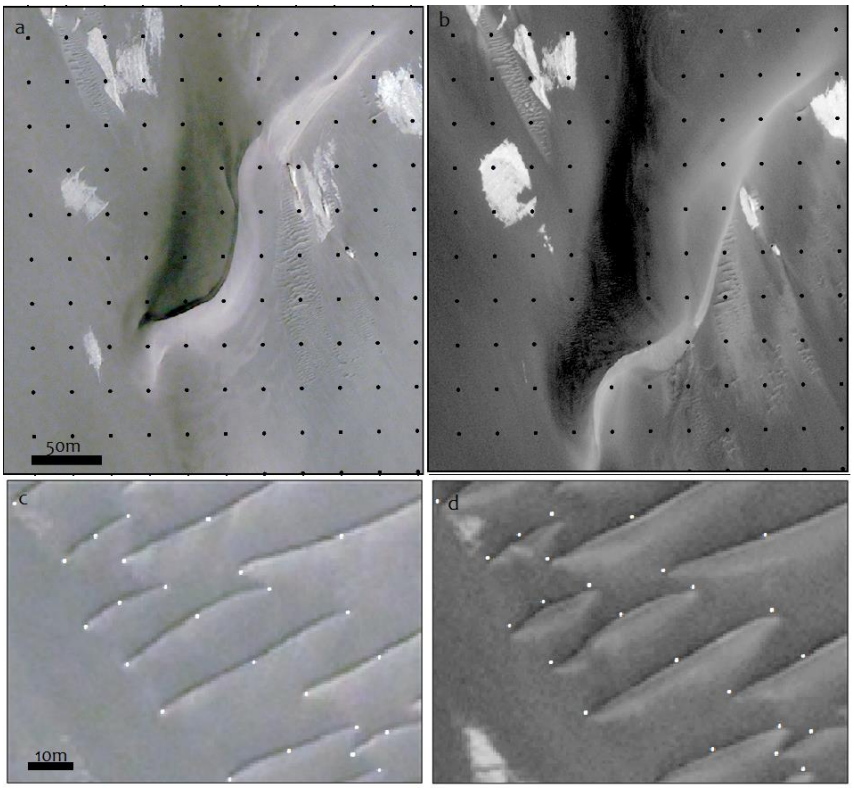

Figure 4. 11. a & b) Barchan dune movement in the south part of the study area. The spots indicate co-registered geographical points in both images. (left 2004, right 2012); c & d) change and migration of close TAR-like features in the same direction as well. The spots on both images show location of defect and middle points of the features in 2004. (left 2004, right 2012).

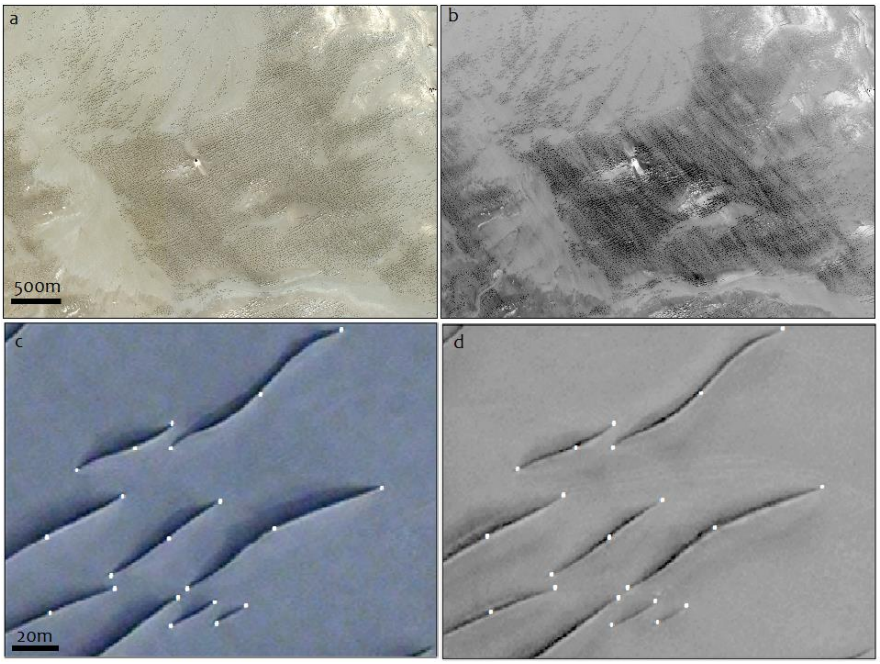

Figure 4 12. a & b) DDT formation and change in the middle part of the study area (left 2004, right 2012); b & c) TAR like features in this area had not moved during the study period. The spots on both images show location of defect and middle points of the features in 2004. (left 2004, right 2012).

Multi-temporal images in this region show DDTs overlying TAR-like bedforms (Figure 4.12). DDTs in this area can be classified as 'continuous dark' based on the DDT classification scheme of Reiss and Lorenz (2016). Formation of these DDTs is initiated by dust layer removal and they fade gradually, which implies that dust settling onto the surface demolishes the tracks (e.g., Malin and Edgett, 2001; Cantor et al., 2006; Greeley et al., 2010). DDTs in the Lut desert can be observed up to a width of 130 meters on TAR-like bedforms, which is much wider than DDTs that have been studied on Mars (Verba et al., 2010; Reiss and Lorenz, 2016). DDTs show different widths, lengths and directions in the study area; however, their length seems to be limited to the central bedform field dimensions, which based on our measurements, is up to 2.5 km. The concentration of DDTs on TAR-like bedforms confirms the idea by Greeley et al., (2005) and also terrestrial analog studies by Reiss et al. (2010), that the albedo difference between the DDTs and its background is related to the exposure of larger grain sizes within the track area (Reiss et al. 2016). Furthermore, they just exist on immobile TAR-like features. However, because DDTs are short-lived features and lots of unknown factors affected them, makes them very unpredictable and tricky to interpret based on changing morphology. Nevertheless, their changes can be a sign of a highly active aeolian environment.

We can divide the Lut TAR-like bedforms into four different groups. The first group consists of TAR-like features at the northwest end of the site near yardangs and ventifacts with dark sediments and migration to the northwest. They have small wavelengths, shorter and more sinuous forms and are very similar to bedforms in Meridiani Planum. The second group contains more than 95% of TAR-like features in the area that did not show any change during our study timeframe, have the darkest sediments compared to other groups and have DDTs overlying them with different wavelengths and include bedforms with the largest metrics. The third group are the features almost at the south-east edge, with light sediments and migrating to the south-east toward the dunes. Most of the features in this group have the entire feature replacement rather than change in form and sinuosity. The fourth group are the ones close to and in between barchans at the southeast of the area, which have the lightest sediments. Features in this group have some changes in their sinuosity, in contrast to the previous group, as well and some of them have migrated and align with the barchans to the southeast. This group contains a unique pattern of bedforms called 'raked pattern TARs' which have been described by Foroutan and Zimbelman (2016).

One interesting observation in the fourth group is the initiation of some small TAR-like features in the form of the raked pattern, although we didn't observe any change in the raked pattern TARs that existed from 2004 to 2012. These features are surrounded by sand sheets and suggest that TARs' initiation and formation might be affected by finer grain materials.

Apart from salts that have been recognized in between many of these features, some of the TAR-like bedforms in the study area that are close to fluvial features covered by lighter deposits. This transformation makes their morphology different, including lighter albedo, rougher texture, blunt crests and serrated edges (Figure 4.13). These features may be similar to TARs interpreted to be dust deposits in Syria Planum on Mars, previously identified by Geissler (2014). Geissler concluded that the Martian deposits built up vertically over time from dust and sand carried across the surface by horizontal winds. Our observations in the Lut desert implies that such features may be buried TARs that have been covered by other lighter deposits, probably salt. Based on the fact that these types of bedforms have been found near a fluvial landform, we believe that an induration mechanism may be responsible for the creation of this kind of bedform on Mars.

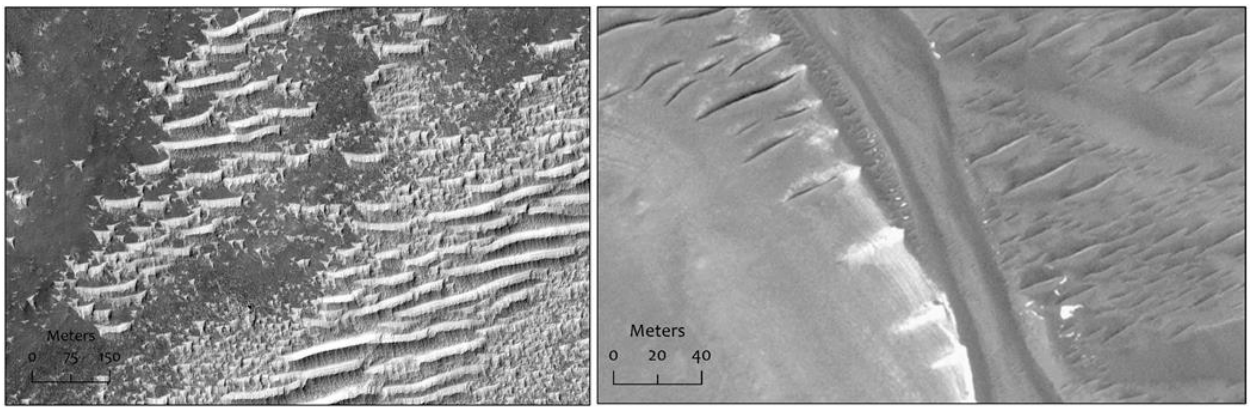

Figure 4.13. Right: Buried TARs in the Lut desert seems to be similar in morphology to the features (left) that have been identified by Geissler (2014) as dust deposits in Syria Planum on Mars (HiRISE,ESP-042124-1665).

4-5- CONCLUSION

TAR-like features in the Lut desert of Iran have been mapped using the ANN semi-automatic method and the morphometry of more than 2 million of these bedforms have been extracted and evaluated in this study. In addition, height and width of about 2000 of these bedforms have been extracted manually. Also in order to acquire sufficient sample size of Martian TARs for comparison, about 2000 Martian TARs have been examined manually using publicly released HiRISE DTM. We studied these factors to identify the relationship between metrics, for comparison to Martian TARs and to define controlling factors. Furthermore, this research also includes a multi-temporal study of aeolian features at the Lut desert study site.

Classified maps of the metrics in the Lut desert show there is a correlation between locations which contain features with longer crest lengths and larger wavelengths. In addition, orientation mapping of these bedforms shows a grouping in their orientation. Orientation differences exist between bedforms that are in juxtaposition with abrasion features and under the effect of strong winds strengthened by yardangs, compared to those in the most mature areas farther from yardangs. Wind data from the closest weather station show a slight change in the wind direction and speed during the 20 years of data examined here, which could be a reason that the orientation grouping in this area may be related to their age. Some of these bedforms near fluvial features seem to be buried by salts and could be considered as a terrestrial analog for what has been identified in Syria Planum as wind-sculpted dust deposits. The Lut features may have the same formation mechanism as the eroded TARs described on Mars by Geisler (2014).

TAR-like features in the study area change and migrate in two opposite directions, which is an indicator of a dominant bi-directional wind regime. Although the known prevailing wind is NNW-SSE, the response of bedforms with different grain size and orientation can be different within the same wind regime. A regional classification exists in this area among TAR-like features regarding their color (or albedo), proximity to abrasion features, migration rate, orientation, overall dimension and relative albedo. Results show that the Lut depression contains four different TAR-like features:

i) TAR-like features in the northwest of the depression, close to the yardangs and ventifacts, have darker sediments which seem to be composed of larger sediments than in other parts of this desert. Migration in the northwest direction of up to 2.5 meters was documented during 8 years of available image coverage. Bedforms with different sizes and metrics may be included in this group, but these other features are relatively small and do not represent the features with the maximum metrics.

ii) TAR-like features in the central part of the study area, which can be defined as 'mature', represent more than 95 percent of the bedforms in this study. They are mainly long features and include bedforms with maximum metric values. These bedforms are completely immobile and can be considered to be the bedforms that are at the lowest part of the site. DDTs (dust devil tracks) are clearly superposed on the TAR-like features in this area and they have the darkest sediments in the area.

iii) TAR-like features before the sand dune region with relatively lighter sediments had migration to the southeast but didn't have any change in their sinuosity; instead, they underwent an entire feature replacement during the study's timeframe.

iv) TAR-like features that are in between and close to barchan dunes in the south part of the study area include what has been called 'raked pattern' TARs (Foroutan and Zimbelman, 2016). These features have the lighter sediments than others within the study area and may contain finer sediments in comparison to the other two groups. These features move in the same direction as the nearby barchans. They have displayed more changes in their sinuosity during the 8-year study relative to the first and third class of features. Initiation of TAR-like features is observed just in this group in the form of the raked pattern.

The comparison of the metrics of these features to other terrestrial analogs and to previously published results for Martian TARs, along with results from HiRISE DTMs, doesn't indicate a complete overlap between the Lut features and TARs on Mars. The range of width for features on Earth and

Mars have stronger differences, which implies their different environment based on sediment availability. Based on this comparison, it has been recognized that TAR-like bedforms in the Lut desert should be the best analog for simple TARs on Mars. However, we conclude that there is no terrestrial analog yet for TARs displaying bifurcation and branching, such as 'forked' and 'feathery' TARs (Balme, et al., 2008). We suggest that the bifurcated type of TARs seems to be unique to Mars. Additional studies with a larger sample size need to be done regarding to this unique type of feature.

4-6- REFERENCES

Alizadeh-Choobari, O., Zawar-Reza, P., & Sturman, A. (2014). The "wind of 120days" and dust storm activity over the Sistan Basin. Atmospheric Research, 143, 328-341.

Bagnold, R.A., (1941). The Physics of Blown Sand and Desert Dunes. Chapman and Hall, London.

Baker, V. R. (2014). Terrestrial analogs, planetary geology, and the nature of geological reasoning. Planetary and Space Science, 95, 5-10.

Balme, M., & Greeley, R. (2006). Dust devils on Earth and Mars. Reviews of Geophysics, 44(3).

Balme, M., Berman, D.C., Bourke, M.C., et al., 2008. Transverse aeolian ridges (TARs) on Mars. Geomorphology 101 (4), 703–720.

Berman, D.C., Balme, M.R., Rafkin, S.C., et al., 2011. Transverse aeolian ridges (TARs) on Mars II: distributions, orientations, and ages. Icarus 213 (1), 116–130.

Bourke, M.C., Wilson, S.H., Zimbelman, J.R., 2003. The variability of TARs in troughs on Mars. LPSC XXXIV [CDROM] Abstract # 2090.

Bourke, M.C., Balme, M.R., Beyer, R.A., Williams, K.K., Zimbelman, J.R., 2006. A comparison of methods used to estimate the height of sand dunes on Mars. Geomorphology. 81(3-4), 440-452.

Bridges, N.T., Geissler, P., Silvestro, S., and Banks, M., 2013, Bedform migration on Mars: Current results and future plans: Aeolian Research, v. 9, p. 133–151, doi:10.1016/j.aeolia.2013.02.004.

Bridges, N. T., Spagnuolo, M. G., de Silva, S. L., Zimbelman, J. R., & Neely, E. M. (2015). Formation of gravel-mantled megaripples on Earth and Mars: Insights from the Argentinean Puna and wind tunnel experiments. Aeolian Research, 17, 49-60.

Cantor, B. A., Kanak, K. M., & Edgett, K. S. (2006). Mars Orbiter Camera observations of Martian dust devils and their tracks (September 1997 to January 2006) and evaluation of theoretical vortex models. Journal of Geophysical Research: Planets, 111(E12).

Chojnacki, M., Johnson, J. R., Moersch, J. E., Fenton, L. K., Michaels, T. I., & Bell, J. F. (2015). Persistent aeolian activity at Endeavour crater, Meridiani Planum, Mars; new observations from orbit and the surface. Icarus, 251, 275-290.

de Silva, S., 2010, The largest wind ripples on Earth: Com- ment: Geology, v. 38, p. e218, doi:10.1130/G30780C.1.

de Silva, S.L., Spagnuolo, M.G., Bridges, N.T., et al., 2013. Gravel-mantled megaripples of the Argentinean Puna: A model for their origin and growth with implications for Mars. Geol. Soc. Am. Bull 125 (11-12), 1912–1929.

Dong, Z., Lv, P., Lu, J., Qian, G., Zhang, Z., & Luo, W. (2012). Geomorphology and origin of yardangs in the Kumtagh Desert, Northwest China. Geomorphology, 139, 145-154.

Ehsani, A.H., Quiel, F., 2008. Application of Self Organizing Map and SRTM data to Characterize Yardangs in the Lut Desert, Iran. Remote Sensing of Environment 112 (7), 3284-3294. doi: 10.1016/j.rse.2008.04.007.

Ellwood, J.M., Evans, P.D., Wilson, I.G. 1975. Small scale aeolian bedforms. Journal of Sedimentary Petrology 45: 554–561.

Fenton, L.K., Michaels, T.I., Chojnacki, M., 2015. Late Amazonian aeolian features, gradation, wind regimes, and sediment state in the vicinity of the Mars explo- ration rover opportunity, Meridiani Planum. Mars. Aeolian Res 16, 75–99.

Foroutan, M., 2015. Ripple-like features on mars, characteristics and classification. 2015 GSA Fall Meeting. Geological Society of America.

Foroutan, M., Zimbelman, J.R., 2016. Mega-ripples in Iran: A new analog for transverse aeolian ridges on Mars. Icarus 274, 99-105. doi: 10.1016/j.icarus.2016.03.025.

Foroutan, M., Zimbelman, J.R., (under Review). Semi-automatic mapping of linear-trending bedforms using ‘self-organizing maps’ algorithm. Geomorphology.

Geissler, P.E., 2014. The birth and death of transverse aeolian ridges on Mars. J. Geo- phys. Res.: Planets 119 (12), 2583–2599.

Golombek, M., Robinson, K., McEwen, A., Bridges, N., Ivanov, B., Tornabene, L., & Sullivan, R. (2010). Constraints on ripple migration at Meridiani Planum from Opportunity and HiRISE observations of fresh craters. Journal of Geophysical Research: Planets, 115(E7).

Greeley, R., Arvidson, R., Bell, J. F., Christensen, P., Foley, D., Haldemann, A., ... & Squyres, S. W. (2005). Martian variable features: new insight from the Mars Express Orbiter and the Mars Exploration Rover Spirit. Journal of Geophysical Research: Planets, 110(E6).

Greeley, R., Waller, D. A., Cabrol, N. A., Landis, G. A., Lemmon, M. T., Neakrase, L. D., ... & Whelley, P. L. (2010). Gusev Crater, Mars: Observations of three dust devil seasons. Journal of Geophysical Research: Planets, 115(E7).

Hamidian Pour, M., Mofidi, A., Salighe, M. (2016). Analysis of the nature and structure of Sistan wind. Iranian Journal of Geophysics, 10 (2).

Jessar, A.D., Zimbelman, J.R., Hennig, L.A. (2015). TARs on Mars: A study of the spatial variability and physical characteristics of Martian Transverse Aeolian Ridges. Fourth International Planetary Dunes Workshop. Abs# 8022.

Lorenz, R. D., & Zimbelman, J. R. (2014). Dune Worlds. Springer Berlin Heidelberg.

Maghsoudi, M., Hajizadeh, A., Nezam, M. M. A., Bayati, S. Z. (2015). Assessment of paleo environmental conditions of ovoid yardangs using granolumetry. Geographical Data 24, 51-64.

Malin, M. C., & Edgett, K. S. (2001). Mars global surveyor Mars orbiter camera: interplanetary cruise through primary mission. Journal of Geophysical Research: Planets, 106(E10), 23429-23570.

Murphy, J.D., 1973. The Geology of Eagle Cove at Bruneau, Idaho. M.S. Thesis, State Univ. New York at Buffalo. 77p.

Reiss, D., Raack, J., Rossi, A. P., Di Achille, G., & Hiesinger, H. (2010). First in-situ analysis of dust devil tracks on Earth and their comparison with tracks on Mars. Geophysical Research Letters, 37(14).

Reiss, D., & Lorenz, R. D. (2016). Dust devil track survey at Elysium Planitia, Mars: Implications for the InSight landing sites. Icarus, 266, 315-330.

Sakamoto-Arnold, C.M. 1988. Eolian features produced by the December 1977 windstorm Southern San Joaquin Valley, California. Journal of Geology 89: 129–137.

Sharp, R. P. (1963). Wind ripples. The Journal of Geology, 617-636.

Shockey, K.M., and Zimbelman, J.R., 2013, Analysis of transverse aeolian ridge profi les derived from HiRISE images of Mars: Earth Surface Processes and Land- forms, v. 38, p. 179–182, doi:10.1002/esp.3316.

Spagnolo, M., Clark, C. D., & Hughes, A. L. (2012). Drumlin relief. Geomorphology, 153, 179-191.

Sullivan R, Banfield D, Bell JF, Calvin W, Fike D, Golombek M, Greeley R, Grotzinger J, Herkenhoff K, Jerolmack D, Malin M. (2005). Aeolian processes at the Mars exploration rover Meridiani Planum landing site. Nature, 436(7047), 58-61.

Tanner, W. F. (1967). Ripple mark indices and their uses. Sedimentology, 9(2), 89-104.

Verba, C. A., Geissler, P. E., Titus, T. N., & Waller, D. (2010). Observations from the high resolution imaging science experiment (HiRISE): Martian dust devils in Gusev and Russell craters. Journal of Geophysical Research: Planets, 115(E9).

Williams, S.H., Zimbelman, J.R., Ward, A.W., 2002. Large ripples on Earth and Mars. Lunar and Planetary Science XXXIII, 1508.

Wilson, S.A., Zimbelman, J.R., 2004. Latitude-dependent nature and physical characteristics of transverse aeolian ridges on Mars. J. Geophys. Res. 109, E10 0 03.

Yizhaq, H., Katra, I., 2015. Longevity of aeolian megaripples. Earth and Planetary Science Letters 422, 28-32. doi: 10.1016/j.epsl.2015.04.004.

Zimbelman, J.R., 2003. Decameter-scale ripple-like features in Nirgal Vallis as revealed in THEMIS and MOC imaging data. Sixth international conference on Mars, abstract 3028.

Zimbelman, J.R., R.P. Irwin, S.H. Williams, F. Bunch, A. Valdez, and S. Stevens, 2009. The rate of granule ripple movement on Earth and Mars, Icarus 203, 71-76, doi: 10.1016/j.icarus.2009.03.033.

Zimbelman, J.R., 2010. Transverse aeolian ridges on Mars: First results from HiRISE images. Geomorphology 121, 22–29.

Zimbelman, J.R., Williams, S.H., Johnston, A.K., 2012. Cross-sectional profiles of sand ripples, megaripples, and dunes: A method for discriminating between forma- tional mechanisms. Earth Surface Process. Landforms 37 (10), 1120–1125.

Zimbelman, J.R., Scheidt, S.P., 2014. Precision topography of a reversing sand dune at Bruneau Dunes, Idaho, as an analog for transverse aeolian ridges on Mars. Icarus 230, 29–37.

4-7 SUPPLEMENTARY MATERIAL

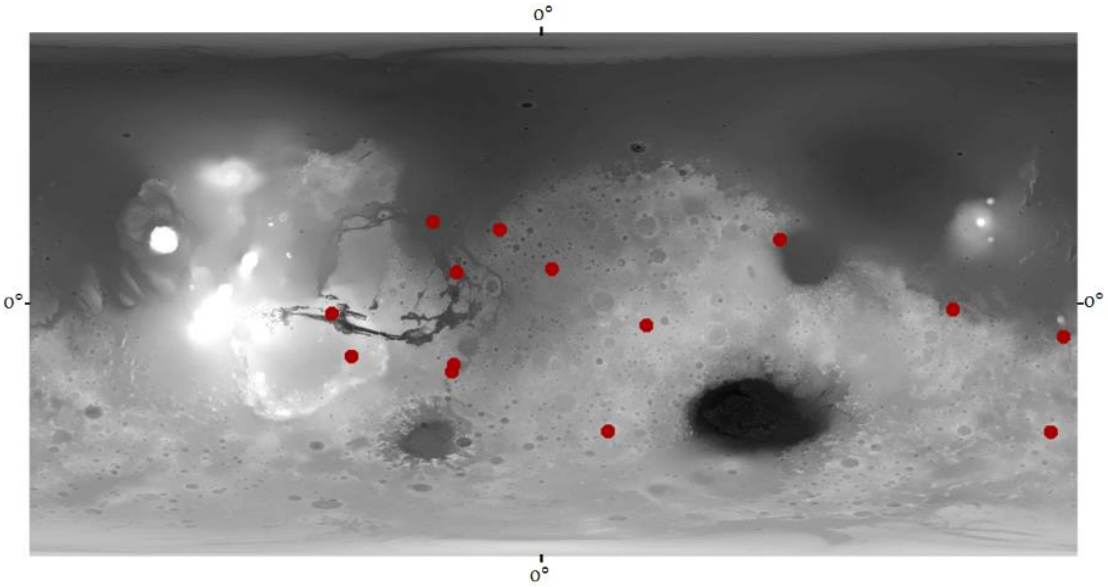

Figure 4.S1- location of studied HiRISE DTMS on Mars (Mola DEM base map).

Table 4.S.1- List of studied HiRISE DTMS.

No.	HiRISE DTM code number	Location on Mars
1	DTEEC_001336_1560_001534_1560_U01	Eberswalde Crater
2	DTEEC_001481_1875_002167_1880_U01	Mojave Crater
3	DTEEC_001488_1750_001752_1750_U02	Gale Crater Interior Mound
4	DTEEC_001513_1655_001777_1650_U01	Gusev Crater
5	DTEEC_001521_2025_001719_2025_U01	Chryse Planitia
6	DTEEC_001918_1735_001984_1735_U01	Southwest Candor Chasma
7	DTEEC_002047_1890_001902_1890_U01	Crater in Western Arabia Terra
8	DTEEC_002074_2025_002140_2025_U01	Mawrth Vallis
9	DTEEC_002088_1530_002154_1530_U01	Fan Surfaces in West Holden Crater
10	DTEEC_002353_1585_003408_1585_A01	Martin Crater
11	DTEEC_002387_1985_003798_1985_A01	Jezero Crater
12	DTEED_021688_1325_021754_1325_A01	Crater in Terra Cimmeria

13	DTEED_025240_1690_025728_1690_A01	Crater in Sinus Sabaeus
14	DTEEC_007110_1325_006820_1325_A01	Gullied Crater in Kaiser Crater Dune Field

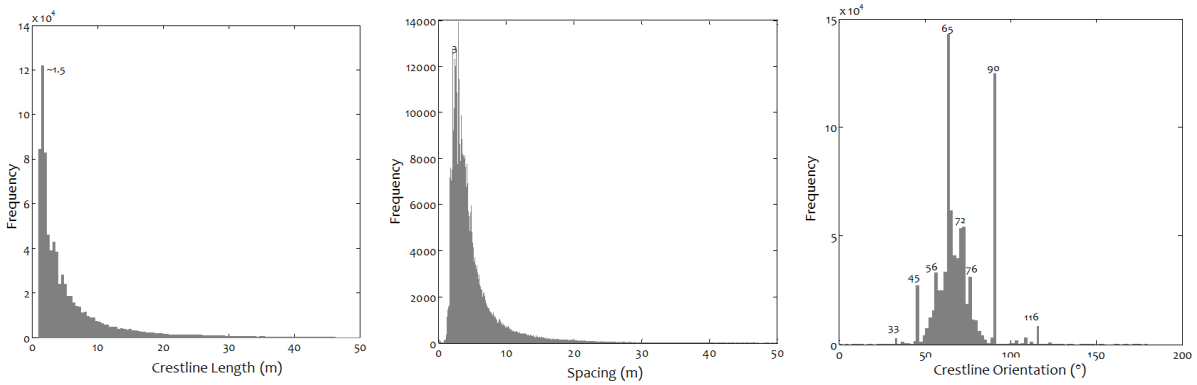

Figure 4.S2- Distribution of length, spacing and orientation of more than 2 million features in the Lut desert of Iran.

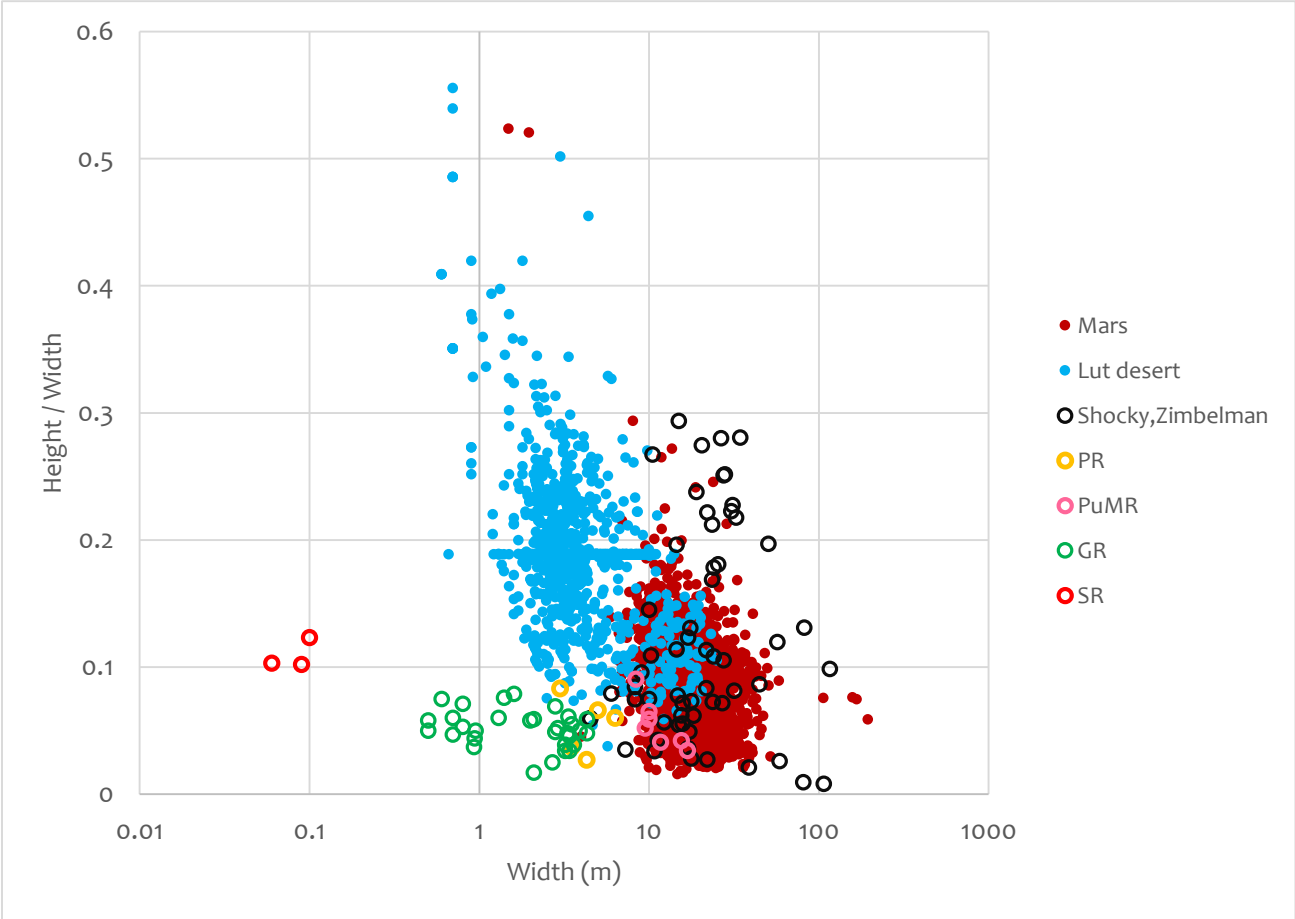

Figure 4.S3- The scatter plot of features' height scaled by width, shown as a function of feature width using a logarithmic scale, which shows good agreement with new data extracted from HiRISE DTMs and also previous extracted data from Mars. Mars and the Lut desert values (filled red and blue symbols) show the data from this study. PuMR: Punian Arganitina mega-ripples results (de Silva et al., 2013). SR: sand ripples; GR: granule ripples; PR: pebble ripples from Zimbelman et al., 2012. Shocky, Zimbelman: illustrates Martian TAR data from Shockey and Zimbelman (2013).

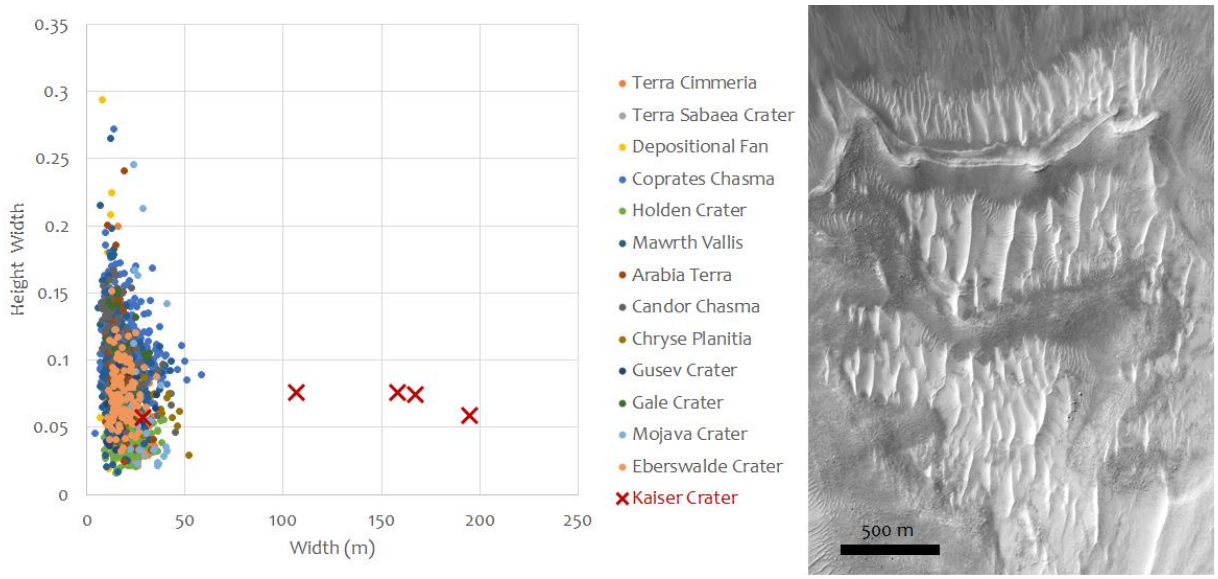

Figure 4.S4- Huge TARs in Kaiser crater and difference of their metrics comparing to other locations on Mars.

Table 4.S2- test of TARs morphometric parameters between Earth and Mars. Which demonstrates differences between metrics of TARs on Mars and TAR-like features on Earth. With significant difference of width. (Note: just data from this study have been considered in this analysis, otherwise difference between length parameter of these features are not that much when we consider all previous studies as well.)

Morphometric parameter				**Test statistics**		
	h	p-value	ci	tstat	df	sd
Height	1	4.8111e-145	-0.7868 -0.6817	-27.3895	2556	0.6779
Width	1	0	-14.0746 -13.1742	-59.3423	2556	5.8060
Height/Width	1	0	0.0961 0.1034	53.9948	2556	0.0467
Length	1	1.269e-263	-88.7906 -80.3313	-39.2027	2556	54.5473
Sinuosity	1	3.9005e-16	-0.0076 -0.0046	-8.1955	2556	0.0188

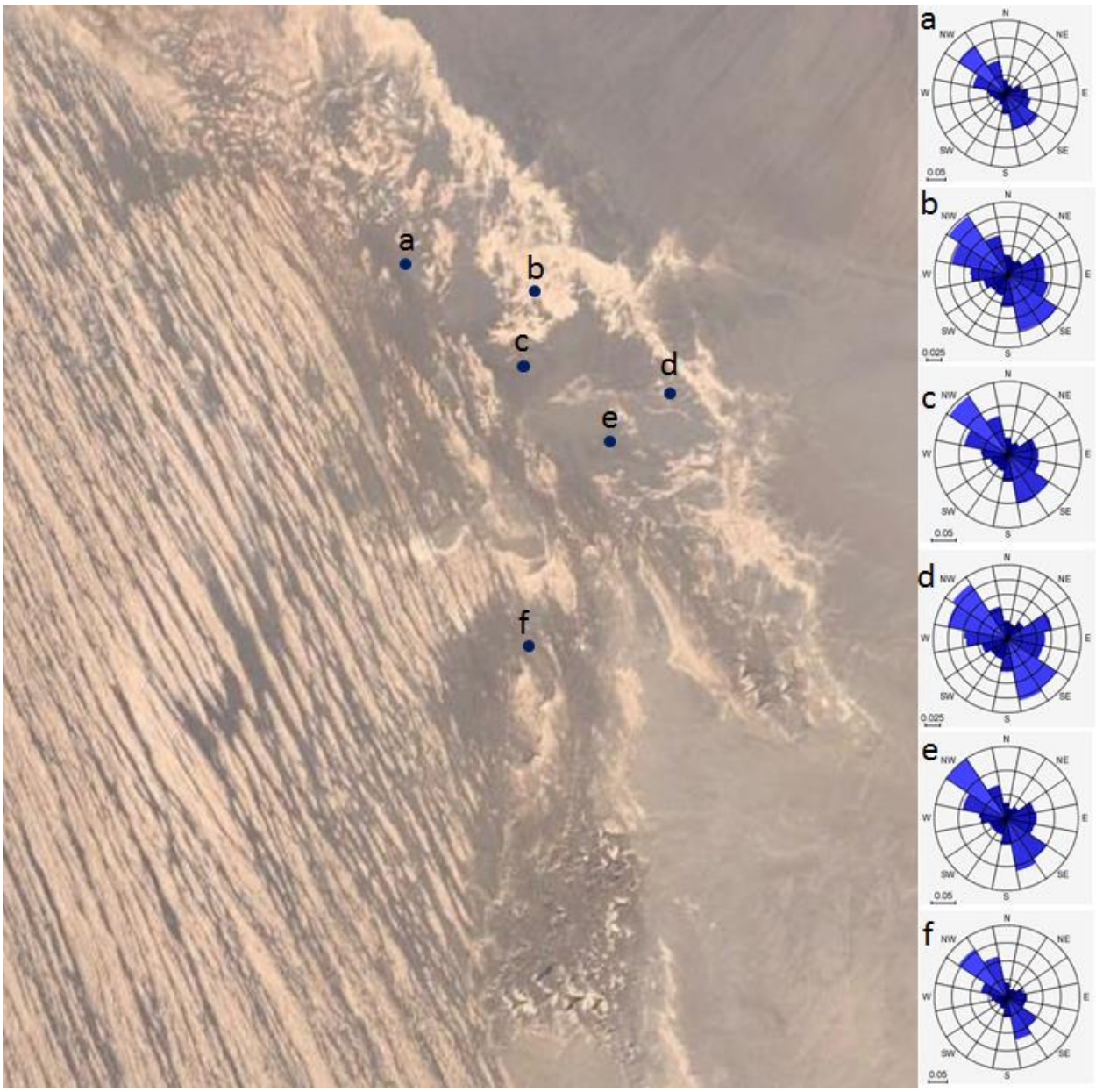

Figure 4.S5- Wind roses in different spots of the study area, have been extracted form using the AWS Truepower's MesoMap® system, which show there isn't a uni-directional wind regime in the study area.

CHAPTER 5

SUMMARY AND CONCLUSIONS

TARs are enigmatic aeolian bedforms on Mars. Being intermediate in size between sand dunes and mega-ripples on Earth makes it harder to find a viable terrestrial analog for TARs. In this research, we introduce a new site as a terrestrial analog of TARs, which is located in the middle of the Lut Desert in Iran. The TAR field in this area is in a huge depression of about 250 km^2 in between a field of mega-yardangs and a large sand erg. The TAR-like features at this location come in a variety of different classes based on a published TAR classification scheme (Berman et al., 2008). Various crestline morphologies, such as simple and barchan-like, and different populations such as saturated, singular, and widely spaced have been recognized in the Lut desert. The study of TAR-like features in this area shows that they have the same horizontal length-scale as most TARs on Mars. The Lut bedforms are surrounded by a Quaternary sand sheet and alluvial fan deposits, which are surrounded by salt-rich terrains. Some TARs are also found in the corridors between yardangs. The features are composed of a surface covering of sediments generally 3-4 mm in diameter. Based on superposition evidence, the TAR-like features in the Lut desert seem to be old relative to their adjacent features, consistent with the current lack of any documented movement for TARs on Mars (Bridges et al., 2013).

A new methodology for mapping small linear-trending features, such as TARs and ripples, has been introduced as part of this study. One of the restrictions in studying small linear-trending features in remote sensing data is their small footprint and difficulty of mapping many individual features. The semi-automatic Artificial Neural Network (ANN) method known as Self Organizing Maps (SOM), within the simple framework presented in this study, was conducted using high-resolution satellite images of Earth and Mars, in order to digitize the aeolian bedforms. An assessment of the accuracy of this method indicates its capability for providing a precise delineation between small linear features, such as TARs and ripples, and other morphologic features present in the satellite images. The network settings and layers were examined in order to define how accurately the maps captured the mega-ripple crestlines and outlines from the satellite images. This framework and module are applicable and adjustable to all types of images which contain linear features. The framework greatly facilitates image analysis using planetary remote sensing along with improving the accuracy of the final results. This technique is applicable to many different environmental management and geophysical issues, such as climate change, aeolian geomorphology, glaciology and even other disciplines outside of remote sensing.

The ANN mapping method was used for processing images from TAR-like features in the Lut desert of Iran. Morphometry of more than 2 million of these bedforms have been extracted and evaluated. In addition, height and width of about 2000 of these bedforms have been extracted manually using HiRISE DTMs on Mars and a similar number of World-view satellite images of Earth. We studied these factors for the identification of the relationship between metrics, comparison to Martian TARs, and defining geomorphological controlling factors. Correlation between bedform parameters on Earth is significantly higher that Martian bedforms. In addition, orientation maps and graphs of these bedforms show a grouping in their orientation. Orientation is different between bedforms that are in juxtaposition to yardangs compared to the ones located in the more mature areas farther from the yardangs. Some of these bedforms near fluvial features seem to be buried under salt and dust, which could be a terrestrial analog for what has been identified in Syria Planum on Mars as dust-related TAR deposits. TAR-like features in the Lut desert have different relations to the wind during the eight-year time span of multi-temporal images from the study area. Apart from the large number of static bedforms, the TARs that migrated have different directions of migration and degrees and forms of morphology alteration, and there seems to be a regional classification for these changes, which may be separated into four different classes.

The comparison of TAR-like features in the Lut desert to Martian TARs using the new semi-automatic mapping technique indicates a good agreement and overlap between the Lut features and TARs on Mars. The Lut bedforms may now be considered the best analog for simple TARs on Mars. However, we believe that there is still no terrestrial analog for TARs with bifurcation and branching, such as 'forked' TARs (Balme, et al., 2008) or 'centipede-shaped' TARs (Figure 1.2). We suggest that these types of TARs are unique to Mars. We hypothesise that forked and centipede-shaped TARs might have finer grain sizes than simple TARs. More studies need to be done in terrestrial analog areas, along with an expanded exploration for TARs on Mars, in order to understand these curious bedforms. We believe that our new terrestrial analog site and the innovative methodology applied here to map the bedforms have paved the way for further explorations of TARs on both Earth and Mars.

FUTURE WORK

The priority of this new analog site compared to previous areas suggests an extensive field study in the site in order to get more understanding about their evolution and composition. There is lots of information that we cannot get from the orbital data alone. Taking sediment samples for investigating their formation and differences throughout the study area is definitely a preference. In addition, regarding the lack of accurate wind data at the local scale, measuring the wind characteristics of the area would be very beneficial in studying these features. An investigation into the cross-sectional profile and structure of sediments in the features, as well as getting stereo images for more understanding of their size and shape would lead to a more rigorous outcome. Furthermore, application of drones for DTM extraction and 3D mapping of the area could be considered.

The raked pattern region (Group 4 in chapter 4) is a unique location for studying the evolution and origin of these enigmatic features. Examining more multi-temporal images should give us enough evidence to develop a hypothesis about the initiation and formation of TAR-like features, which might provide hints abut the formation of TARs on Mars. Also higher resolution satellite images are highly recommended throughout this site. The nature of this location with different active aeolian features could definitely improve our understanding about aeolian activity on Earth and Mars.

Regarding the technical part of the thesis, developing the current semi-automatic mapping technique to a completely automatic mapping module would be a laudable future goal. The framework introduced here was promising and applicable on all our available raster data, but we need to define every step in setting criteria for the module in order to make it much easier to use. Nowadays we have an extensive number of new high-resolution images from different satellites, planets and missions, such as images from New Horizons of Pluto, where enigmatic dunes have been described on some of the nitrogen plains (Stern et al., 2015), which is a big motivator for producing an adaptive module. This may be more easily achieved by applying a greater variety of satellite and airborne images and different target features with diverse density.

BIBLIOGRAPHY

Alizadeh-Choobari, O., Zawar-Reza, P., & Sturman, A. (2014). The "wind of 120days" and dust storm activity over the Sistan Basin. Atmospheric Research, 143, 328-341.

Allen, M., Jackson, J., & Walker, R. (2004). Late Cenozoic reorganization of the Arabia-Eurasia collision and the comparison of short-term and long-term deformation rates. Tectonics, 23(2).

Almeida, M.P., Parteli, E.J.R., Andrade, J.S., Herrmann, H.J., 2008. Giant saltation on Mars. Proceedings of the National Academy of Sciences. 105(17), 6222-6226.

Bagnold, R.A., 1941. The Physics of Blown Sand and Desert Dunes. Chapman and Hall, London.

Baker, V. R. (2014). Terrestrial analogs, planetary geology, and the nature of geological reasoning. Planetary and Space Science, 95, 5-10.

Balme, M., & Greeley, R., 2006. Dust devils on Earth and Mars. Reviews of Geophysics, 44(3).

Balme, M., Berman, D.C., Bourke, M.C., Zimbelman, J.R., 2008. Transverse Aeolian Ridges (TARs) on Mars. Geomorphology. 101(4), 703-720.

Barlow, N., 2008. Mars: An introduction to its interior, surface and atmosphere. Cambridge University Press.

Berman, D.C., Balme, M.R., Rafkin, S.C.R., Zimbelman, J.R., 2011.Transverse Aeolian Ridges (TARs) on Mars II: distributions, orientations, and ages. Icarus. 213(1), 116-130.

Berman, D. C, Michalski, J. R., Balme, M. R., 2015. Analyses of transverse aeolian ridges on mars. 46th Lunar and Planetary Science Conference Abstract #2210.

Bodansky, E., Gribov, A., & Pilouk, M., 2001. Smoothing and compression of lines obtained by raster-to-vector conversion. In International Workshop on Graphics Recognition (pp. 256-265). Springer Berlin Heidelberg.

Bourke, M.C., Williams, S.H., Zimbelman, J.R., 2003. The variability of TARs in troughs on Mars. LPSC XXXIV [CDROM].

Bourke, M.C., Balme, M.R., Beyer, R.A., Williams, K.K., Zimbelman, J.R., 2006. A comparison of methods used to estimate the height of sand dunes on Mars. Geomorphology. 81(3-4), 440-452.

Bourke, M.C., Goudie, A.S., 2009. Varieties of barchans form in the Namib Desert and on Mars. Aeolian Research. 1(1-2), 45-54.

Bourke, M.C., Lancaster, N., Fenton, L.K., Parteli, E.J., Zimbelman, J.R., Radebaugh, J., 2010. Extraterrestrial dunes: An introduction to the special issue on planetary dune systems. Geomorphology. 121(1), 1-14.

Bridges, N.T., Ayoub, F., Avouac, J., Leprince, S., Lucas, A., Mattson, S., 2012a. Earth-like sand fluxes on Mars. Nature. 485, 339-342.

Bridges, N.T., Bourke, M.C., Geissler, P.E., Banks, M.E., Colon, C., Diniega, S., Golombek, M.P., Hansen, C.J., Mattson, S., McEwen, A.S., Mellon, M.T., Stantzos, N., Thomson, B.J., 2012b. Planet-wide sand motion on Mars. Geology. 40, 31-34.

Bridges, N.T., Geissler, P.E., Silvestro, S., Banks, M.E., 2013. Bedform migration on Mars: Current results and future plans. Aeolian Research. 9, 133-151.

Bridges, N. T., Spagnuolo, M. G., de Silva, S. L., Zimbelman, J. R., Neely, E.M., 2015. Formation of gravel-mantled megaripples on Earth and Mars: Insights from the Argentinean Puna and wind tunnel experiments. Aeolian Research. 17, 49-60.

Cantor, B. A., Kanak, K. M., & Edgett, K. S. (2006). Mars Orbiter Camera observations of Martian dust devils and their tracks (September 1997 to January 2006) and evaluation of theoretical vortex models. Journal of Geophysical Research: Planets, 111(E12).

Cardinale, M., Silvestro, S., Vaz, D. A., Michaels, T., Bourke, M. C., Komatsu, G., & Marinangeli, L., 2016. Present-day aeolian activity in Herschel Crater, Mars. Icarus, 265, 139-148.

Carr, M.H., 2006. The surface of Mars. Cambridge University Press.

Chapman, M.G., 2007. The Geology of Mars: Evidence from Earth-based analogs. Cambridge University Press, Cambridge.

Chavez, P., Sides, S. C., & Anderson, J. A., 1991. Comparison of three different methods to merge multiresolution and multispectral data- Landsat TM and SPOT panchromatic. Photogrammetric Engineering and remote sensing, 57(3), 295-303.

Chojnacki, M., Burr, D.M., Moersch, J.E., Michaels, T.I., 2011. Orbital observations of contemporary dune activity in Endeavour Crater, Meridiani Planum, Mars. Journal of Geophysical Research. 116(E7), E00F19.

Chojnacki, M., Johnson, J. R., Moersch, J. E., Fenton, L. K., Michaels, T. I., & Bell, J. F., 2015. Persistent aeolian activity at Endeavour crater, Meridiani Planum, Mars; new observations from orbit and the surface. Icarus, 251, 275-290.

Church, M., 2010. The trajectory of geomorphology Progress in Physical Geography. Progress in Physical Geography. 34, 265-286.

Claudin, P., Andreotti, B., 2006. A scaling law for aeolian dunes on Mars, Venus, Earth, and for subaqueous ripples. Earth and Planetary Science Letters. 252, 30-44.

Coops, N. C., Johnson, M., Wulder, M. A., & White, J. C., 2006. Assessment of QuickBird high spatial resolution imagery to detect red attack damage due to mountain pine beetle infestation. Remote Sensing of Environment, 103(1), 67-80.

Craddock, R.A., 2011. Aeolian processes on the terrestrial planets: Recent observations and future focus. Progress in Physical Geography. 36(1), 110-124.

de Silva, S.L., Bailey, J.E., Mandt, K.E., Viramonte, J.M., 2010a. Yardangs in terrestrial ignimbrites: Synergistic remote and field observations on Earth with applications to Mars. Planetary and Space Science. 58(4), 459-471.

de Silva, S., 2010b. The largest wind ripples on Earth: Comment: Geology, v. 38, p. e218, doi:10.1130/G30780C.1.

de Silva, S.L., Spagnuolo, M.G., Bridges, N.T., Zimbelman, J.R., 2013. Gravel-mantled megaripples of the Argentinean Puna: A model for their origin and growth with implications for Mars. Geological Society of America Bulletin. 125(11-12), 1912-1929.

DigitalGlobe, (2008a). WorldView-1 products quick reference guide, Longmont, CO, 2008. [Online]: http://digitalglobe.com

DigitalGlobe, (2008b). QuickBird imagery products: Product guide. Longmont, CO, 2008. [Online]: http://digitalglobe.com

Dong, Z., Lv, P., Lu, J., Qian, G., Zhang, Z., & Luo, W. (2012). Geomorphology and origin of yardangs in the Kumtagh Desert, Northwest China. Geomorphology, 139, 145-154.

Duda, T., Canty, M., 2002. Unsupervised classification of satellite imagery: choosing a good algorithm. International Journal of Remote Sensing 23, 2193–2212.

Edgett, K.S., Malin, M.C., 2000. New views of Mars aeolian activity, materials, and surface properties: Three vignettes from the Mars Global Surveyor Mars Orbiter Camera. Journal of Geophysical Research. 105, 1623-1650.

Ehsani, A. H., & Quiel, F., 2008. Application of self organizing map and SRTM data to characterize yardangs in the Lut desert, Iran. Remote Sensing of Environment, 112(7), 3284-3294.

Ellwood, J.M., Evans, P.D., Wilson, I.G. 1975. Small scale aeolian bedforms. Journal of Sedimentary Petrology 45: 554–561.

Ewing, R.C., Kocurek, G., Lake, L.W., 2006. Pattern analysis of dune-field parameters. Earth Surface Processes and Landforms. 31(9), 1176-1191.

Ewing, R. C., Peyret, A. P. B., Kocurek, G., & Bourke, M., 2010. Dune field pattern formation and recent transporting winds in the Olympia Undae Dune Field, north polar region of Mars. Journal of Geophysical Research: Planets, 115(E8).

Ewing, R.C., Hayes, A.G., Lucas, A., 2015. Sand dune patterns on Titan controlled by long-term climate cycles. Nature Geoscience. 8(1), 15-19.

Fenton, L.K., Michaels, T.I., Chojnacki, M., Beyer, R.A., 2014. Inverse maximum gross bedform-normal transport 2: Application to a dune field in Ganges Chasma, Mars and comparison with HiRISE repeat imagery and MRAMS. Icarus. 230, 47-63.

Fenton, L.K., Michaels, T.I., Chojnacki, M., 2015. Late Amazonian aeolian features, gradation, wind regimes, and Sediment State in the Vicinity of the Mars Exploration Rover Opportunity, Meridiani Planum, Mars. Aeolian Research. 16, 75-99.

Foroutan, M., Kompanizare, M., & Ehsani, A. H., 2013. Semiautomatic morphometric land surface segmentation of an arid mountainous area using DEM and self-organizing maps. Arabian Journal of Geosciences, 6(12), 4795-4810.

Foroutan, M., 2015. Ripple-like features on mars, characteristics and classification. 2015 GSA Fall Meeting. Geological Society of America.

Foroutan, M., & Zimbelman, J. R., 2016. Mega-ripples in Iran: A new analog for transverse aeolian ridges on Mars. Icarus, 274, 99-105.

Foroutan, M., Zimbelman, J.R., (under Review). Semi-automatic mapping of linear-trending bedforms using 'self-organizing maps' algorithm. Geomorphology.

Fryberger, S.G., 1979. Dune forms and wind regime. A Study of Global Sand Seas, USGS Professional Paper, US Geological Survey and United States National Aeronautics and Space Administration, Washington. 1052, 137– 169.

Gabriel, A., 1938. The southern Lut and Iranian Baluchistan. Geographical Journal. 92, 193–208.

Geissler, P. E., 2014. The birth and death of transverse aeolian ridges on Mars. Journal of Geophysical Research: Planets, 119(12), 2583-2599.

Golombek, M., Robinson, K., McEwen, A., Bridges, N., Ivanov, B., Tornabene, L., & Sullivan, R., 2010. Constraints on ripple migration at Meridiani Planum from Opportunity and HiRISE observations of fresh craters. Journal of Geophysical Research: Planets, 115(E7).

Greeley, R., Iverson, J.D., 1985. Wind as geological process on Earth, Mars, Venus and Titan. Cambridge University Press, Great Britain, Oxford.

Greeley, R., Kraft, M.D., Kuzmin, R.O., Bridges, N.T., 2000. Mars Pathfinder landing site: Evidence for a change in wind regime from lander and orbiter data. Journal of Geophysical Research: Planets (1991-2012). 105(E1), 1829-1840.

Greeley, R., Arvidson, R., Bell, J. F., Christensen, P., Foley, D., Haldemann, A., ... & Squyres, S. W., 2005. Martian variable features: new insight from the Mars Express Orbiter and the Mars Exploration Rover Spirit. Journal of Geophysical Research: Planets, 110(E6).

Greeley, R., Waller, D. A., Cabrol, N. A., Landis, G. A., Lemmon, M. T., Neakrase, L. D., ... & Whelley, P. L., 2010. Gusev Crater, Mars: Observations of three dust devil seasons. Journal of Geophysical Research: Planets, 115(E7).

Greeley, R., 2013. Introduction to Planetary Geomorphology. Cambridge University Press.

Hamidian Pour, M., Mofidi, A., Salighe, M. (2016). Analysis of the nature and structure of Sistan wind. Iranian Journal of Geophysics, 10 (2).

Hansen, C.J., Bourke, M.C., Bridges, N.T., Byrne, C., Colon, C., Diniega, S., Dundas, C., Herkenhoff, K., McEwen, A.S., Mellon, M.T., Portyankina, G., Thomas, N., 2011. Seasonal erosion and restoration of Mars northern. Science. 331(6017), 575-578.

Hargitai, H., & Kereszturi, Á. (Eds.)., 2015. Encyclopedia of Planetary Landforms. Springer.

Jessar, A.D., Zimbelman, J.R., Hennig, L.A. (2015). TARs on Mars: A study of the spatial variability and physical characteristics of Martian Transverse Aeolian Ridges. Fourth International Planetary Dunes Workshop. Abs# 8022.

Jianwen, M., Bagan, H., 2005. Land-use classification using ASTER data and self-organized neutral networks. International Journal of Applied Earth Observation and Geoinformation 7, 183–188.Kohonen, T., 2001. Self Organizing Maps, 3rd Ed. Springer, New York.

Kerber, L., Head, J.W., 2012. A progression of induration in Medusae Fossae Formation transverse aeolian ridges: evidence for ancient aeolian bedforms and extensive reworking. Earth Surface Processes and Landforms. 37, 422-433.

Kocurek, G., Ewing, R.C., 2005. Aeolian dune field self -organization – Implications for the formation of simple versus complex dune field patterns. Geomorphology. 72(1-4), 94-105.

Kocurek, G., Ewing, R.C., Mohrig, D., 2010. How do bedform patterns arise? New views on the role of bedform interactions within a set of boundary conditions. Earth Surface Processes and Landforms. 35(1), 51-63.

Kok, J.F., Parteli, E.J., Michaels, T.I. and Karam, D.B., 2012. The physics of wind-blown sand and dust. Reports on Progress in Physics, 75(10), p.106901.

Koua, E.L., MacEachren, A., Kraak, M.J., 2006. Evaluating the usability of visualization methods in an exploratory geovisualization environment. International Journal of Geographical Information Science 20, 425–448.

Lillesand, T., Kiefer, R. W., & Chipman, J., 2014. Remote sensing and image interpretation. John Wiley & Sons.

Lorenz, R.D., Zimbelman, J.R., 2014. "Dune Worlds": How Windblown Sand Shapes Planetary Landscapes. Springer, Washangton, USA.

Maghsoudi, M., Hajizadeh, A., Nezam, M. M. A., Bayati, S. Z., 2015. Assessment of paleo environmental conditions of ovoid yardangs using granolumetry. Geographical Data 24, 51-64.

Murphy, J.D., 1973. The Geology of Eagle Cove at Bruneau, Idaho. M.S. Thesis, State Univ. New York at Buffalo. 77p.

Malin, M.C., Edgett, K.S., 2001. Mars Global Surveyor Mars Orbiter Camera: Interplanetary cruise through primary mission. Journal of Geophysical Research. 106, 23429-23570.

Marchant, D.R., Head III, J.W., 2007. Antarctic dry valleys: Microclimate zonation, variable geomorphic processes, and implications for assessing climate change on Mars. Icarus. 192(1), 187-222.

Marini, F., Zupan, J., Mageri, A.L., 2005. Class-modeling using Kohonen artificial neural networks. Analytica Chimica Acta 544, 306–314.

McEwen, A.S., et al., 2007. Mars Reconnaissance Orbiter's High Resolution Imaging Science Experiment (HiRISE), Journal of Geophysical Research, 112, E05S02, doi: 10.1029/2205JE002605.

Mildrexler, D.J., Zhao, M., Running, S.W., 2011. Satellite finds highest land skin temperatures on Earth. Bulletin of the American Meteorological Society. 92, 855-860.

Nickling, W. G., & Neuman, C. M., 2009. Aeolian sediment transport. In Geomorphology of desert environments (pp. 517-555). Springer Netherlands.

Parikh, J. A., DaPonte, J. S., DiNicola, E. G., & Pedersen, R. A., 1992. Selective detection of linear features in geological remote sensing data. In Aerospace Sensing (pp. 963-972). International Society for Optics and Photonics.

Parteli, E.J.R., Almeida, M.P., Durán, O., Andrade Jr., J.S., Herrmann, H.J., 2009. Sand transport on Mars. Computer Physics Communications. 180, 609-611.

Pedersen, A., Kocurek, G., Mohrig, D., & Smith, V., 2015. Dune deformation in a multi-directional wind regime: White Sands Dune Field, New Mexico. Earth Surface Processes and Landforms, 40(7), 925-941.

Radebaugh, J., Lorenz, R.D., Farr, T., Paillou, P., Savage, C., Spencer, C., 2010. Linear dunes on Titan and earth: initial remote sensing comparisons. Geomorphology. 121(1-2), 122-132.

Raiche, A., 1991. A pattern recognition approach to geophysical inversion using neural nets. Geophysical Journal International, 105(3), 629-648.

Reiss,D., Raack,J., Rossi,A.P., DiAchille,G., Hiesinger,H., 2010. First in-situ analysis of dust devil tracks on Earth and their comparison with tracks on Mars. Geophysical Research Letters.37, L14203.

Reiss, D., & Lorenz, R. D., 2016. Dust devil track survey at Elysium Planitia, Mars: Implications for the InSight landing sites. Icarus, 266, 315-330.

Rossi, A.P., Marinangeli, L., 2004. The first terrestrial analogue to Martian dust devil tracks found in Ténéré Desert, Niger. Geophysical research letters, 31(6). Geophysical Research Letters. 31(6), L06702.

Sakamoto-Arnold, C.M., 1988. Eolian features produced by the December 1977 windstorm Southern San Joaquin Valley, California. Journal of Geology 89: 129–137.

Savage, C.J., Radebaugh, J., Christiansen, E.H., Lorenz, R.D., 2014. Implications of dune pattern analysis for Titan's surface history. Icarus. 230, 180-190.

Sefton-Nash, E., Teanby, N.A., Newman, C., Clancy, R.A., Richardson, M.I., 2014. Constraints on Mars' recent equatorial wind regimes from layered deposits and comparison with general circulation model results. Icarus. 230, 81-95.

Sharp, R. P., 1963. Wind ripples. The Journal of Geology, 617-636.

Shockey, K.M., Zimbelman, J.R., 2013. Analysis of transverse aeolian ridge profiles derived from HiRISE images of Mars. Earth Surface Processes and Landforms. 38(2), 179-182.

Silvestro, S., Fenton, L.K., Vaz, D.A., Bridges, N.T., Ori, G.G., 2010. Ripple migration and dune activity on Mars: Evidence for dynamic wind processes. Geophysical Research Letters. 37(20), L20203.

Silvestro, S., Vaz, D.A., Fenton, L.K., Geissler, P.E., 2011. Active aeolian processes on Mars: A regional study in Arabia and Meridiani Terrae. Geophysical Research Letters. 38(20), L20201.

Silvestro, S., Fenton, L.K., Michaels, T.I., Valdez, A., Ori, G.G., 2012. Interpretation of the complex dune morphology on Mars: dune activity, modelling and a terrestrial analogue. Earth Surface Processes and Landforms. 37(13), 1424-1436.

Silvestro, S., Vaz, D. A., Di Achille, G., Popa, I. C., & Esposito, F., 2015. Evidence for different episodes of aeolian construction and a new type of wind streak in the 2016 ExoMars landing ellipse in Meridiani Planum, Mars. Journal of Geophysical Research: Planets, 120(4), 760-774.

Smalley, I.J., Krinsley, D.H., 1979. Eolian sedimentation on Earth and Mars: some comparisons. Icarus. 40(2), 276-288.

Sobel I. E., 1970. Camera models and machine perception. Ph.D. Thesis, Electrical Engineering Department, Stanford University, Stanford, CA.

Spagnolo, M., Clark, C. D., & Hughes, A. L. (2012). Drumlin relief. Geomorphology, 153, 179-191.

Stern, S. A., Bagenal, F., Ennico, K., Gladstone, G. R., Grundy, W. M., McKinnon, W. B., ... & Young, L. A., 2015. The Pluto system: Initial results from its exploration by New Horizons. Science, 350(6258), aad1815.

Sullivan R, Banfield D, Bell JF, Calvin W, Fike D, Golombek M, Greeley R, Grotzinger J, Herkenhoff K, Jerolmack D, Malin M., 2005. Aeolian processes at the Mars exploration rover Meridiani Planum landing site. Nature, 436(7047), 58-61.

Szynkiewicz, A., Ewing, R.C., Moore, C.H., Glamoclija, M., Bustos, D., Pratt, L.M., 2010. Origin of terrestrial gypsum dunes implications for Martian gypsum-rich dunes of Olympia Undae. Geomorphology. 121(1), 69-83.

Tanner, W. F. (1967). Ripple mark indices and their uses. Sedimentology, 9(2), 89-104.

Thomas, P.C., Malin, M.C., Carr, M.H., Danielson, G.E., Davies, M.E., Hartmann, W.K., Ingersoll, A.P., James, P.B., McEwen, A.S., Soderblom, L.A., Veverka, J., 1999. Bright dunes on Mars. Nature. 397, 592-594.

Thomas, M., Clarke, J.D., Pain, C.F., 2005. Weathering, erosion and landscape processes on Mars identified from recent rover imagery, and possible Earth analogues. Australian Journal of Earth Sciences. 52(3), 365-378.

Vaz, D. A., & Silvestro, S., 2014. Mapping and characterization of small-scale aeolian structures on Mars: An example from the MSL landing site in Gale Crater. Icarus, 230, 151-161.

Verba, C. A., Geissler, P. E., Titus, T. N., & Waller, D. (2010). Observations from the high resolution imaging science experiment (HiRISE): Martian dust devils in Gusev and Russell craters. Journal of Geophysical Research: Planets, 115(E9).

Walker, A.S., 1986. Chapter 8: Plate E-19. M. Nicholas, S. Short, J. Robert, W. Blair (Eds.), Geomorphology from Space, NASA.

Ward, A.W., 1979. Yardangs on Mars: Evidence of recent wind erosion. Journal of Geophysical Research: Solid Earth. 84(B14), 8147-8166.

White, B.R. (1979) Soil transport by wind on Mars. Journal of Geophysical Research, 84, 4643-4651.

Williams, S.H., Zimbelman, J.R., Ward, A.W., 2002. Large ripples on Earth and Mars. Lunar and Planetary Science XXXIII, 1508.

Wilson, S.A., Zimbelman, J.R., 2004. Latitude-dependent nature and physical characteristics of transverse aeolian ridges on Mars. Journal of Geophysical Research. 109, (E10003).

Wu, J., Bauer, M. E., Wang, D., & Manson, S. M., 2008. A comparison of illumination geometry-based methods for topographic correction of QuickBird images of an undulant area. ISPRS journal of photogrammetry and remote sensing, 63(2), 223-236.

Yizhaq, H., Kok, J.F., Katra, I., 2014. Basaltic sand ripples at Eagle Crater as indirect evidence for the hysteresis effect in Martian saltation. Icarus. 230, 143-150.

Yizhaq, H., Katra, I., 2015. Longevity of aeolian megaripples. Earth and Planetary Science Letters 422, 28-32. doi: 10.1016/j.epsl.2015.04.004.

Zambito, J. J., & Benison, K. C., 2013. Extremely high temperatures and paleoclimate trends recorded in Permian ephemeral lake halite. Geology, 41(5), 587-590.

Zimbelman, J.R., 1987. Spatial resolution and the geologic interpretation of Martian morphology: Implications for subsurface volatiles. Icarus. 71, 257-267.

Zimbelman, J.R., 2003. Decameter-scale ripple-like features in Nirgal Vallis as revealed in THEMIS and MOC imaging data. Sixth international conference on Mars, abstract 3028.

Zimbelman, J.R., Irwin III, R.P., Williams, S.H., Bunch, F., Valdez, A., Stevens, S., 2009. The rate of granule ripple movement on Earth and Mars. Icarus. 203(1), 71-76.

Zimbelman, J.R., 2010. Transverse Aeolian Ridges on Mars: First results from HiRISE images. Geomorphology. 121, 22-29.

Zimbelman, J. R., Williams, S. H., & Johnston, A. K., 2012. Cross-sectional profiles of sand ripples, megaripples, and dunes: a method for discriminating between formational mechanisms. Earth Surface Processes and Landforms. 37(10), 1120-1125.

Zimbelman, J.R., Scheidt, S.P., 2014. Precision topography of a reversing sand dune at Bruneau Dunes, Idaho, as an analog for Transverse Aeolian Ridges on Mars. Icarus. 230, 29-37.